DETERMINATION OF VIBROACOUSTICAL BEHAVIOR OF PLATES BY INTENSITY METHODS

A THESIS SUBMITTED TO
THE GRADUATE SCHOOL OF NATURAL AND APPLIED SCIENCES
OF
MIDDLE EAST TECHNICAL UNIVERSITY

BY

MURAT İNALPOLAT

IN PARTIAL FULFILLMENT OF THE REQUIREMENTS FOR THE DEGREE OF
MASTER OF SCIENCE

IN

MECHANICAL ENGINEERING

JUNE 2004

Approval of the Graduate School of Natural and Applied Sciences

_____

Prof. Dr. Canan ÖZGEN
Director

I certify that this thesis satisfies all the requirements as a thesis for the degree of Master of Science.

_____

Prof. Dr. S. Kemal İDER
Head of Department

This is to certify that we have read this thesis and that in our opinion it is fully adequate, in scope and quality, as a thesis for the degree of Master of Science.

_____

Prof. Dr. Mehmet ÇALIŞKAN
Supervisor

Examining Committee Members

Prof. Dr. Y. Samim ÜNLÜSOY	(METU, ME)	_____
Prof. Dr. Mehmet ÇALIŞKAN	(METU, ME)	_____
Prof. Dr. Bülent E. PLATİN	(METU, ME)	_____
Prof. Dr. H. Nevzat ÖZGÜVEN	(METU, ME)	_____
Assoc. Prof. Dr. Yusuf ÖZYÖRÜK	(METU, AEE)	_____

I hereby declare that all information in this document has been obtained and presented in accordance with academic rules and ethical conduct. I also declare that, as required by these rules and conduct, I have fully cited and referenced all material and results that are not original to this work.

Name, Last name : Murat İNALPOLAT

Signature :

ABSTRACT

DETERMINATION OF VIBROACOUSTICAL BEHAVIOR OF PLATES BY INTENSITY METHODS

İnalpolat, Murat
M.S., Department of Mechanical Engineering
Supervisor : Prof. Dr. Mehmet Çalışkan

June 2004, 141 pages

In this study, sound radiation and power flow characteristics of plates which constitute the bodies of common engineering applications like cars and household appliances are investigated. Three different vibro-acoustical measurement techniques are used in an integrated manner and results obtained are compared with those obtained from analytical models developed.

Two-microphone sound intensity measurement with a probe utilizing side-by-side configuration is used to analyze the near-field radiation characteristics of a square steel plate excited by a shaker at its midpoint. Surface intensity is simultaneously measured on the plate with another probe consisting of a condenser microphone and an eddy-current non-contact displacement transducer to compare the results with those obtained from two-microphone sound intensity measurement. Surface intensity is also measured with a probe consisting of a condenser microphone and an accelerometer as an alternative configuration. Structural intensity is used to identify the power flow patterns on the plate. All measurements

are repeated for externally damped configuration of the same plate and results are analyzed. Easily adoptable two distinct, lumped parameter models of the plate are developed to compute the sound power radiated by the structure. In these models, the plate is modeled by employing the pulsating sphere and vibrating piston as the elementary source types, alternatively. In the model employing vibrating piston in the baffle, results are obtained with and without mutual interaction among partitions. Results obtained from these models are compared with the experimental results. Error analysis is also conducted for all of the measurement techniques employed.

Keywords: Sound Intensity, Structural Intensity, Power Flow, Vibro-acoustics of Plates, Lumped Parameter Modelling

ÖZ

PLAKALARIN TİTREŞİMSEL VE AKUSTİK DAVRANIŞLARININ YEĞİNLİK YÖNTEMLERİYLE BELİRLENMESİ

İnalpolat, Murat

Yüksek Lisans, Makina Mühendisliği Bölümü

Tez Yöneticisi : Prof. Dr. Mehmet Çalışkan

Haziran 2004, 141 sayfa

Bu çalışmada, otomobiller ve beyaz eşyalar gibi bilinen mühendislik uygulamalarının gövdelerini oluşturan plakaların ses radyasyon ve güç akış karakteristikleri araştırılmıştır. Üç farklı tireşimsel ve akustik yöntem bütünleşik olarak kullanılmış ve sonuçları, geliştirilen analitik modellerin sonuçları ile karşılaştırılmıştır.

Yan yana mikrofon konfigurasyonunu kullanan bir düzenek ile yapılan iki mikrofon ses yeğinliği ölçümü, ortasından titreştirici ile tahrik edilen kare çelik bir plakanın yakın alan ses radyasyon karakteristiğinin anlaşılmasında kullanılmıştır. Yüzey yeğinliği eşzamanlı olarak, bir sığasal mikrofon ile girdap akımlı temassız bir deplasman ölçerden oluşan başka bir düzenek ile sonuçlarını iki mikrofon ses yeğinliği ölçümünün sonucu ile karşılaştırmak üzere ölçülmüştür. Yüzey yeğinliği alternatif bir konfigürasyon olarak bir mikrofon ile bir ivmemetreden oluşan bir düzenek ile de ölçülmüştür. Yapısal yeğinlik, plakalardaki güç akış desenlerinin belirlenmesi için kullanılmıştır. Bütün ölçümler aynı plakanın dışarıdan sönümlenmiş hali için tekrarlanmış ve sonuçlar analiz edilmiştir. Plakanın iki ayrı,

kolaylıkla uygulanabilir, toplanmış parametreli modeli, yapı tarafından yayılan ses gücünün hesaplanması için geliştirilmiştir. Bu modellerde, plaka ritmik atımlı küre ve titreşen pistonu temel kaynak tipi alarak değişimli olarak modellenmiştir. Sonsuz düzlem içinde titreşen pistonlu modelde sonuçlar, her bir bölme arasında akustik etkileşim varken ve yok iken elde edilmiştir. Bu modellerden elde edilen sonuçlar deneysel sonuçlarla karşılaştırılmıştır. Kullanılan bütün ölçüm teknikleri için hata analizi de gerçekleştirilmiştir.

Anahtar Kelimeler: Ses Yeğinliği, Yapısal Yeğinlik, Güç Akışı, Plakaların Titreşim ve Akustiği, Toplanmış Parametreli Modelleme

To My Family

ACKNOWLEDGEMENTS

The author wishes to express his deepest gratitude to his supervisor, Prof. Dr. Mehmet Çalışkan, for his guidance, advice, criticism, encouragement and insight throughout the research. In addition, the author is thankful to Prof. Dr. H. Nevzat Özgüven, Prof. Dr. Y. Samim Ünlüsoy, Prof. Dr. Bülent E. Platin and Assoc. Prof. Dr. Yusuf Özyörük for serving on the Thesis Committee.

The author would like to thank Dr. Hakan Şerafettinoğlu of Arçelik for his invaluable support and criticism. The author truly thanks Mr. Bülent İrfanoğlu for his patient support and also for the lengthy discussions concerning this study. A special thanks is extended to Ms. Berna Çetinkaya for her precious friendship and support which made this study possible to be completed.

Appreciation is extended to the technical staff of METU. In particular, appreciation is due Mr. İmdat Uğursu, Mr. Özdemir Emen and Mr. Yusuf Papur for the technical support they have provided throughout this study.

Finally the author wishes to express his sincere thanks to his family and special friends whose encouragement and support were invaluable throughout this work.

TABLE OF CONTENTS

LIST OF FIGURES

NOMENCLATURE

$p(t)$: Time-varying acoustic pressure (Pa)

$u(t)$: Time-varying particle velocity (m/s)

I : Active part of sound intensity (W/m^2)

J : Reactive part of sound intensity (W/m^2)

ρ_o : Density of air (kg/m^3)

Δr : Microphone spacing (m)

Δx : Accelerometer spacing (m)

c : Speed of sound in air (m/s)

P : Amplitude of acoustic pressure

U : Amplitude of particle velocity

δ : Dirac-delta function

$\tilde{u}(t)$: Complex valued particle velocity

∇ : Gradient operator

j : Unit imaginary number ($\sqrt{-1}$)

$G_{P_2P_1}$: One-sided cross spectrum between P_2 and P_1 $(N/m^2)^2$

$G_{P_1P_1}$: One-sided power spectrum of P_1 $(N/m^2)^2$

λ : Wavelength (m)

k : Wavenumber (1/m)

B_o : Bandwidth of measurement (Hz)

B_e : Resolution Bandwidth (Hz)

T : Total averaging time (s)

N : Number of averaged samples

H : Frequency response function of measurement channel

$G^{sw}_{P_2P_1}$: One-sided cross spectrum between P_2 and P_1 measured after the microphone switching procedure is accomplished $(N/m^2)^2$

A : Amplitude of acceleration

X : Amplitude of displacement

ϕ : Phase mismatch angle (deg)

a(t) : Time-varying acceleration (m/s^2)

V : Translational surface velocity (m/s)

θ : Angular velocity (rad/s)

M_{xy} : Twisting moment (N.m)

Q : Shear force (N)

η : Surface displacement of the plate (m)

B : Flexural (Bending) stiffness (N.m)

W : Structural intensity (W/m)

c_f : Flexural phase velocity (m/s)

m : Mass per unit area of the plate (kg/m^2)

S : Total area of measurement surface (m^2)

ΔS : Area of each partition on the measurement surface (m^2)

σ : Radiation efficiency

G_u : Particle velocity spectrum

ε_b : Normalized bias error

ε_r : Normalized random error

γ : Coherence estimate

a : Radius of pulsating sphere type sound source (m)

Ω : Solid angle (Steradian)

J_1 : Bessel function of the first order

S_1 : Struve function of the first order

Z : Radiation impedance

CHAPTER 1

INTRODUCTION

1.1 General

Noise produced by machinery in situ affects our daily life, both physiologically and psychologically. This unwanted part of sound should be reduced to levels, low enough to avoid people to be damaged. Having realized this fact, governments publish legislations related with the sound abatement procedures. Yet, these procedures include more information about the limit values of noise that the human-being should be exposed, than the control procedures of noise. Consequently, noise control specialists must develop different strategies to control noise radiated by a wide range of different cases.

Even though strategies differ in details, the general procedures are based on the same principles. A straightforward approach to solve a noise control problem is to examine the problem in terms of its three fundamental elements: source, path and receiver.

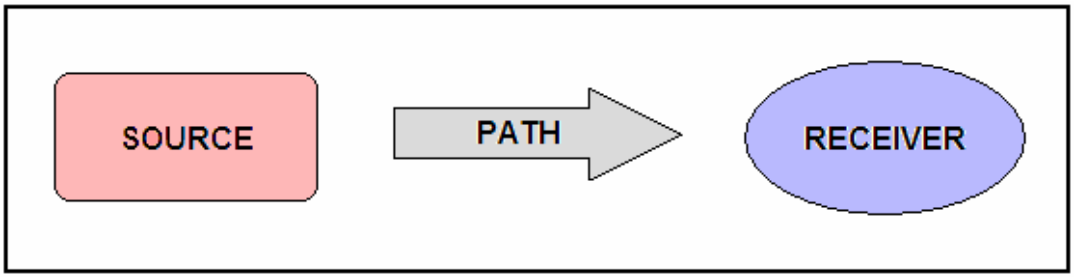

Figure 1.1 Fundamental Elements of Noise Control Procedures

The most appropriate solution to a given noise control problem requires alternation or modification of any or sometimes all of the fundamental elements shown in Figure 1.1. Solution that can achieve the desired amount of noise reduction by using the lowest expenses and causing least inconvenience to the occupant activities is the most appropriate one. One must analyse the three fundamental elements of noise control, i.e. source, path and receiver to be able to diagnose the problem and find the best solution to reduce sound that can reach the receiver.

1.2 Scope and Objective of the Thesis

In this particular study, it is aimed to analyse the “source” in terms of its vibroacoustical properties. Plate-like structures are typical sources considered in this particular study. Radiation and power flow characteristics of such structures are studied because they constitute bodies of the well-known engineering applications like cars and household appliances which appear to be the most encountered sound sources in everyday life. It is the best choice to control the noise at the source and especially at the design stages for these applications. Although it is probably the most expensive solution to the problem, it provides the most reliable and permanent solution.

Cross-spectral measurement techniques are employed to identify the representative near-field sound radiation paths together with the power flow paths on a square, steel plate. It is also aimed to determine the total sound power radiated from the plate and its radiation efficiency. Sound power radiated is the unique parameter that can be used for comparison and labelling of the machinery, particularly household appliances. This is due to the fact that, sound power is a characteristic property of a product, i.e. it does not depend on the measurement conditions. Consequently, it is used for comparison by the customers on the market and requires proper labelling of the machinery manufactured for fair competition.

Two-microphone sound intensity technique is employed to determine the near-field sound energy radiation paths as well as to find the radiated sound power

and the corresponding radiation efficiency. Side-by-side microphone configuration is used to make measurements in the near-field of the plate. Surface intensity technique is used to accomplish the same objective while it provides the chance to compare the results with the ones obtained by the two-microphone sound intensity measurements. Errors associated with these two acoustical techniques and their elimination methods are emphasized and an error analysis is also carried out within the scope of this study. Structural intensity is measured using a probe comprising of two accelerometers. In fact, the objective of the structural intensity measurements is to observe the propagation paths of the bending waves which couple very well with the sound field and cause the dominant part of the sound radiated by the plate. It has become possible to determine the structural intensity via the measurement of frequency response functions with a frequency domain formulation derived in this particular study. This derivation is based on modelling of the measurement system with a Single Input / Multiple Output System. Error analysis for the structural intensity technique is also performed. All of the measurements are carried on the plate without external damping and for the same plate after damping treatment is applied via damping patches. Comparison of the results obtained for these two cases are made possible in terms of the near-field sound intensity maps, sound power and radiation efficiency spectra and power flow maps. Intensity mapping techniques are utilized to visualize the results.

A lumped parameter model of the plate is developed by using three different lumped source types. The plate is thought to be divided into 36 partitions with equal areas and each partition is modeled by a lumped parameter source model. Firstly, the plate is modeled by using pulsating sphere type sound sources with equal areas and functioning in their own true phases. Secondly, it is modeled by a collection of small, circular, baffled pistons with equal areas functioning in their own true phases. It is assumed that there is no mutual acoustical interaction between each element in modelling. As a last model, it is assumed that the pistons utilized within the previous model have mutual interaction between them and the model is again formed by using the circular baffled pistons. Results of these

analytical models are compared with the ones obtained from the experimentation. Collected spectra are post-processed via 30 distinct Matlab® routines.

The purpose of this research is to use the experimental methods mentioned herein this study in such an integrated manner that the vibroacoustical characteristics of plates are determined completely. A lumped parameter model of the plate is developed as a powerful as well as a practical tool to determine the total sound power radiated and the radiation efficiency of plates. This particular model is also used to check the results of the experimental methods employed. The results are very encouraging because it is observed that the experimental methods yield reasonably close results, at especially low frequencies, and analytical results obtained from the model display a similar trend with the experimental results. It should also be noted that the entire procedure accomplished within this study is very convenient to use in industrial applications as well as to use in laboratory conditions. It is not required to have special measurement systems to fulfill this procedure and this makes it more valuable.

The next chapter presents a literature review of the state-of-the-art in four main subjects of this study.

Chapter 3 is dedicated both to the derivation of the mathematical expressions that will be frequently used throughout this study and the interpretation of the physics underlying the whole subject in hand.

Chapter 4 presents the application of the experimental methods and their results along with the error analysis associated with these methods.

Lumped parameter modelling of plates is explained in Chapter 5. The plate is modelled by using three distinct lumped parameter source types and the results are presented in comparison with the results obtained by the application of the measurement techniques employed.

In Chapter 6, the results and conclusions of most significance are summarized. Recommendations for future work are also presented within this chapter.

CHAPTER 2

LITERATURE REVIEW

The literature review which follows is presented in four sections. Each corresponds to a field of study pertinent to the present study on determination of radiation characteristics of plate-like structures. These sections include : 1) Sound intensity and its applications, 2) Measurement of surface intensity comparison to sound intensity, 3) Structural intensity and its measurement, 4) Lumped parameter vibroacoustic modelling of plates.

2.1 Sound Intensity and Its Applications

Even though H.F. Olson started the era of sound intensity in 1932, it has taken 45 years that the measurement and application of sound intensity become possible in a practical manner. At 1977, F.J. Fahy and J.Y. Chung have ignited the idea of applying digital signal processing techniques to the theory with their independent studies. From that time to the time being, sound intensity has become a fabulous tool for noise control engineers in measuring, analyzing and controlling vibration and noise.

In 1932 H.F. Olson received a patent for a device to measure acoustic intensity at a point in the sound field by combining the signals from a pressure microphone and a velocity microphone so that the ultimate output indicated intensity [40]. It is reported again by H.F. Olson that, this device had problems with the thermocouple used in power conversion [41]. After this influential work of Olson, there had been other studies [42,43,44,45,46] on the same objective of designing an intensity meter which has a wide dynamic range, low temperature stability and which is appropriate to measure intensity in reverberant fields. Yet,

efforts had been insufficient to measure intensity with reasonably low errors. Much research had been conducted using the two-microphone technique and digital signal analysis after the suggestion of Burger et al. [48]. In 1977 Pavic published a thorough analysis of the theory and errors associated with the two-microphone sound intensity technique [47]. He reported that the major drawback of this technique was a rather low upper frequency limit. However, he suggested that better results could be obtained by using digital signal analysis techniques. In the same year F.J. Fahy published results of intensity measurements using the cross-spectral density of two microphone signals [6]. Results were encouraging except that major problems were encountered due to phase mismatch between the channels of the measurement system employed. At the end of 1977 J.Y. Chung has ended up with a new technique involving the mechanical interchange of the positions of two microphones. The method had claimed to be applicable to any acoustic field subject to the condition that the product of the wave number and the microphone spacing remained small. This technique has been applied to measurements of intensity on diesel engines with apparent success [49]. In 1981, Krishnappa presented a new method of eliminating phase mismatch error [14]. In this method, the phase and gain mismatch errors are corrected by measuring the transfer function between the two microphone systems exposing them to the same sound over a wide range of frequencies. The accuracy of the measurement was claimed to be verified by producing a sound field in an anechoic room and by generating plane-wave propagation inside a long length of pipe with an anechoic termination.

In the following years, much more attention is attracted to the determination of sound power, radiation efficiency and surface velocity using sound intensity methods [32,51,52,53,58]. Moreover, errors inherent are published by several authors [5,11,54,55,56,57]. All of these analysis are integrated and a standart has been published by International Standarts Organisation at 1993 and named as “ISO 9614-1, Measurement at Discrete Points”. Errors associated with the technique is determined, evaluated and corrected via some factors called as field indicators

within this standart. After the standartization, sound intensity has taken a stronger place in sound power measurement.

Application of sound intensity based measurement techniques to the problems involving plates has been one of the most popular research topics since the development of the frequency domain formulation of sound intensity. Tichy and Kihlman presented a study displaying the sound field in front of plates with and without damping [59]. Cervera et al. carried out an analytical calculation together with the measurement of sound intensity above a vibrating plate [60]. As a practical example, Singh et al. determined sound power and radiation efficiency of the top plate of a gearbox housing [61]. He also compared the results with the results obtained by using FEM/BEM. As a more recent study, İnalpolat and Çalışkan published a comparative study including two-microphone sound intensity measurements over a steel plate [36]. Side-by-side microphone configuration is used and the results of the sound intensity measurements together with the ones obtained from surface intensity measurements are compared with the results obtained by using a lumped parameter model of the vibrating plate.

2.2 Measurement of Surface Intensity in Comparison to Sound Intensity

If the surface vibration data taken from the vibrating object along with the sound pressure signal from the microphone is exploited, the resulting acoustic intensity is referred as the "surface intensity" (W/m^2) [36]. This method is mainly proposed to be used when there is limited access to the surface of the machine. Hodgson laid the foundations of this method with his influential work in which surface intensity is utilized for source identification and ranking purposes of a centrifugal chiller [16]. The feasibility of the method has claimed to be checked by calculating the radiation efficiencies of the noise radiators in addition to the measurement procedure and the results were found to be encouraging. McGary and Crocker focused on the phase shift problems of this technique [20]. They developed a simple set-up for measuring and correcting instrumentation phase

mismatch. A piston, excited by a shaker fed with white noise is located at one end of a duct with other end anechoically terminated. An accelerometer is mounted on the piston and the waves generated by the piston are transduced by a microphone put apart a known distance from the piston. Total phase was measured and the calculated field phase was subtracted from the total phase measured giving the phase mismatch between the two measurement channels. Field measurements were corrected by means of the determined phase mismatch angle and the results were claimed to be successful. Reinicke published a study which compares the surface intensity technique with the two-microphone sound intensity technique by using measurements carried out on a centrifugal fan [19]. Following the utilization of the probe presented by Hodgson which comprises an accelerometer with a condenser microphone, attempts have continued to be made to design and utilize some other kinds of probes. Boone designed a fibre optic lever displacement transducer, a non-contacting probe to measure surface displacement by using fibre-optic principles [17]. Another different type of surface intensity probe is designed by Driesch et al. This probe combines a highly sensitive piezoelectric ceramic accelerometer and an inexpensive electric condenser microphone within a common titanium housing [18]. Even though several researches have tried to develop a surface intensity probe without phase mismatch between the measurement channels, none of them could have ended up with such a probe. Moreover, no practical method of measuring phase mismatch between acoustical and vibrational phenomena could have been found to date.

2.3 Structural Intensity and Its Measurement

Structural Intensity is the analogous quantity to sound intensity with the exception that the medium through which waves propagate is solid. This novel technique for measuring the vibrational intensity (power flow per unit width of cross-section) in uniform plates and beams vibrating in flexure was first proposed by Noiseux [21]. After this influential work of Noiseux, Pavic stated the time domain formulation of structural intensity in a more clear fashion [22]. He

considered only the flexural waves in the derivation since such waves couple the sound field very well. Studies of Fahy and Pierri [62] and Verheij [26] ignited the idea of transforming the time domain formulation of structural intensity to frequency domain. Frequency domain formulation of structural intensity for beams was given by Lyon [30]. Transfer formulation for measurement of structural intensity was adopted for beams by Kim and Tichy [27] and for plates by using a single input/multiple output model for the measurement system by İnalpolat and Çalışkan [36]. The two-accelerometer structural intensity technique first proposed by Pavic has been applied to a variety of problems involving plate vibrations. For example, Rasmussen [65] measured structural intensity successfully on a fuselage structure simulating a helicopter cabin. Zhang and Mann analyzed the influence of attachments on the vibratonal behavior of plates by using the structural intensity method [63].

A second method of measuring structural intensity called as SIMAP (Structural Intensity from the Measurement of Acoustic Pressure) has been proposed by Williams et al. [23]. Normal surface velocity of a vibrating structure is reconstructed by means of pressure measurements on a fine mesh in a plane close to the vibrating surface. If the normal velocity is reconstructed on a fine enough mesh on the surface of the vibrating surface, then the 2-dimensional structural intensity vector in the vibrating surface can be calculated by finite difference methods. Measurement of pressure was achieved by a non-contact method utilizing a scanning hydrophone. It should be noted that, the SIMAP is regarded within ***Inverse Problem*** formulation methods which are beyond the scope of this study.

2.4 Lumped Parameter Modelling of Plates

Plate-like structures have been first proposed to be modelled by using simple sound source types by Cremer et al. [25]. In Cremer's study, it is suggested to combine monopoles that are of the same strength and where neighbouring sources are 180° out of phase with each other. This model has been shown to be valid especially for short bending wavelengths. A more realistic model in which all

of the simple sources are proposed to be combined in such a manner that they radiate in their own true phases was presented by Johnson and Elliott [64] and in a distinct study by Hashimoto [38]. Plates have been proposed to be modelled by circular vibrating piston type sound sources that radiate in their own true phases. It has been stressed that there is an acoustical mutual interaction between these vibrating piston type sources within these studies. Results of these models are checked by means of experimental procedures and claimed to be in harmony.

In this particular study, the plate used throughout the experimental stages is modelled by a collection of pulsating sphere type sources and circular vibrating pistons in a baffle. Influence of mutual interaction have also been examined. It should be noted that, lumped parameter modelling provides an easy and practical means of estimating total sound power radiated by plate-like structures even if dimensions of structure is large with respect to the wavelength of the sound considered.

2.5 Criticism on the Existing Literature

Even though there are numerous studies on the topic of intensity, the most cited publications are chosen as the references throughout this study. Although the references are chosen from the most outstanding ones, there are a few numbers of missing or insufficient parts within these studies.

There is an ambiguity in the definition and usage of the cross-spectrum within the frequency domain formulation of sound intensity which is given by Equation 3.27. Some of the references cited in this study call the numerator of this equation as cross-spectrum while others call it as cross-spectral density. A cross-spectrum is defined as the cross-spectral density multiplied by the frequency resolution associated with the finite Fourier transforms [12]. Having known this definition, units associated with the terms in the frequency domain formulation of sound intensity are checked and it is shown that the term that causes the confusion has to be called as cross-spectrum.

The procedure presented by McGary and Crocker [20] to measure the phase mismatch between measurement channels is not found as practical as the authors have claimed. Moreover, measurement frequency is limited by the cut-off frequency of the duct used and the success of the anechoic termination applied. It should be noted that there is no available method for measuring phase shift error of surface intensity measurements even today. It is possible to measure this quantity only within special measurement environments like anechoic chambers which makes the method impractical.

Even though the literature relevant with the subject in hand is reviewed in this chapter, some of the studies that would help the reader in understanding the subject are reminded within the following sections.

CHAPTER 3

THEORETICAL DEVELOPMENT

3.1 Introduction

This chapter is dedicated both to the derivation of the mathematical expressions that will be frequently used throughout the thesis and the interpretation of the physics associated with the phenomenon in hand. As it has already been mentioned, different vibroacoustical methods will be used to analyze the vibroacoustical behaviour of plates in order to obtain the important knowledge about modal behavior, nearfield and farfield radiation characteristics, vibrational power flow patterns, total radiated sound power and radiation efficiency of plates. After acquiring all these information about the plates, results are going to be available to use in the analysis of the machinery that are made up of plate-like structures as in the case of cars and household appliances. All these information is going to be gathered by using acoustical intensity methods which include both the sound intensity and the surface intensity measurement techniques and the structural intensity method for display of power transmission paths on plates. All of the methods mentioned above will first be defined by looking from the physical point of view and then, mathematical derivations will be given in order to make a strong connection in between physics and the governing mathematics of the phenomenon.

3.2 Sound Intensity

Sound intensity can be defined as the net flow of acoustic energy per unit time crossing unit area at a certain point in the sound field. In the SI system of units, the unit for the sound intensity is W/m^2. The most important property that makes sound intensity to be such an important quantity is that the sound intensity is a vector quantity having both magnitude and direction. This property enables the noise control engineer to extract some critical information about the radiation patterns and radiation efficiencies of structures.

Even though sound intensity is a vector propagating in all three dimensions, normally only the projection of the intensity vector in one direction is measured. This gives sufficient information for sound power calculations and simple source location in diagnostics. In order to explore more complex sound fields, the full three dimensional intensity vector may be measured at different points on a predetermined hypothetical surface covering the sound source of interest.

Acoustic intensity or sound intensity is classified according to the type of physical phenomena involved in the measurement and calculation procedures. If the surface vibration data taken from the vibrating structure along with the sound pressure signal is utilized, the resulting acoustic intensity is referred as the surface intensity. The two-microphone intensity, as the name implies, employs the sound pressure signals from two closely spaced microphones in the determination of intensity vector at a point. It is beyond doubt that the two-microphone intensity method is the most popular method among all other methods that it has made the deepest impression on both the academical and commercial areas. This is of course due to some important advantages that establish the superiority of the method among the others. Most important of these advantages can be listed as follows,

- No restrictions are imposed on the place where the sound intensity measurements are performed, provided that the sound field is stationary.

- Measurements may be performed in the near-field. Near-field measurements improve the signal to noise ratio and require less “free space” about the source under test.
- No restrictions are imposed on shape and size of the hypothetical measurement surface.
- Measurements are not influenced by continuous (but steady) background noise.
- Sound intensity can be used to determine the sound power from various parts of machines in a more practicle and better way.

Some of these advantages are provided by the surface intensity method too. Comparison of these two methods and the physical meaning of the advantages of the two-microphone intensity method will be explained in the following sections.

3.2.1 Principles of Measurement of Sound Intensity

From a more physical point of view, it can be said that in a medium without mean flow, the intensity vector is equal to the time averaged product of the instantaneous pressure and the corresponding instantaneous particle velocity at the same position in space.

$$\vec{I} = \overline{p(t) \cdot \vec{u}(t)} \tag{3.1}$$

The bar seen above indicates time averaging. Intensity can also be written in a definite direction of particle motion r as,

$$I_r = \overline{p(t) \cdot u_r(t)} \tag{3.2}$$

It can be easily realized that the above equation has the well known electrical analogy that the power is equal to the voltage times the current at the same branch of a circuit.

With the inspection of the equations above, it is obvious that one must measure the acoustic pressure with the particle velocity at the same point in space to detect the sound intensity flowing in the direction of measurement.

If the sound field is assumed to be sinusoidal, instantaneous pressure can be seen as in Figure 3.1.

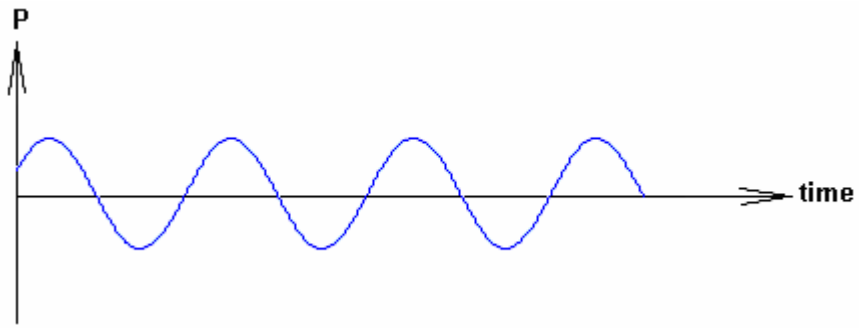

Fig 3.1 Freely Propagating Pressure Wave Constituting the Sinusoidal Sound Field

The particle velocity can also be seen in the form of a sinus wave but actually it can be split up into two components, u^{active} and $u^{reactive}$, where u^{active} is the component that is in phase with the pressure p and $u^{reactive}$ is the component which is 90^{o} out of phase with the pressure p. Active part is associated with the net amount of energy propagating in a sound field while the reactive part is related with the non-propagating part of the energy field. Mostly, active part is the one which is taken into consideration by noise control engineers because only the in-phase particle velocity component, u^{active} will give a time averaged product with pressure which is unequal to zero as shown in Figure 3.2 [1].

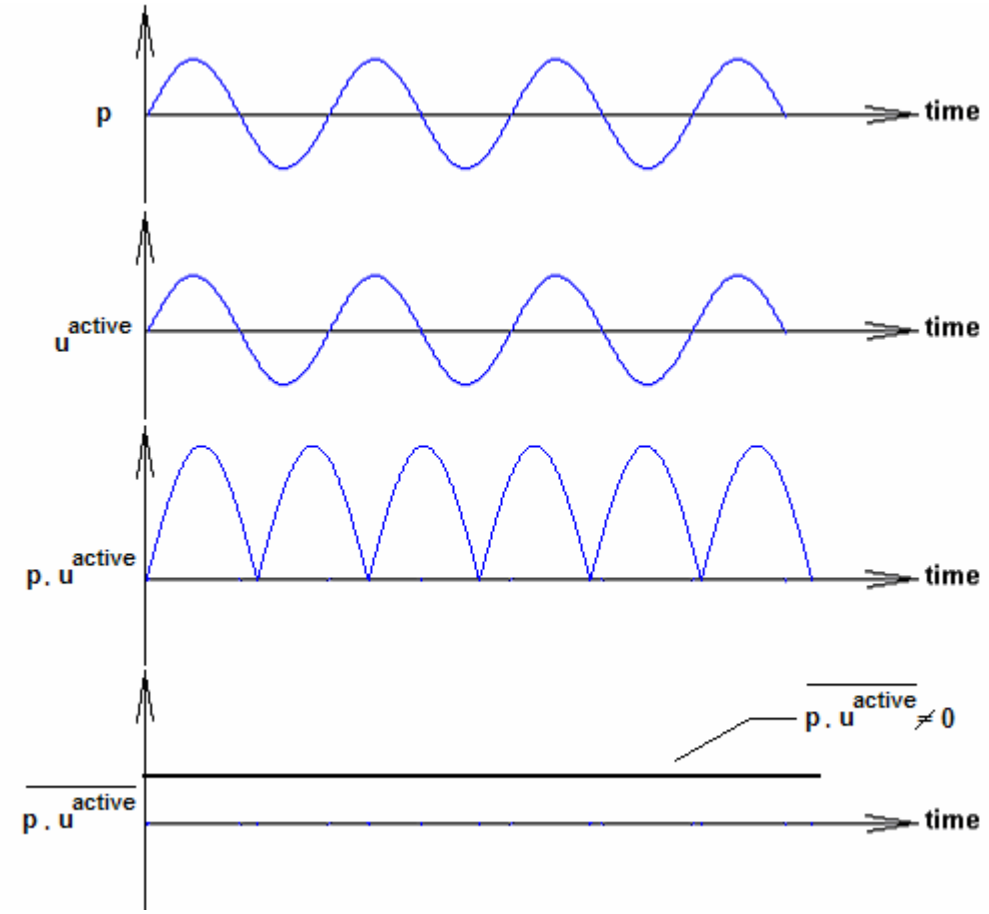

Fig 3.2 Formation of the Active Part of the Sinusoidal Sound Field

Measurement of the active part of sound fields gives the ability of sound source location, sound power and radiation efficiency determination and ranking of the sound sources in order to find the most critical ones. In the meanwhile, measurement of reactive part of sound fields informs us about the near-field radiation patterns, i.e energy circulation paths just above a vibrating object which enlightens the way to learn about the efficiency of transformation of the vibrational energy to the acoustical energy and how it is originated.

It has just mentioned that the particle velocity with the associated pressure at the same point must be measured. It is straightforward to measure the acoustical pressure, but direct measurement of the particle velocity is not as easy as to measure the pressure at the same point in space. The Euler Equation is employed to

calculate the particle velocity. It is the equation which is used to relate the particle velocity to the pressure gradient in a fluid flow and it is based on Newton's second law of motion, basically force is equal to mass times acceleration and can be written as,

$$\rho_o \cdot \frac{\partial \vec{u}}{\partial t} = -\text{grad } p \tag{3.3}$$

where ρ_o is the density of air. In a definite direction r, we can write the same equation as,

$$\rho_o \cdot \frac{\partial u_r}{\partial t} = -\frac{\partial p}{\partial r} \tag{3.4}$$

Knowing that the pressure gradient is proportional to the particle acceleration, the particle velocity can be obtained by just integrating the pressure gradient with respect to time,

$$u_r = -\frac{1}{\rho_o} \cdot \int \frac{\partial p}{\partial r} dt \tag{3.5}$$

At this point, the finite difference method is used to approximate the pressure gradient from two closely spaced microphones located with a small distance in between to sample the pressures, p_1 and p_2. Then, the pressure difference p_2-p_1 is divided by the distance Δr between the two transducers to estimate the particle velocity component u_r in the direction r as,

$$u_r = -\frac{1}{\rho_o \cdot \Delta r} \cdot \int (p_2 - p_1) \cdot dt \tag{3.6}$$

Finite difference approximation is valid for this application as long as the distance between two transducers, Δr, is small enough when compared with the wavelength λ of the soundwave of interest in the measurement.

The approach mentioned above is related only with the two-microphone sound intensity measurement method. Yet, there is another method of transducing sound intensity which requires the use of only one microphone and a particle velocity transducer. The former method is called as the p-p method and the latter is called as the p-u method. Their names arise from the abbreviations of the pressure (p) transducers and the particle velocity transducer (u) employed to form the probes used in transducing the sound intensity. Both methods are discussed and compared below.

3.2.2 Methods used in the Transduction of Sound Intensity

As it is mentioned above, there are two different methods used to transduce sound intensity. Both methods aim the same thing i.e., to measure the instantaneous pressure and the particle velocity associated with the same point in space, but they differ in the transducer types they accommodate.

In the p-u method, pressure signal that comes from the microphone is multiplied by the velocity signal that comes from the particle velocity transducer to find the sound intensity in the direction of the probe axis. Currently there are two kinds of commercially used p-u probes. One of them combines a condenser microphone with an ultrasonic particle velocity transducer[2]. Two parallel ultrasonic beams are sent in opposite directions and their arrival time to their destination deviates from the expected value because of the convection of the ultrasonic waves by the oscillatory air movement. The phase difference of these two ultrasonic beams is used to determine the particle velocity in front of the condenser microphone. It is very important to coincide the point that the particle velocity is measured with the acoustical center of the condenser microphone. Another important point is that the diffraction effects of the probe should be

minimized by taking these effects into consideration during the design stage. There is always a phase mismatching problem due to the use of a probe consisting of two transducers which are based upon entirely different physical mechanisms of transduction. This phase difference between the phase responses has to be compensated electronically. Moreover, each p-u pair produced has to be compensated individually. This causes the production to be more expensive than the expected. Although calibration of the microphone is straightforward, calibration of the particle velocity transducer is a little bit elaborating. It may be calibrated in a spherical progressive sound field against a pressure measurement and the fundamental equation $u = p / \rho_o.c$ is utilized.

Second type of p-u probe is the so-called Microflown which is a relatively new probe invented at the University of Twente at 1994. An acoustical flow measurement sensor called as Microflown and based upon the principles of micro fluid flow sensor is integrated with a conventional type condenser microphone to measure the sound intensity. In fact, Microflown consists of temperature sensors which are implemented as platinum resistors powered by an electrical current dissipating an electrical power causing the resistors to heat-up [3]. An increase in temperature of the sensor causes an increase in electrical resistance as well. Nominal temperature of the sensors stays between 200 $^{\circ}$C and 400 $^{\circ}$C if the particle velocity is zero at the measurement time and all of the heat produced by the sensors are dissipated to the surrounding air. When particle velocity is present, it affects the temperature distribution around the resistors in a different fashion and this difference in the temperature distribution determines the quantitative value of the particle velocity. Its calibraton is usually made by using a standing wave tube since the acoustical impedance is very well understood in the tube and may be used practically. Even though this probe promises hope to the specialists of the field, it is still under development and not in widespread use as the p-p type probes.

These types of probes have some advantages and disadvantages when compared with the widespread p-p type probes. Most important advantages are that the broadband measurements can be made at once and phase-mismatch is not very critical, especially, for normal sound fields. They are suitable for near-field

measurements, too. In contrast, the most important disadvantages of p-u probes are that its measurement takes far much time relative to the calibration of a p-p probe and it is not a standardized method [3].

Figure 3.3 Microflown Type Probe

A standart p-p type sound intensity probe consists of two identical pressure transducers which are combined in such a way that the diffraction effects are minimized. For measurements in air, condenser microphones are used whereas for underwater applications hydrophones are used. Two microphones are placed together in many different configurations before like ‘face-to-face’, ‘side-by-side’, ‘tandem’ and ‘back-to-back’ configurations. The most popular and superior ones are the ‘face-to-face’ and ‘side-by-side’ configurations and they are schematically given below.

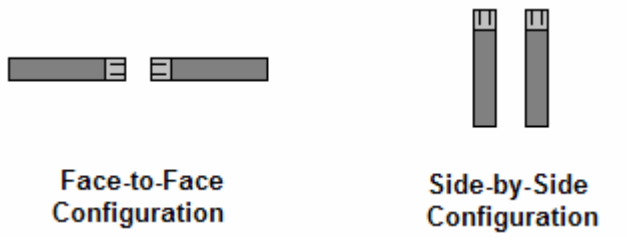

Fig 3.4 Schematical Presentation of Two Types of the P-P Probe Configurations

Even though both configurations are widely used, face-to-face configuration is the one preferred in commercial market, especially for testing and labelling of the appliance/machinery produced. Also, they have a better phase response especially at high frequencies [4]. A p-p type sound intensity probe with a face-to-face configuration is shown below.

Figure 3.5 P-P Type Sound Intensity Probe (B&K Type 3595)

A solid spacer is used between the two microphones which enables both the adjustment of the microphone separation distance Δr and suppression of the unwanted diffraction effects. Another advantage of this type of intensity probe is the practical and easy calibration procedure which provides an important amount of time consumption.

Sound intensity probes which have a side-by-side microphone configuration are frequently used in the research field. It becomes possible to have a knowledge about the near-field radiation characteristics of vibrating objects because it may be placed very close to radiating surfaces. Yet, it has the disadvantage that the

microphones shield each other [5]. Shielding means that one microphone may cause diffraction and cause the other microphone not to receive the net signal. This shielding phenomena creates a relatively sound-free field which is frequently known as ***acoustical shadow*** in acoustics. An intensity probe having a side-by-side configuration which is designed by the author and manufactured at the Department of Mechanical Engineering of METU is shown below.

Fig 3.6 An Intensity Probe Having a Side-By-Side Configuration

This probe is made up of brass and it allows the microphone separation distance to be adjusted. It is used for the preliminary measurements of sound intensity and the results were promising in one direction only. In fact, this probe can be easily mounted so that it can be rotated about its axis of symmetry for field performance checks. Moreover, microphones may accommodate windscreen which is necessary for outdoor use for the sake of suppressing the effect of mean flow.

It does not matter whether its configuration is side-by-side or face-to-face, the principle of transducing sound intensity is the same for all of the configurations of a p-p type intensity probe. As it is aforementioned in Section 3.2.1, pressure at the acoustical center of the sound intensity probe is easy to find. It is just the arithmetic mean of the two pressure values measured at the front of each microphone used and can be calculated as follows,

$$p(t) = \frac{p_2(t) + p_1(t)}{2} \tag{3.6}$$

In the adopted literature used in this study, p_2 is the pressure transduced at the microphone that is closer to the source and p_1 is the pressure transduced by the further microphone. The problem of transduction of particle velocity is solved by using the finite difference technique. Using Equation 3.6, particle velocity is estimated for the acoustical center of the probe again and it is shown in the below scheme.

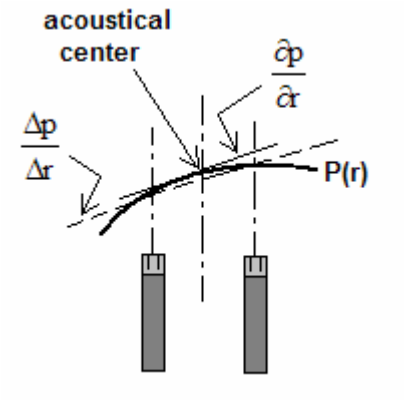

Fig 3.7 Illustration of the Finite Difference Approximation

The logic is simple. The sound field is sampled at two different, but close points by using two identical transducers which should have almost the same phase responses. These samples are used to estimate the acoustical pressure and the particle velocity associated with the point which is called as the ***acoustical center*** of the probe.

Up to this point, everything was just related with the sampling of the sound field and the physics behind the theory, but it is only the starting point to measure the sound intensity. The sampled signal must be processed to find a quantity which is meaningful both mathematically and physically. This duty is achieved by the signal processing methods.

3.2.3 Signal Processing Procedures Employed

There are mainly two different approaches to process the signals sensed by the transducers. First one is the ***Direct Method*** and it is based on the direct filtering technique. The sound intensity is calculated in r direction using the equation given below.

$$\vec{I}_r = \overline{p \cdot u_r} = \frac{1}{2 \cdot \rho_o \cdot \Delta r} \cdot \overline{(p_2 + p_1) \cdot \int (p_1 - p_2) \cdot dt} \qquad (3.7)$$

This is the time domain formulation of sound intensity and it can be implemented by analogue as well as digital techniques. There are many possible means to implement the technique, but it is measured by using a real-time sound intensity meter with 1/3 octave digital filters and it has a working principle modeled by the block diagram below.

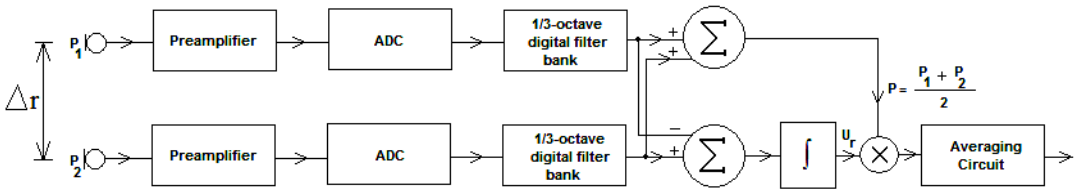

Figure 3.8 Direct Method Employed by a Real-Time Sound Intensity Meter

The second method which is commercially available is the so-called ***Indirect Method*** and it is based up on the FFT (Fast Fourier Transform) technique. Simply, a dual channel FFT Analyzer is adequate for the calculation of intensity but within the limitations of the technique used. After the simultaneous but independent studies of F.J. Fahy [6] and J.Y. Chung [7] and the incredibly fast

development of the digital signal processing techniques, practicle and efficient use of the FFT-based sound intensity analysis methods became possible. Both direct and indirect methods can be used independently as well as in an integrated manner to benefit from the different advantages of both techniques. For example, it is more time consuming to do the same octave band analysis with same random error level using the indirect method relative to the direct method. In the direct method, data is obtained anyway in octave frequency bands, so there is no need to synthesize the acquired data. Yet, in the indirect method, first product is always a narrow band data which is generated using a finite number of spectral lines dividing the whole frequency range. Each octave band should be formed by a sufficient number of spectral lines which require an independent averaging process made from ensemble data. Each averaging takes a definite time and thus, total time consumed during application of the indirect method is longer. Because of the fact that narrow band data is sampled at some special frequencies to divide it into octave bands, the resolution of the FFT-based technique is always far too coarse when compared with the data directly filtered. Another advantage of the direct method is that it gives a particle velocity output directly and the results may directly be used in the calculation of radiation efficiency, acoustic impedance and some other related quantities.

Even though the direct technique has lots of advantages, FFT-based technique is the most popular one, because of the flexibility of the method due to the increasing speed of the digital equipment used for this kind of analysis. Sound intensity is calculated easily from the imaginary part of the cross-spectrum between the two microphone signals. In fact, it is sufficient to implement this cross-spectral formulation into an FFT-Analyzer. The mathematical derivation of this cross-spectral formulation is given in the following section.

3.2.4 Derivation of the Two-Microphone Sound Intensity Formulation

For a given frequency ω_1 , let the pressure and the particle velocity at a point in the medium be,

$$p(t) = P \cdot e^{-j\cdot(\omega_1 \cdot t+\theta)} \tag{3.8}$$

$$u(t) = U \cdot e^{-j\cdot(\omega_1 \cdot t+\Phi)} \tag{3.9}$$

where u(t) is measured in the direction from the near to the far microphone, and P and U are the peak amplitudes of the harmonic pressure and velocity respectively [8]. Complex notation is used for ease in the mathematical computations. Forming the product $p(t).u^*(t)$, using this complex representation yields,

$$p(t) \cdot u^*(t) = P \cdot U \cdot e^{j(\Phi-\theta)} \tag{3.10}$$

At the same time it is very well known that, one need to determine only the real part of this complex statement because of the reason that only the real (active) part of the intensity transfers net energy from one point to another point in space. Taking the real part, one obtains

$$I = \frac{1}{2} \cdot \mathrm{Re}\left\{p(t) \cdot u^*(t)\right\} \tag{3.11}$$

However, if the Fourier Transform of Equations 3.8 and 3.9 are taken, then the RMS spectra become

$$P(\omega) = \left(\frac{P}{\sqrt{2}}\right) \cdot e^{-j\theta} \cdot \delta(\omega - \omega_1) \tag{3.12}$$

$$U(\omega) = \left(\frac{U}{\sqrt{2}}\right) \cdot e^{-j\Phi} \cdot \delta(\omega - \omega_1) \tag{3.13}$$

If Equations 3.12 and 3.13 are integrated around ω_1, result will be as given by Equation 3.16 for any ω value. Comparing Equation 3.14 with the Equations given by 3.16, it can be easily seen that the intensity as a function of ω can be expressed as it is given by Equation 3.15 below.

$$I = \frac{P \cdot U}{2} \cdot \cos(\Phi - \theta) \tag{3.14}$$

$$I(\omega) = \mathrm{Re}\left\{P(\omega) \cdot U^{*}(\omega)\right\} \tag{3.15}$$

Equation 3.15 is a general result valid for any ω where,

$$P(\omega) = \left(\frac{P}{\sqrt{2}}\right) \cdot e^{-j\theta}$$

$$U(\omega) = \left(\frac{U}{\sqrt{2}}\right) \cdot e^{-j\Phi} \tag{3.16}$$

At this point, expressions for $P(\omega)$ and $U^{*}(\omega)$ in terms of two-microphone measurements are desired. The momentum equation for zero mean flow in a non-viscous fluid is

$$\frac{\partial \tilde{u}(t)}{\partial t} = \frac{-1}{\rho_o} \cdot \nabla p(t) \tag{3.17}$$

The component of velocity in direction r (from near to the far microphone) can be related to the pressure gradient in that direction.

$$\frac{\partial u_r(t)}{\partial t} = \frac{-1}{\rho_o} \cdot \left[\frac{p_2(t) - p_1(t)}{\Delta r} \right] \tag{3.18}$$

The one-sided finite Fourier Transform is defined as,

$$X(\omega) = \frac{1}{T} \cdot \int_0^T x(t) \cdot e^{-j \cdot \omega \cdot t} \cdot dt \tag{3.19}$$

where $X(\omega)$ is complex valued. Taking the transform of Equation 3.18 yields,

$$\frac{1}{T} \cdot e^{-j \cdot \omega \cdot t} \cdot u_t(t) \Big|_0^T + j \cdot \omega \cdot \rho_o \cdot U(\omega) = \frac{-1}{\rho_o \cdot \Delta r} \left[P_2(\omega) - P_1(\omega) \right] \tag{3.20}$$

If a transient acoustic disturbance is entirely contained during $0 < t < T$, then $u_r(0) = u_r(T) = 0$ and

$$U(\omega) = \frac{j}{\omega \cdot \rho_o \cdot \Delta r} \cdot \left[P_2(\omega) - P_1(\omega) \right] \tag{3.21}$$

The pressure p(t) is approximated by the average between $p_1(t)$ and $p_2(t)$. By linearity of Equation 3.19, $P(\omega)$ can be expressed as,

$$P(\omega) = \frac{P_1(\omega) + P_2(\omega)}{2} \tag{3.22}$$

Equations 3.21 and 3.22 are substituted into Equation 3.15 to obtain the acoustic intensity in terms of pressure measurements $p_1(t)$ and $p_2(t)$.

$$I(\omega) = \mathrm{Re}\{\frac{-j}{2 \cdot \omega \cdot \rho_o \cdot \Delta r} \cdot (P_1(\omega) \cdot P_2^*(\omega) - P_1(\omega) \cdot P_1^*(\omega) + P_2(\omega) \cdot P_2^*(\omega) - P_2(\omega) \cdot P_1^*(\omega))\} \tag{3.23}$$

The product of terms $P_i(\omega).P_i^*(\omega)$ is real and will not contribute to the intensity, and therefore

$$I(\omega) = \mathrm{Re}\{\frac{-j}{2 \cdot \omega \cdot \rho_o \cdot \Delta r} \cdot (P_1(\omega) \cdot P_2^*(\omega) - P_2(\omega) \cdot P_1^*(\omega))\} \tag{3.24}$$

Noting that $z_1z_2^*-z_2z_1^* = 2.j.\mathrm{Im}[z_1z_2^*]$ for z_1 and z_2 complex, Equation 3.24 becomes

$$I(\omega) = \frac{\mathrm{Im}\left[P_1(\omega) \cdot P_2^*(\omega)\right]}{\omega \cdot \rho_o \cdot \Delta r} \tag{3.25}$$

The product $P_1(\omega).P_2^*(\omega)$ is just the one-sided cross spectrum between $p_2(t)$ and $p_1(t)$.

$$G_{P_2P_1}(\omega) = P_2^*(\omega) \cdot P_1(\omega) \tag{3.26}$$

Therefore, the two-microphone technique relates the intensity to the one-sided cross-spectrum between microphones 2 and 1 through Equation 3.27.

$$I(\omega) = \frac{\mathrm{Im}\left[G_{P_2P_1}(\omega)\right]}{\omega \cdot \rho_o \cdot \Delta r} \tag{3.27}$$

As it is already mentioned, Equation 3.27 gives only the active part of sound intensity. Active part represents the net amount of energy propagating in a sound field and it is related with the phase gradient of the sound field. Equation 3.27 is in fact the so-called ***"frequency domain formulation"*** of sound intensity and it can be easily implemented to a dual-channel spectrum analyzer. Through such implementation, one can identify and locate the noise sources of the machinery under investigation and find the total sound power output even in the presence of background noise, i.e. in the presence of other working machinery close to the machinery under investigation.

Even though the most useful part is the active part, there is still another part of sound intensity which is an indicator of the non-propagating acoustical power existing especially at the near-field of vibrating surfaces. It is of course the reactive part. It can yield information about the near-field radiation characteristics and energy transfer paths of a vibrating structure. It can also be used to realize the presence of a standing wave if there exists any. Reactive intensity can also be determined by just carrying out the same procedure which is used to determine its active counter-part. The spectral formulation which is employed to determine the reactive part is given below and it can be easily derived by just taking the imaginary part of the Equation 3.10.

$$J(\omega)=\frac{G_{p_1p_1}(\omega) - G_{p_2p_2}(\omega)}{2\cdot\rho_o\cdot\omega\cdot\Delta r} \tag{3.28}$$

Both, Equations 3.27 and 3.28 have been used throughout the experimental part of this study and all of the results found by using these equations are presented in the next chapter.

3.2.5 Errors and Limitations Associated with the Technique

All measurement techniques doubtlessly have some limitations due to the error bounds that should not be overlooked. This is also true for the case of sound intensity measurement using FFT-based cross-spectral technique. This measurement technique employs some approximations like finite difference and Fast Fourier Transform. Moreover, measured data most likely shows a random behavior. In the analysis of random data, one can come across two different types of error. The first one is a haphazard scatter in the results from one analysis to the next of different samples of the same random data, and is called the ***Random Error*** [9]. Random error always exists in the measured data of this type because averaging operation must unavoidably be carried out over a finite number of sample records which are finite in length. The second type of error is a systematic error which is inherent in the process of measuring random data. It is called as the ***Bias Error*** and always appear with the same magnitude and in the same direction from one analysis to the next. A thorough classification of the error types that appear in the measurement of sound intensity is presented below.

1) Bias Errors (Systematic = Inherent Errors)

- Phase mismatch error (low frequency limitation)
- Finite difference approximation error (high frequency limitation)
- Probe diffraction effects
- Calibration errors

2) Random Errors (Non-Systematic Errors)

- Spatial sampling error
- Spectral estimation error

It is the phase difference between the microphones that is measured when the sound intensity is said to be measured. That's why, it is said that the active part of sound intensity is directly proportional with the phase gradient of the sound field as shown in Figure 3.9. The sound wave must propagate so that a phase difference occurs between two close points on the propagation path of the sound wave. This

phase gradient is in fact the proof of energy propagation and the sign of measured intensity depends on the sign of the phase gradient.

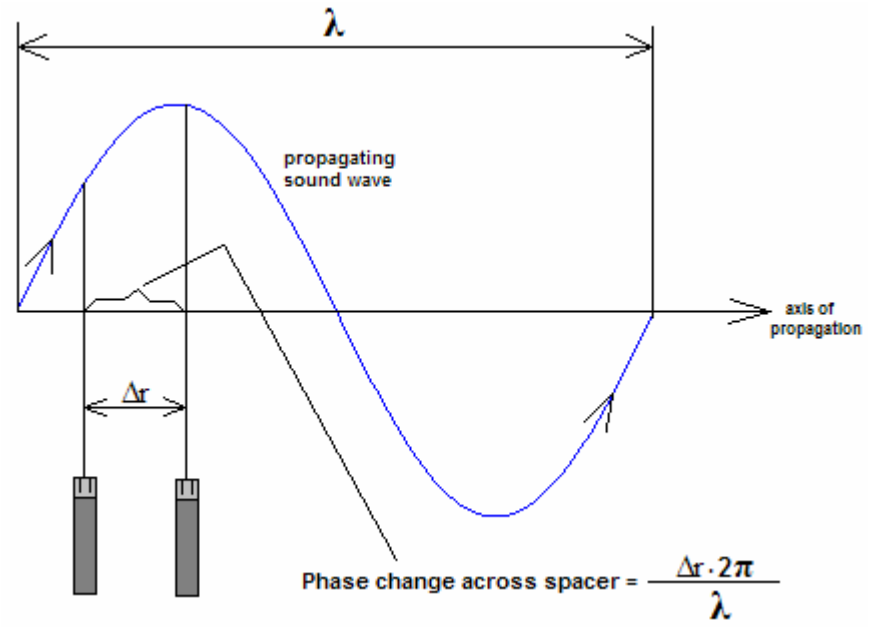

Figure 3.9 Free Field Phase Change over the Microphone Separation Distance

This phase change is also equivalent to the time taken for the wave to propagate over the microphone spacing distance Δr. The time separation must be preserved to measure the correct intensity. However, in all analyzing systems there will be a small time delay between the two channels which introduces a small phase change [10]. This is called as ***Phase Mismatch Error***. Formation of phase mismatch is shown in phasor form in Figure 3.10.

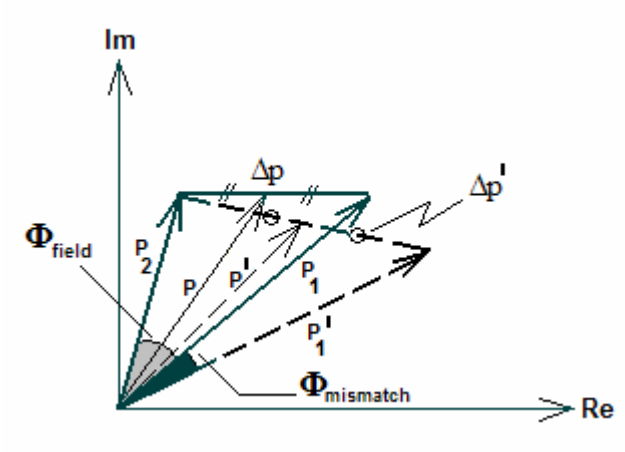

Figure 3.10 Demonstration of the Phase Mismatch Using the Phasor Form

The erroneous pressure P_1' is measured instead of the pressure P_1 due to the phase mismatch inherent in the system. This is the first type of the bias errors and causes a low frequency limitation for the measurement of sound intensity. This limitation arises from the fact that there will be a smaller fraction of a wavelength between the microphones for a low frequency sound wave when compared with a high frequency sound wave, i.e. the probe can sense a smaller free field phase change so that the ratio of the phase angle due to the mismatch to the free field phase change becomes larger, increasing the value of the phase mismatch error. For this reason, there occurs a frequency limitation depending on the microphone separation distance of a probe. Larger microphone separation distances must be used for the measurement of lower frequency sounds. Roughly speaking, the wavelength of the measured sound wave must be at least six times the microphone separation distance to be able to obtain an almost negligible high frequency sampling error. Even though true microphone separation distances are chosen and the ratio of the mismatch phase angle to the normal field phase angle is seen to be low enough, it is still observed a constant value of phase mismatch error related with the nature of the measurement system used. Phase mismatch error is in fact the only error source that can be reliably evaluated and its cancellation is possible. The cancellation method will be explained throughout the next section.

Finite difference approximation error arises from the erroneous choice of the microphone separation distance Δr with respect to the frequency content of the sound measured. As mentioned before, in the determination of the particle velocity, finite difference method is used to approximate the gradient of the sound pressure curve left within the microphone separation distance with a straight line fit between the acoustical centers of the two microphones. If the chosen microphone spacing is larger than it should be with respect to the measured sound of relatively low frequency then the pressure gradient would most probably be approximated erroneously and it is schematically shown in the below figure. This fact introduces a high frequency limitation. Equations are developed which describe the errors in intensity measurements for simple sources such as monopoles, dipoles and lateral quadrupoles and the best procedure is declared to be the selection of measurement parameters based on the quadrupole non-dimensional analysis as a "worst-case" design [11].

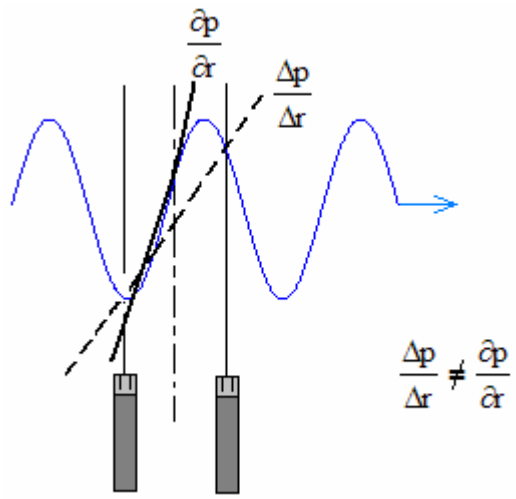

Figure 3.11 Illustration of the Finite Difference Approximation Error

It is recommended to choose the parameters in such a way that they would satisfy the parameter limits given as,

$$0.1 \le k \cdot \Delta r \le 1.3 \qquad \text{and} \qquad 0 \le \frac{\Delta r}{r} \le 0.5 \tag{3.29}$$

At last it can be said that, it has to be assumed that the plane wave form of finite difference error is appropriate and it is found using the below formula.

$$L_{\varepsilon} = 10 \cdot \log\left[\frac{\sin(k \cdot \Delta r)}{k \cdot \Delta r}\right] \tag{3.30}$$

Importance of choosing the appropriate microphone separation distance Δr is easily understood from the above statements and can be schematically summarized by the below figure.

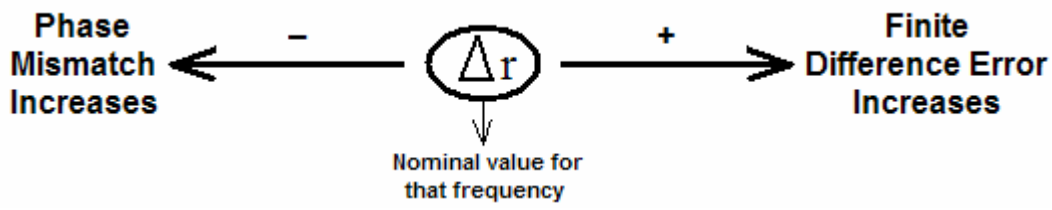

Figure 3.12 Navigator Diagram that Indicates the Boundaries of the Value of Δr

The other two types of bias errors, i.e. probe diffraction effects and calibration errors are generally assumed to have been adequately suppressed.

Spatial sampling error is the first type of random errors and it is a function of the spatial irregularity of the distribution of the normal intensity component over the measurement surface. It can be avoided by using sufficiently large number of measurement points over the measurement surface. In the meanwhile, spectral

estimation error is determined principally by the bandwidth-averaging time product (B_o.T) of the intensity estimate and the coherence between the two microphone signals. Normalized standard deviation E_I of an intensity measurement on random data can be approximated by the formula,

$$E_I \approx c \cdot \frac{1}{\sqrt{B_o \cdot T}} \cdot \frac{P^2}{\hat{I}} \tag{3.31}$$

The standard deviation σ_I of the intensity measurement is then given by Equation 3.32, where B_o is the bandwidth and T is the total averaging time of the intensity estimate and c is a constant.

$$\sigma_I = \varepsilon_I \cdot \hat{I} \approx c \cdot \frac{1}{\sqrt{B_o \cdot T}} \cdot P^2 \tag{3.32}$$

The random error of estimates of intensity associated with the particular signal processing system employed is influenced by the nature of the sound field, through the relative phase of pressure and particle velocity and the degree of coherence between the two transducer signals. In practical measurements, if lengthy computations of coherence are to be avoided, it is necessary to use sufficiently long averaging times to keep the random error within acceptable limits accompanying with the assumption that the extraneous noise is diffuse. As a last word about the errors associated with the sound intensity technique, it is recommended to decrease the bandwidth or increase the averaging time to be able to reduce the bias errors. Even though the B_o.T product corresponding to each spectrum is a constant value, it is possible to increase the overall B_o.T product by averaging over several independent spectra thus effectively increasing the value of T. Again as a rule of

thumb recommendation, the number of averaged samples (N) or the bandwidth (B_o) can be increased to be able to reduce the random errors associated with the measurement.

3.2.6 Elimination of Instrument Phase Mismatch Error

Even though there is no need to make a correction for the phase mismatch of the recently used modern sound intensity measurement systems, it is still necessary to make this correction when the research is carried on with the laboratory equipment and conditions. It is known for a long time that the Equation 3.27 which is used for the calculation of sound intensity is highly sensitive to mismatch error and it should be manipulated to eliminate this type of error. There exist three commonly used correction methods and they will be discussed throughout this section.

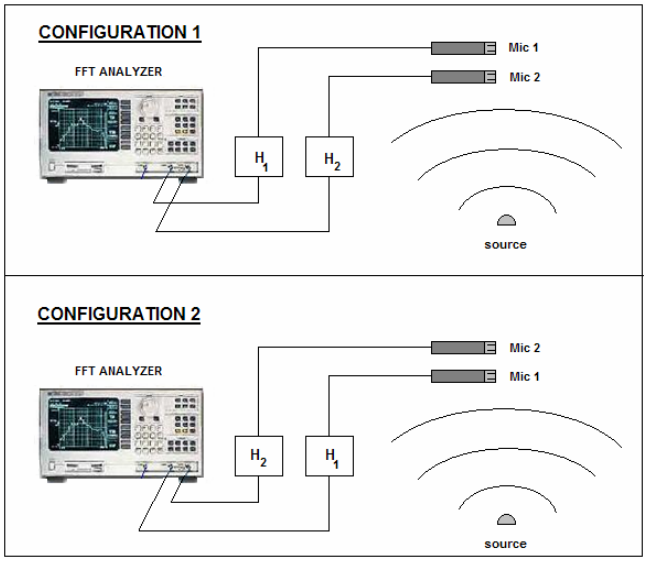

Figure 3.13 Schematic Representation of the Microphone Switching Procedure

Microphone switching method is the first method and it has been proposed by J. Y. Chung in 1978. For the correction of the phase mismatch it is proposed to interchange the measurement positions of the two microphones in space in order to obtain a phase-corrected intensity spectrum. This easy manipulation is schematically shown in Figure 3.13.

In Figure 3.13, H_1 and H_2 are the transfer functions (frequency responses) of the two measuring channels. $\tilde{G}_{12}$ is the cross spectrum measured when the set-up is in the form of configuration 1 and $\tilde{G}_{12}^{sw}$ is the cross spectrum measured after the microphone switching procedure is accomplished, i.e. the set-up is seen like in the configuration 2. Both cross spectra can be expressed as shown below if the instrument transfer functions are taken into account [12].

$$\tilde{G}_{12} = G_{12} \cdot \left(H_1 \cdot H_2^* \right) \tag{3.33}$$

$$\tilde{G}_{12}^{sw} = G_{12} \cdot \left(H_1^* \cdot H_2 \right) \tag{3.34}$$

Multiplying these two equations and rearranging, we obtain the corrected cross spectrum as

$$G_{12} = \sqrt{\frac{\left[\tilde{G}_{12} \cdot \tilde{G}_{12}^{sw} \right]}{\left[\left(H_1 \cdot H_1^* \right) \cdot \left(H_2 \cdot H_2^* \right) \right]}} \tag{3.35}$$

and as a result, the corrected cross spectrum can be written as

$$G_{12} = \frac{\sqrt{\left(\tilde{G}_{12} \cdot \tilde{G}_{12}^{sw}\right)}}{|H_1| \cdot |H_2|} \tag{3.36}$$

It is noteworthy to see that the instrument phase response vanishes. It is well understood that knowledge about the gain factors $|H_1|$ and $|H_2|$ of the measuring channels is enough for the determination of the corrected cross spectrum. Vectorial meaning of this switching procedure can be easily understood by considering Figure 3.9 again. It is in fact the procedure of taking a second measurement with a new vector P_1'. This new vector is symmetric to the first P_1' with respect to P_1 and can be determined by just averaging the two P' phasors to obtain the corrected P value. Returning to Equation 3.36, selection of the proper root is critical as this determines the indicated direction of the intensity vector [13]. For this selection, one or more of the following physical assumptions may be used,

- The sound propagates from a known direction.
- The phase angle of the true cross spectrum is "small", i.e. it lies between $\pm \pi$.
- The phase mismatch is small, hence the true cross spectrum bisects the smaller angle between the two measured cross spectra.

Another method for the correction of the unmatched systems can be said to be the ***transfer function method.*** In this method, the phase and gain mismatch errors are corrected by measuring the transfer function between the two microphone systems exposing them to the same sound (phase and pressure levels) over a wide range of frequencies [14]. Both microphones are mounted on a plate that can be rigidly attached to the end of a duct for which the cut-off frequency is known and is well beyond the highest frequency of the measurement carried on. The transfer function H_{12} between the two channels is then measured and used for correction of all subsequent measurements, since H_{12} contains information of phase and amplitude differences between two channels. The formula given below is used for the determination of the corrected cross-spectrum.

$$G_{12} = \frac{\tilde{G}_{12}}{H_{12} \cdot |H_1|^2} \tag{3.36}$$

Calculations are carried out easily but the determination of the transfer function is a little bit problematic due to the resonances of the duct system used. Transfer function can also be measured by using an acoustical coupler or electrostatic actuators driven with a random excitation [15].

There is a third method for the correction of the phase and gain mismatch of the measurement system in hand. It is called as the ***modified microphone switching method*** and is a compromise between the two methods previously described. This method allows accurate calibration and avoids the additional measurement time and complex square root problems. Using modified microphone switching technique, phase calibration can be performed from a ratio of transfer functions between the microphones (original and switched) exposed to "similar" sound fields. It is only assumed that the sound field is stationary while using this method and there is no limitation at high frequencies. At the first stage (first calibration) the measured quantity is,

$$K_1 = \frac{\tilde{G}_{12}}{\tilde{G}_{11}} = \frac{G_{12} \cdot H_1^* \cdot H_2}{G_{11} \cdot H_1^* \cdot H_1} \tag{3.37}$$

The second calibration with the microphones interchanged gives,

$$\frac{\tilde{G}_{12}^{sw}}{\tilde{G}_{22}} = \frac{G_{21} \cdot H_1^* \cdot H_2}{G_{11} \cdot H_2^* \cdot H_2} \tag{3.38}$$

Or it can be written as,

$$K_2 = \frac{\left(\tilde{G}_{12}^{sw}\right)^*}{\tilde{G}_{22}} = \frac{G_{12} \cdot H_2^* \cdot H_1}{G_{11} \cdot H_2^* \cdot H_2} \tag{3.39}$$

Combining Equations 3.37 and 3.39, one can write

$$\sqrt{\frac{K_1}{K_2}} = \frac{H_2}{H_1} \tag{3.40}$$

When this equation is inserted into the Equation 3.36, instead of H_{12}, gives

$$G_{12} = \frac{\tilde{G}_{12}}{|H_1|^2 \cdot \sqrt{\frac{K_1}{K_2}}} \tag{3.41}$$

Equations 3.36 and 3.41 are directly implemented into Equation 3.27 to determine the corrected sound intensity values.

3.3 Surface Intensity

Surface intensity is the second method of measuring sound intensity which is based upon the FFT technique. It is in fact the method which employs a pressure transducer and a surface vibration transducer. Condenser microphones are used to

transduce pressure and generally an accelerometer is used for the transduction of the velocity of the vibrating surface. Optical probes have also been used for the transduction of the vibration velocity. Yet, a classical non-contact displacement transducer is used for the transduction of the vibration velocity in this study as a distinction from the other methods employed before. Use of the non-contact displacement transducer avoids the mass loading of the transducer that affects the modal behavior of the vibrating sources as it is especially the case when an accelerometer is used for the transduction of the vibration velocity of the relatively light structures. This technique is firstly proposed by Hodgson for source identification and ranking purposes of a centrifugal chiller [16]. He used a combination of an accelerometer and a condenser microphone which is placed in close proximity to the point of vibration measurement. Following the utilization of this probe, attempts are continued to be made to design and utilize some other kinds of probes. Boone designed a fiber optic lever displacement transducer which is a non-contacting probe, too [17]. Another different type of surface intensity probe is the one designed by Driesch and combines a highly sensitive piezoelectric ceramic accelerometer and an inexpensive electric condenser microphone within a common titanium housing [18]. Type of the sensor does not change the objective of the measurement. Pressure and the associated particle velocity is always the goal of this type of measurements. Surface intensimetry is declared to have advantages compared to 2-microphone intensimetry in cases without aerodynamic sources when [19],

- Errors due to absorption in the boundary layer are larger than those due to internal losses
- The radiation efficiency σ shall be determined, or
- There is limited access to the machine surface which does not allow for measurements on an enveloping surface.

3.3.1 Derivation of Microphone / Accelerometer Surface Intensity Formulation

Assume that a(t) is the acceleration signal taken with an accelerometer from a point belonged by the vibrating surface and p(t) is the pressure measured with a condenser microphone which is close to the same point. If the acceleration signal can be decomposed into Fourier components, then, as a function of angular frequency ω, the velocity and acceleration are related as:

$$U(\omega) = \frac{-1}{j \cdot \omega} \cdot A(\omega) \tag{3.42}$$

It can be assumed that the fluid at the surface of the vibrating surface remains in contact with the surface itself. Thus, the surface velocity u(t) will then be equal to the velocity of the fluid particles at the body surface. Substituting Equation 3.42 and the finite Fourier transformed form of the surface pressure p(t) into Equation 3.15, one gets

$$I(\omega) = \mathrm{Re}\left[P(\omega) \cdot \frac{1}{j \cdot \omega} \cdot A^{*}(\omega) \right] \tag{3.43}$$

Dividing and multiplying by the complex number j,

$$I(\omega) = \mathrm{Re}\left[\frac{-j}{\omega} \cdot P(\omega) \cdot A^{*}(\omega) \right] \tag{3.44}$$

Note that $P(\omega).A^{*}(\omega)$ is the one-sided cross-spectrum between the accelerometer and the microphone so that the cross-spectral formulation for surface intensity can be written as,

$$I(\omega) = -\frac{\mathrm{Im}\left[G_{AP}(\omega)\right]}{\omega} \tag{3.45}$$

3.3.2 Derivation of Microphone / Displacement Transducer Surface Intensity Formulation

It is already mentioned that a classical non-contact displacement transducer is used for the transduction of the vibration velocity in this study as a distinction from the other methods employed before. Thus, the formulation relating the displacement history of the point on a vibrating surface and its associated pressure to the intensity will be derived here. If the displacement can be decomposed into Fourier components, velocity and displacement can be related as

$$U(\omega) = -j \cdot \omega \cdot X(\omega) \tag{3.46}$$

Substituting Equation 3.46 and the finite Fourier transformed form of the surface pressure p(t) into Equation 3.15, we get

$$I(\omega) = \mathrm{Re}\left[P(\omega) \cdot j \cdot \omega \cdot X^{*}(\omega)\right] \tag{3.47}$$

$$I(\omega) = \omega \cdot \mathrm{Im}\left[P(\omega) \cdot X^{*}(\omega) \right] \tag{3.48}$$

It is obvious that $P(\omega).X^{*}(\omega)$ multiplication is the cross-spectrum between the pressure and the displacement signals. So, it can be deduced as

$$I(\omega) = \omega \cdot \mathrm{Im}\left[G_{XP}(\omega) \right] \tag{3.49}$$

Thus, one can determine the intensity by just measuring the one-sided cross-spectrum between the signals obtained from the microphone and the non-contact displacement transducer.

3.3.3 Elimination of Phase Mismatch for the Surface Intensity Technique

In general, there are two choices available for the phase mismatch elimination process. The first choice is to measure the total phase between the two channels and then, to measure the field phase that occurs because of the spacing in between the two transducers. The field phase is extracted from the total phase between the channels to obtain the phase mismatch. Once the phase mismatch between the two channels is determined, it is then straightforward to use this phase mismatch value and find the true intensity values for each measurement. The value of phase mismatch is a constant value for a particular measurement system and does not change from one measurement to the other. The second choice is to take a measurement and then, take another measurement with the two channels are totally interchanged. Even though there is no method available that uses the second choice of interchanging the two channels for the phase mismatch elimination, there is one method in literature that utilizes the principle of the first choice mentioned above.

This method is proposed by McGary and Crocker and a simple set-up is used for the measurement of the field phase between the two channels [20]. A circular tubing with an anechoically terminating horn attached at its end is used to guide the plane waves propagating down the length of the tube itself. The horn is used to reduce reflected plane waves that are formed due to the excitation of the air by a rigid circular piston attached to a shaker that is fed with white noise. A tiny accelerometer is fixed on the piston and a microphone is pushed through a cylindrical brass mounting port which is welded to the side of the piston tube. The set-up is schematically shown in Figure 3.14.

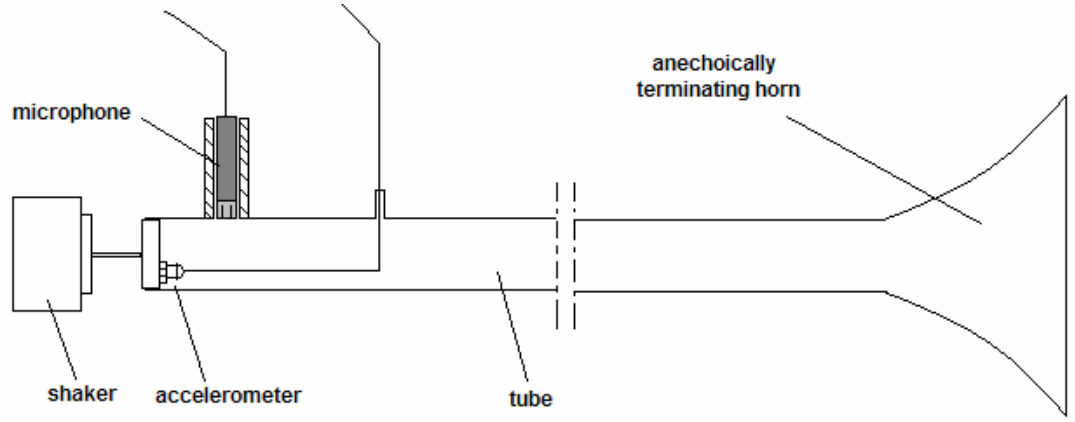

Figure 3.14 Set-up Used for the Determination of the Field Phase Shift

Field phase shift is determined using the set-up shown and it is subtracted from the total phase between the channels. The result is the phase mismatch ϕ and knowing the value of the mismatch, the true intensity can be found by the equation below.

$$\left|\vec{I}\right| = \frac{1}{2\cdot\pi}\cdot\int_0^{\infty}\frac{\left\{\mathrm{Im}\left(G_{pa}(f)\right)\cdot\cos\phi+\mathrm{Re}\left(G_{pa}(f)\right)\cdot\sin\phi\right\}}{f}\cdot df \qquad (3.50)$$

where $G_{pa}(f) / f$ is equal to the one-sided cross-spectral density in this equation and f is the frequency. It can be easily seen that the intensity value is much more related with the imaginary part of the cross-spectrum when the phase mismatch is nearer to zero. Error in intensity caused by this uncorrected phase shift can be calculated in terms of decibels by using Equation 3.51.

$$\mathrm{Err} = 10 \cdot \log \left\{ \cos\phi + \left(\frac{\mathrm{Re}\left(G_{pa}\right)}{\mathrm{Im}\left(G_{pa}\right)} \cdot \sin\phi \right) \right\} \tag{3.51}$$

3.4 Structural Intensity

All mechanical systems have to be supplied with power in order to vibrate. Supplied power causes acoustical and vibrational energy to come out and gives rise to mechanical malfunction of the structure or machinery in some working conditions. This is why, it becomes such critical to understand how the power is delivered to the system, how it flows inside the system and how it is absorbed and removed from the system. To get a better understanding of the power flow inside and outside of the system and the paths of the power flow, the development of measurement methods is very important. In this respect, a practical method called as the structural intensity method which relates the vibratory motion of the structures with the structural power flow inside the same structure is developed. It is a quantity analogous to sound intensity. It is the net energy transmitted through a unit surface but this time the surface is a solid surface differentiating the definition of structural intensity from acoustic intensity. If the surface area of the structure is large compared to an acoustic wavelength, acoustic intensity is a good indicator of dynamic activity. If the area is small compared to a wavelength at the frequencies

of interest then the structural intensity measurement using the vibratory motion on the structure surface may be a good indicator.

3.4.1 Measurement of Structural Intensity

There are mainly two approaches for the measurement of structural intensity. First of them is the method which employs two accelerometers to determine power flow due to flexural waves propagating on surface of the plate. Only kinematic variables are needed to calculate the structural intensity. After Noiseux's influential work [21], Pavic made the subject clearer and showed the necessary procedures for the measurement of structural intensity in some special cases with his essential work [22]. Only flexural waves are considered in his formulations since they are excited easily and often constitute an efficient mechanism for sound radiation.

Two accelerometers are located a distance (Δx) apart on the vibrating surface and measures the projection of the flowing intensity on the line joining the centers of the two accelerometers. Accelerometers may be combined with a magnet that provides a constant separation distance in between them and also used as a mounting method. The configuration shown in Figure 3.15 measures the intensity component flowing in the direction r, i.e. from the accelerometer 1 to 2. The component of intensity at the perpendicular direction to the definite direction of sound propagation r, can be measured by just mounting the probes in a perpendicular direction with respect to their first position. Power flow magnitudes and directions in a plate can also be determined and visualized by measuring the intensity on these two orthogonal directions for a few points on the plate.

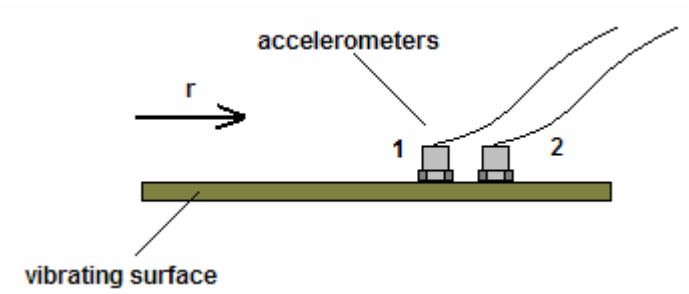

Figure 3.15 Schematical Representation of the Structural Intensity Probe

The second method of determining the structural intensity is the so-called SIMAP (Structural Intensity from the Measurement of Acoustic Pressure) technique. In this method, the pressure measured in a plane close to the vibrating surface is used to reconstruct the normal velocity (both amplitude and phase) on the surface of the vibrating structure [23]. If the normal velocity is reconstructed on a fine enough mesh on the surface of the vibrating surface, then the 2-dimensional structural intensity vector in the vibrating surface can be calculated by finite difference methods. Power delivered to the system and the power absorbed from the system can be calculated from the integral representation of the 2-dimensional divergence of the structural intensity in a vibrating structure. It should be noted that, the SIMAP is regarded within ***Inverse Problem*** formulation methods which are beyond the scope of this study. Derivation of the structural intensity formulation will be shown in the next section for the sake of understanding the functions of the sensors used and the application of the measurement technique.

3.4.2 Derivation of the Structural Intensity Formulation

Power is the rate at which work is done by one system on another system as shown in the below figure.

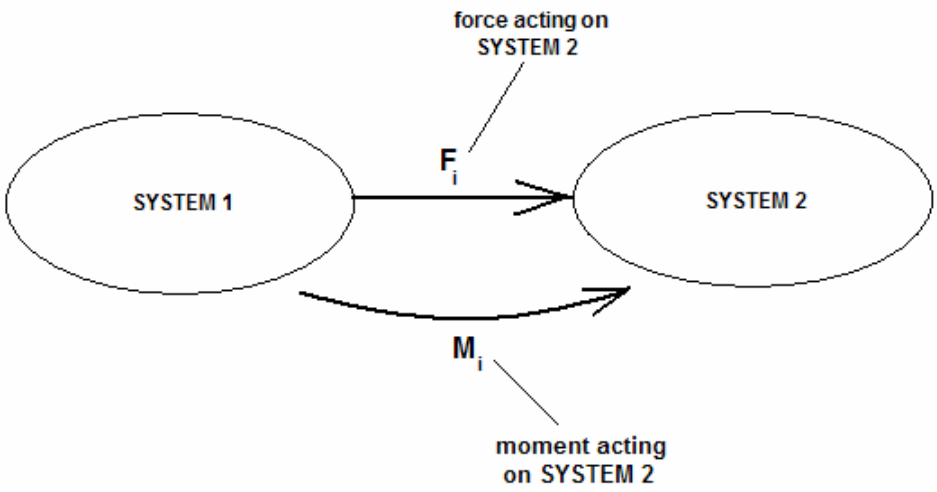

Figure 3.16 Illustration of Power Flow from One System to Another

Here, system 1 acts on system 2 with a force F_i which gives system 2 a resulting velocity V_i and a moment M_i which creates an angular velocity $\dot{\theta}_i$. For vibrating structures the time averaged power is used and it can be expressed as the products of the forces and the moments with their associated velocities which are in the same direction as the forces and the moments applied on the system.

$$\langle P_i \rangle_t = \langle F_i \cdot V_i \rangle_t + \langle M_i \cdot \theta_i \rangle_t \tag{3.52}$$

where $\langle\ \rangle_t$ denotes a time averaging. The flow of power on plates is described by the intensity, i.e. the power per unit width of the plate [24]. The intensity in the x-direction passing through a small cross-section of a plate is transported by the work done by the bending and twisting moments M_x and M_{xy}, and the shear force Q_x as it

is shown in Figure 3.17. Multiplying these inputs by the corresponding translational velocity and the angular velocities and divide by the width Δl of the cross-section, one can find the structural intensity as it is given by Equation 3.53:

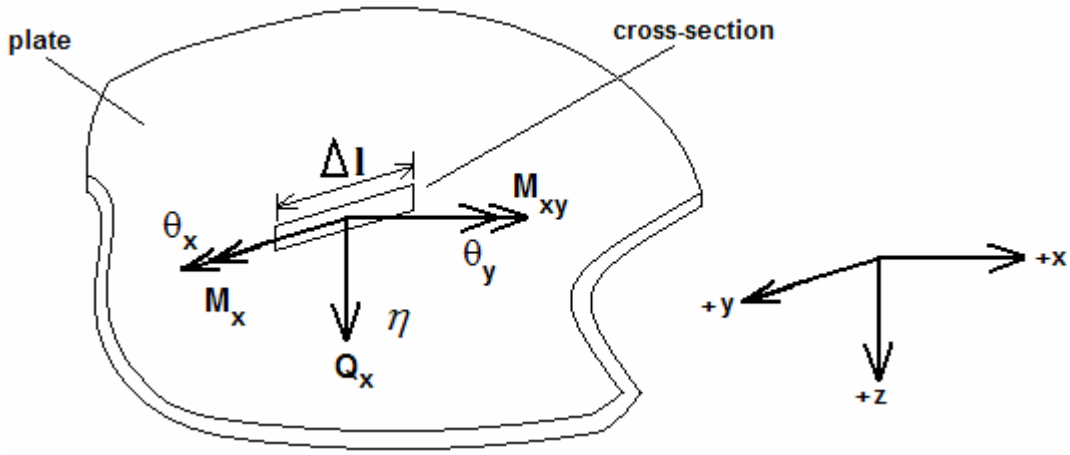

Figure 3.17 Force and Moments Applied on the Cross-Section of a Plate

$$W_x(x,t) = \frac{Q_x}{\Delta l} \cdot \frac{\partial \eta}{\partial t} + \frac{M_{xy}}{\Delta l} \cdot \dot{\theta}_y + \frac{M_x}{\Delta l} \cdot \dot{\theta}_x \tag{3.53}$$

where η represents the displacement of the plate in normal direction (+z) and the angular velocities are given by:

$$\dot{\theta}_x = \frac{\partial^2 \eta}{\partial t \cdot \partial x} \tag{3.54}$$

$$\dot{\theta}_y = \frac{\partial^2 \eta}{\partial t \cdot \partial y} \tag{3.55}$$

The force and the moments can be expressed in kinematic quantities as given below.

$$Q_x = B \cdot \Delta l \cdot \frac{\partial}{\partial x}\left(\nabla^2 \eta\right) \tag{3.56}$$

$$M_x = -B \cdot \Delta l \cdot \left(\frac{\partial^2 \eta}{\partial x^2} + \nu \cdot \frac{\partial^2 \eta}{\partial y^2} \right) \tag{3.57}$$

$$M_{xy} = -B \cdot \Delta l \cdot (1-\nu) \cdot \frac{\partial^2 \eta}{\partial x \cdot \partial y} \tag{3.58}$$

where ν is the Poisson's ratio of the plate, ∇^2 is the two-dimensional Laplace operator and B is the flexural (bending) stiffness per unit width of the plate and it is expressed as [25] :

$$B = \frac{E \cdot h^3}{12 \cdot \left(1-\nu^2\right)} \tag{3.59}$$

In this equation, E represents the modulus of elasticity and h is the height of the cross-section of the plate shown in Figure 3.17. Substituting and rearranging Equations 3.54 to 3.58 into Equation 3.53, one can obtain the expression for structural intensity.

$$W_x(x,t) = B \cdot [\frac{\partial}{\partial x}(\nabla^2 \eta) \cdot \frac{\partial \eta}{\partial t} - \left(\frac{\partial^2 \eta}{\partial x^2} + \nu \cdot \frac{\partial^2 \eta}{\partial y^2}\right) \cdot \frac{\partial^2 \eta}{\partial x \cdot \partial t} - (1-\nu) \cdot \frac{\partial^2 \eta}{\partial x \cdot \partial y} \cdot \frac{\partial^2 \eta}{\partial y \cdot \partial t}] \quad (3.60)$$

Assuming that flexural waves can propagate in one direction only (e.g., as in the case of a beam) and this direction coincides with the x-axis, Equation (3.60) reduces to:

$$W_x(x,t) = B \cdot \left[\left(\frac{\partial^3 \eta}{\partial x^3}\right) \cdot \frac{\partial \eta}{\partial t} - \left(\frac{\partial^2 \eta}{\partial x^2}\right) \cdot \frac{\partial^2 \eta}{\partial x \cdot \partial t}\right] \quad (3.61)$$

The wave equation for the case of sinusoidal motion, $\nabla^2(\nabla^2 \eta) - k^4 \eta = 0$ assumes, for a one-dimensional field, a simpler form of $\frac{\partial^4 \eta}{\partial x^4} \propto \eta$ which implies a well-known solution:

$$\eta(x,t) = Re\left\{\left[\bar{A}_+ \cdot \exp(-ikx) + \bar{A}_- \cdot \exp(ikx) + \bar{C}_+ \cdot \exp(-kx) + \bar{C}_- \cdot \exp(kx)\right] \cdot \exp(i2\pi ft)\right\}$$

$$= Re\left\{\bar{\eta}(x,t)\right\} \quad (3.62)$$

This solution represents traveling progressive waves and an exponentially decreasing, phase-conserving near-field (evanescent waves) [22]. Here, k is the wave number. Both progressive waves and evanescent waves are produced because of the boundary conditions applied, but evanescent waves die out within the limits of the near-field belonging to the boundary condition. It should be noted that the

bar above the amplitudes of the waves means that the amplitudes may be complex-valued numbers. Positive and negative going progressive and evanescent waves are illustrated on the below figure.

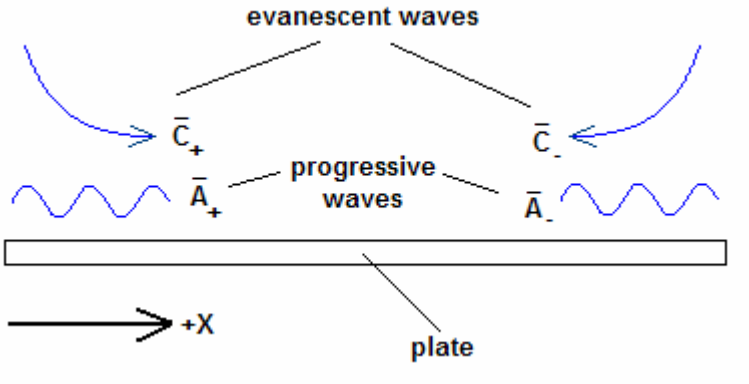

Figure 3.18 Propagating Progressive Flexural Waves and Evanescent Waves

For this case, it is easy to obtain an expression for the averaged intensity in terms of the progressive wave amplitudes A_+ and A_- and near field amplitudes $C_+\exp(-kx)$ and $C_-\exp(kx)$ after substituting Equation 3.62 into Equation 3.61:

$$\left\langle W_x \right\rangle_t = 2\cdot\pi\cdot B\cdot k^3\cdot f\cdot\left[A_+^2 - A_-^2 - 2\cdot C_+\cdot C_-\cdot\sin\left(\Psi_+ - \Psi_-\right)\right] \qquad (3.63)$$

where A_+, A_-, C_+ and C_- are the amplitudes of the waves. Values of the phases can be stated as $\Psi_+ = \arctan\left(\mathrm{Im}\,\bar{C}_+ / \mathrm{Re}\,\bar{C}_+\right)$ and $\Psi_- = \arctan\left(\mathrm{Im}\,\bar{C}_- / \mathrm{Re}\,\bar{C}_-\right)$. Contribution of the evanescent wave amplitudes are small and equal for the near-field measurements and negligible for the far-field measurements, so they can be thought as if they are negligible i.e., the cross-term in Equation 3.63 vanishes for

the far-field measurements. It can be thus concluded that the near-field can be neglected in power flow considerations and the Equation 3.63 reduces to,

$$\left\langle W_x \right\rangle_t = 2 \cdot \pi \cdot B \cdot k^3 \cdot f \cdot \left[A_+^2 - A_-^2 \right] \tag{3.64}$$

The normal velocity can be written as,

$$\frac{\partial \eta}{\partial t} = \mathrm{Re}\left\{ (i2\pi f) \cdot \left[\bar{A}_+ \exp(-ikx) + \bar{A}_- \exp(ikx) \right] \cdot \exp(i2\pi ft) \right\} \tag{3.65}$$

and the angular acceleration can be written as,

$$\frac{\partial^3 \eta}{\partial x \cdot \partial t^2} = \mathrm{Re}\left\{ (2\pi f)^2 \cdot (ik) \cdot \left[\bar{A}_+ \exp(-ikx) - \bar{A}_- \exp(ikx) \right] \cdot \exp(i2\pi ft) \right\} \tag{3.66}$$

The time-averaged product of normal velocity and angular acceleration is found to be,

$$\left\langle \left(\frac{\partial \eta}{\partial t} \right) \cdot \left(\frac{\partial^3 \eta}{\partial x \cdot \partial t^2} \right) \right\rangle_t = \frac{1}{2} \cdot (2\pi f)^3 \cdot k \cdot \left(A_+^2 - A_-^2 \right) \tag{3.67}$$

From the comparison of Equations 3.67 and 3.64, one can obtain the below equation for the intensity of sinusoidal flexural waves:

$$\left\langle W_x \right\rangle_t = \left(\frac{2 \cdot B}{c_f^2} \right) \cdot \left\langle \left(\frac{\partial \eta}{\partial t} \right) \cdot \left(\frac{\partial^3 \eta}{\partial x \cdot \partial t^2} \right) \right\rangle_t \tag{3.68}$$

where $c_f = 2.\pi.f / k$ is the flexural phase velocity. Applying the finite difference approximation, two transducers 1 and 2, spaced symmetrically about the point x_o where the intensity is measured at a distance Δx, will produce signals for estimating the quantity

$$\left\langle \dot{\eta} \cdot \frac{\partial \ddot{\eta}}{\partial t} \right\rangle_t \simeq \left\langle \frac{\dot{\eta}_1 + \dot{\eta}_2}{2} \cdot \frac{\dot{\eta}_1 - \dot{\eta}_2}{\Delta x} \right\rangle_t = \frac{\left\langle \ddot{\eta}_1 \cdot \dot{\eta}_2 \right\rangle_t}{\Delta x} \tag{3.69}$$

and finally

$$\left\langle W_x \right\rangle_t \simeq \left(\frac{2 \cdot B}{\Delta x \cdot c_f^2} \right) \cdot \left\langle \ddot{\eta}_1 \cdot \dot{\eta}_2 \right\rangle_t = \frac{\sqrt{B \cdot m}}{\Delta x \cdot \pi \cdot f} \cdot \left\langle \ddot{\eta}_1 \cdot \dot{\eta}_2 \right\rangle_t \tag{3.70}$$

Here, m is the mass per unit area of the plate. It can be concluded from Equation 3.70 that by averaging the acceleration and the velocity at two closely spaced points in the direction of the power flow, one can determine the value of the net intensity flowing from transducer 1 towards transducer 2. The net value of structural intensity in y-direction can be calculated by mounting the transducers along the y-axis and using Equation 3.70 by replacing x with y only.

Equation 3.70 is the time-domain formulation for structural intensity measurements on a plate's surface. It involves an averaging of the product of two measured signals in the time-domain with switched channels. Even though the time-domain formulation is declared to be succeeded in measurements, a frequency domain formulation is obviously needed for quick and easy measurement of

structural intensity. Frequency domain formulation of structural intensity is developed and explained below. Equation 3.70 can also be written in terms of two acceleration signals as,

$$\langle W_x \rangle_t \simeq \frac{\sqrt{B \cdot m}}{\Delta x \cdot \pi \cdot f} \cdot \left\langle a_1 \cdot \int a_2 d\tau \right\rangle_t \tag{3.71}$$

Frequency domain equivalent of the time-averaged quantity in Equation 3.71 is given as [26],

$$\left\langle a_1 \cdot \int a_2 d\tau \right\rangle_t \overset{f}{=} \frac{1}{2 \cdot \omega} \cdot \mathrm{Im}\left[a_1^*(f) \cdot a_2(f) \right] \tag{3.72}$$

Definition of the cross spectrum is given as [9],

$$G_{a_1 a_2}(f) = 2 \cdot E[a_1^*(f) \cdot a_2(f)] \tag{3.73}$$

where E[ ] represents an expected value operation. First implementing Equation 3.73 into Equation 3.72 and then Equation 3.72 into Equation 3.71 and rearranging, one can end up with the frequency domain formulation of the structural intensity as given below.

$$W_x(f) \simeq \frac{2 \cdot \sqrt{B \cdot m}}{\Delta x \cdot \omega^2} \cdot \mathrm{Im}[G_{a_1 a_2}(f)] \tag{3.74}$$

If the measurement system is treated as a single-input/multiple-output system where the forcing applied by the shaker is assumed to be the input and the two acceleration signals measured by the accelerometers are assumed to be the two outputs of the system as shown on the below figure, Equation 3.74 can be decomposed into Equation 3.76 by using the relation given in Equation 3.75 [9].

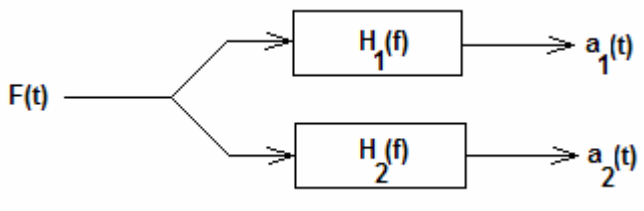

Figure 3.19 Modeling the System as a SI/MO (Single Input/Multiple Output) System

$$G_{a_1 a_2}(f) = H_1^*(f) \cdot H_2(f) \cdot G_{FF}(f) \tag{3.75}$$

$$W_x(f) \simeq \frac{2 \cdot \sqrt{B \cdot m}}{\Delta x \cdot \omega^2} \cdot \mathrm{Im}[H_1^*(f) \cdot H_2(f) \cdot G_{FF}(f)] \tag{3.76}$$

where H_1 and H_2 are the complex frequency response functions between linear accelerations at positions 1 and 2 respectively, with respect to the reference force F and G_{FF} is the auto-spectrum of the reference force signal.

3.4.3 Elimination of Errors Associated with the Structural Intensity Technique

In general, there are two types of errors that are of great importance and can be eliminated. They are the finite difference error and the instrument phase mismatch error. The equations on the actual structural intensity should be corrected for finite difference error so that the corrected expression becomes [27]:

$$W_{x_{actual}} = W_{x_{measured}} \cdot \left[\frac{k \cdot \Delta x}{\sin(k \cdot \Delta x)} \right] \tag{3.77}$$

For the measurement of structural intensity with the two-accelerometer technique, a theoretical formula is used to find the wave number k as given below,

$$k = \sqrt{\frac{m \cdot \omega^2}{B}} \tag{3.78}$$

Phase mismatch errors can be eliminated by using the sensor (accelerometer) switching technique and taking the average value as the true intensity value as it was the case in the 2-microphone sound intensity measurement.

3.5 Sound Power Level and Radiation Efficiency

A principal application of the direct measurement of sound intensity is determination of sound power radiated by a machine installed in-situ. The sound intensity method allows sound power determinations to be performed even in the

presence of stationary background noise. Radiated sound power can be determined from intensity measurements on a suitable hypothetical (imaginary) surface enclosing the source because the intensity describes the power passing through a unit area.

$$W=\int\int_S \vec{I}\cdot d\vec{S}=\int\int_S I_n\cdot dS \tag{3.79}$$

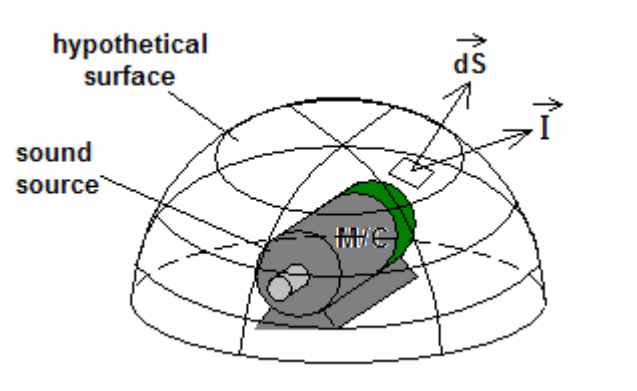

Figure 3.20 Hypothetical Surface around the Sound Source

The integration of the intensity component normal to the surface (I_n) over the aforementioned hypothetical surface will directly give the sound power of the source, W. Logarithm of the sound power of a source with respect to the reference value $W_{ref}=10^{-12}$ Watt gives the sound power level of the source. However, in practice, the sound power is often calculated using,

$$W\cong\sum_{p=1}^{n}\vec{I}_p\cdot(\Delta S)_p \tag{3.80}$$

where p is the number of discrete measurement points on hypothetical surface. If n tends to approach infinity, then Equations 3.79 and 3.80 will be equal to each other.

Another way of making both equations equal to each other, in practice, is to scan the intensity probe continuously around the measurement location over the hypothetical surface. During the scanning process, the probe is continuously traversed over the surface enclosing the source at a constant rate by hand or by the help of a controllable robot manipulator. Both methods of measuring intensity mentioned above are called as the ***discrete point measurement method*** and the ***scanning method***, respectively. Example arrangements of measurement points for the discrete point measurement method and sweeping path of the probe for the scanning method are shown schematically on the figure below.

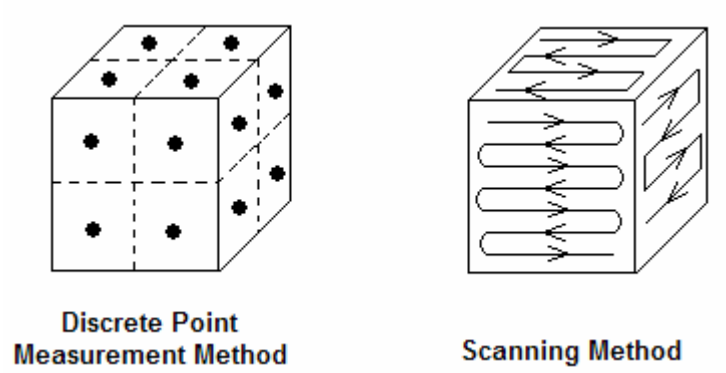

Figure 3.21 Measurement Points and Paths on the Hypothetical Surface

Both methods are suitable for determining sound power level of sources, but they differ from each other by some measurement characteristics. Even though it is possible to measure sound power levels in a faster and reliable manner by the scanning method, it does not allow measuring intensity vectors and near-field identification of sources. Scanning method is mathematically a better approximation to the continuous space integral, consequently it is often more accurate. But care needs to be taken to sweep the probe at a constant speed and to cover the surface equally [10]. For discrete point measurements, repeatability is high, but closely spaced points are needed for an irregular sound field. Discrete point measurement method is used throughout this study because it is more suitable

for an academic study which includes the measurement of intensity vectors, near-field intensity mapping and determination of sound power level at the same time.

Sound power level information is useful for the following purposes [28]:

- It allows comparison of the noise-producing properties of different machines
- It allows verification that the noise produced by a particular machine meets specifications for noise-control purposes
- It provides a means for predicting expected noise levels in reverberant spaces and in the free field when directivity information is also known.

Nowadays, it is more frequently used for labeling and comparison of machinery by the manufacturers. They need a reasonable quantity which can be quickly and easily measured and sound power level is the most suitable one for these purposes. Because it can be measured in situ or on the production line, sound intensity is the most popular way of measuring sound power levels of machinery for manufacturers and noise control engineers. As it is mentioned before, sound intensity method allows sound power determinations to be performed in the presence of stationary background noise. This can be explained by a result of the Gauss' Theorem. The total intensity, I, leaving the surface which encloses the sound source multiplied by the area of the surface yields the sound power of the source.

When the source is situated outside the closed hypothetical surface, the total intensity leaving the closed surface is zero. Mathematically,

$$\int_S \vec{I} \cdot \vec{dS} = 0 \tag{3.81}$$

For this situation of the source, one will always measure some energy flowing in on a side of the hypothetical surface but the energy will flow out on other sides of the closed surface. Consequently the contribution to the sound power radiated from the closed surface will be zero. This phenomenon is schematically shown below.

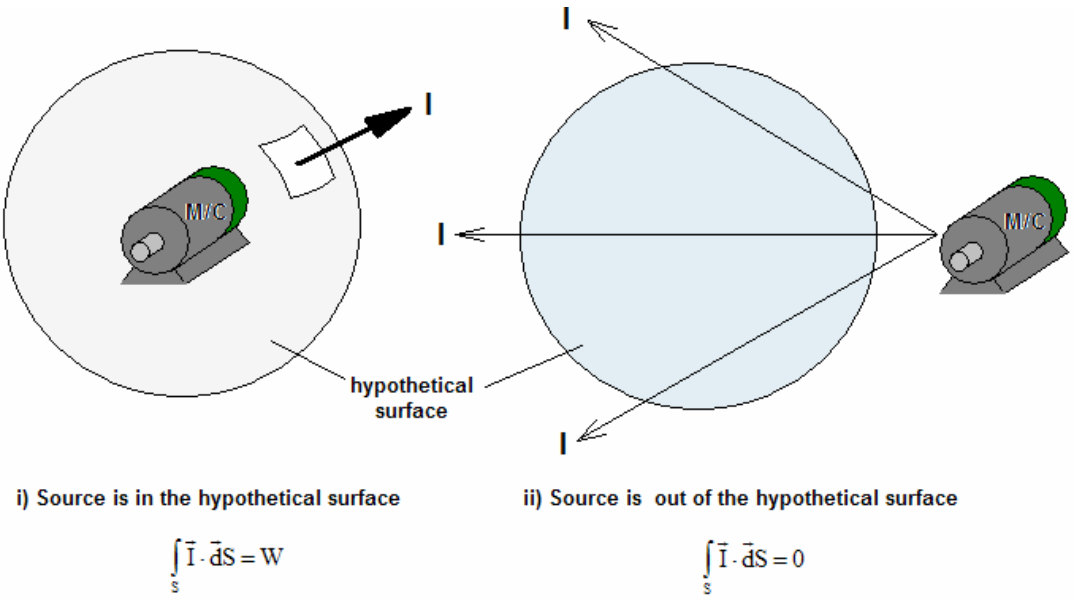

Figure 3.22 Schematical Illustration of the Importance of Location of Source

When employing this physical result of the Gauss' Theorem in practice, one must ensure that there is no mean flow of the air, that there is no absorption within the closed surface and that noise from external sources is stationary during the measurements.

The hypothetical surface used throughout the measurements may be of any shape as long as it can be reasonably divided into imaginary partitions. It is important to note that there are two important statements that apply to sound intensity measurements [29]. They are:

- The space averaged sound power radiated by a source is independent of the shape and size of the enclosing surface defined around the source.
- The net sound power radiated by a collection of sources is the sum of the sound powers radiated by the individual sources provided they are uncorrelated broad band noise sources without pure tones.

Another vital benefit of the sound power knowledge is that it allows the radiation efficiency of a vibrating structure to be determined. Radiation efficiency

is the best tool to master the link between vibrational behavior and the noise radiated and it measures the ability of a sound source to radiate sound in comparison to an ideal plane wave radiator. Ideal plane wave radiator has a radiation efficiency value of 1 as a reference value. In order to determine the radiation efficiency of a vibrating surface, it is necessary to determine separately the radiated sound power and the space-averaged mean square normal vibration velocity of the surface.

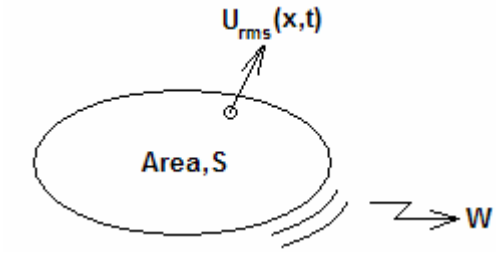

Figure 3.23 An Arbitrary Vibrating Object

The relationship between sound power and radiation efficiency is given by the below equation:

$$\sigma = \frac{W}{\rho_o \cdot c \cdot S \cdot \left\langle U_{rms}^2 \right\rangle_{s,t}} \tag{3.82}$$

Note that the vibration velocity U in Equation 3.82 is a both space and time averaged quantity. S is the total area of the vibrating surface, c is the speed of sound and ρ_o is the density of the medium as it has already been mentioned. It shall be found that radiation efficiency is affected by the geometry and boundary conditions of the structure and by the structural dynamics, i.e. the kinds of modes of vibration that exist in the machine structure [30]. Radiation efficiency is utilized for the investigation of the radiation characteristics of vibrating plates throughout

this study and the results supported the information obtained before that, plates radiate in a poor fashion at frequencies under their coincidence (critical) frequency.

CHAPTER 4

MEASUREMENTS AND RESULTS

4.1 Experimentation and Data Acquisition

The experimentation in this study is conducted on a 300 mm x 300 mm steel square plate with a thickness of 1 mm. The critical frequency at which the speed of bending wave propagation is equal to the speed of acoustic wave propagation in the surrounding medium for this particular plate is calculated to be around 13 kHz by using the approximate formula given by Lyon [30]. All of the measurements and the analysis of the resultant data are carried out in the frequency range of 0 and 1600 Hz. It means that the analysis is carried out at subcritical frequencies, i.e the frequencies well-below the critical frequency of the plate.

The plate is excited at its midpoint by a Derritron VP3/3B electromagnetic shaker. HP 35665 A Dynamic Signal Analyzer is used to accomplish to acquire and process data in the analysis. It is also used to generate random or sine swept signals that are fed to the shaker by means of a Derritron TA 300 power amplifier. Two measurement probes are designed and manufactured for the measurement of sound intensity and surface intensity. A general view of the measurement set-up that is built in the Dynamic Systems Laboratory of the Mechanical Engineering Department of METU can be seen in Figure 4.1.

Figure 4.1 Measurement Set-Up in the Dynamic Systems Laboratory

The side-by-side probe configuration is utilized for sound intensity measurements. Two Bruel&Kjaer Type 4165 condenser microphones are put apart at a fixed distance of 18 mm in a plexiglass holder with a special arrangement that keeps the distance between the microphones at a constant value. A wooden manipulator arm is designed as a 3 DOF mechanism so that the probe is integrated in its gripper and it can be easily traversed on all of the possible measurement surfaces. Sound intensity probe and the manipulator arm is shown in Figure 4.2. Bruel&Kjaer Type 2807 power amplifier is used for conditioning of pressure signals sensed by the microphones. Amplitude calibration of the microphones is accomplished using the Bruel&Kjaer Type 4230 Sound Level Calibrator which produces 94 dB at 1000 Hz. Phase calibration and checks are done by using the B&K Type 3541 Sound Intensity Calibrator.

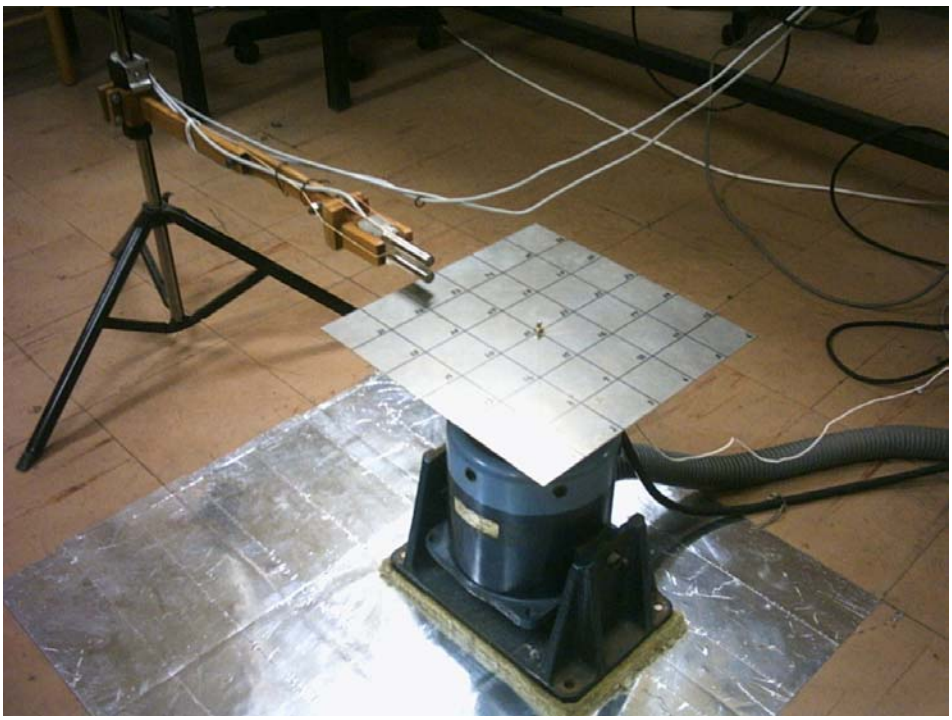

Figure 4.2 The Sound Intensity Probe Integrated to the The Manipulator Arm

It becomes possible to measure the near-field sound intensity and identify the sound energy flow patterns just above the vibrating plate with this type of microphone arrangement as well as the measurement of three dimensional vector intensity. Set-up configuration for the near-field sound intensity measurements is shown in Figure 4.2. The plate is divided into 36 imaginary partitions and intensity is measured at the midpoint of each particular partition. The number of 36 is chosen such that the spatial sampling error is small enough and it helps to map the intensity with enough accuracy. In fact, number of partitions are increased starting from 9 up to 36 and it is observed that there is no considerable change in the results obtained after this number of partitions. Random noise signal is generated by the Dynamic Signal Analyzer and used to vibrate the plate during the measurements. Even though a random signal is fed into the shaker, all of the data is taken and processed between the frequencies of 0 and 1600 Hz. This frequency range is used

because some of the engineering applications that are made-up of plate-like structures, like household appliances, have a working frequency range falling into this range. Sound intensity measurement set-up is schematically shown in Figure 4.3.

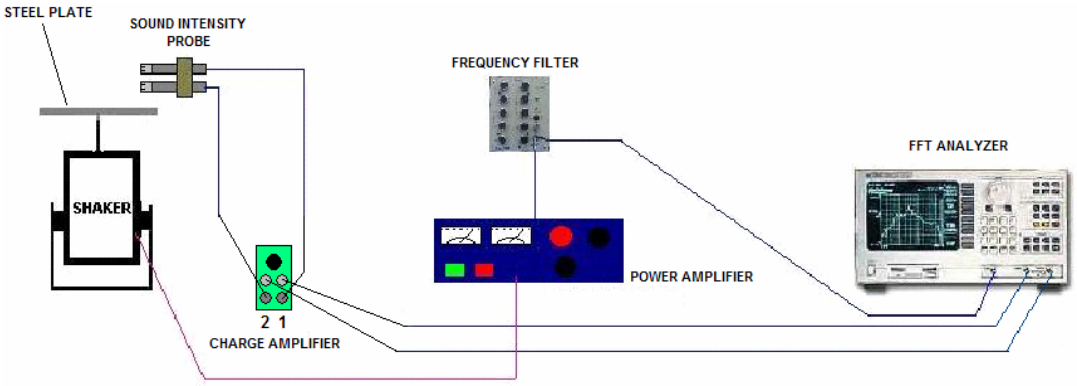

Figure 4.3 Schematical Representation of the Sound Intensity Measurement Set-Up

A box shaped hypothetical surface is used for the measurement of sound intensity when the aim is to find the total sound power radiated by the plate and consequently, the radiation efficiency. The hypothetical surface is a cube with dimensions 365 mm x 365 mm x 365 mm and it is made up of brass frame because of the reason that brass has a low coefficient of sound absorption. There are four different partitioned (meshed) frames that can be assembled onto each particular side of the brass cube. They have 9, 16, 25 and 36 partitions in particular and provide measurements with different spatial averaging. Resolution of intensity maps also changes with the changing number of partitions. The floor is wrapped with an aluminium sheet to avoid the sound waves that impinges upon the floor to be absorbed. The hypothetical surface and sound power measurement procedure is shown in Figure 4.4 below.

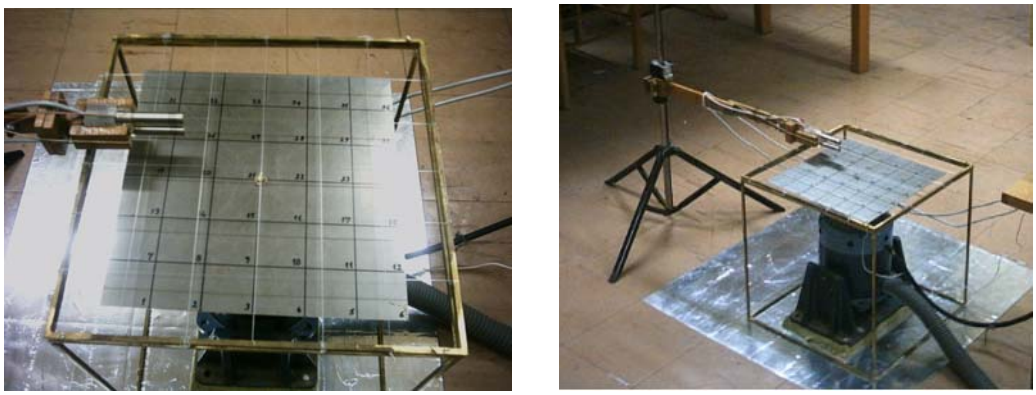

Figure 4.4 Two Different Views of the Sound Power Measurement Set-Up

Lower microphone of the sound intensity probe is used together with an eddy-current, non-contact displacement transducer to measure the surface intensity of the plate. Surface intensity data is taken at the same grid points of the plate as in the case of near-field sound intensity measurement. Non-contact displacement transducer is calibrated with a different technique. The B&K Type 4294 calibration exciter which can supply a constant acceleration value of 10 m/s^2 with an equivalent velocity value of 10 mm/s or with an equivalent displacement value of 10 μm at 159.15 Hz is used to calibrate the probe. Because the probe can only measure the displacement of metallic surfaces, an accelerometer is screwed onto the calibration exciter to form a metal and flat vibrating surface. The constant calibration distance of 1 mm is achieved by using a flat plastic (non-metallic) spacer. Signals received by the transducer is amplified by its power amplifier unit. It is important to note that the plate is grounded with a cable connected between the plate and the power amplifier of the displacement transducer to neutralize the excess charge in the plate. Calibration of the displacement probe is shown in Figure 4.5.

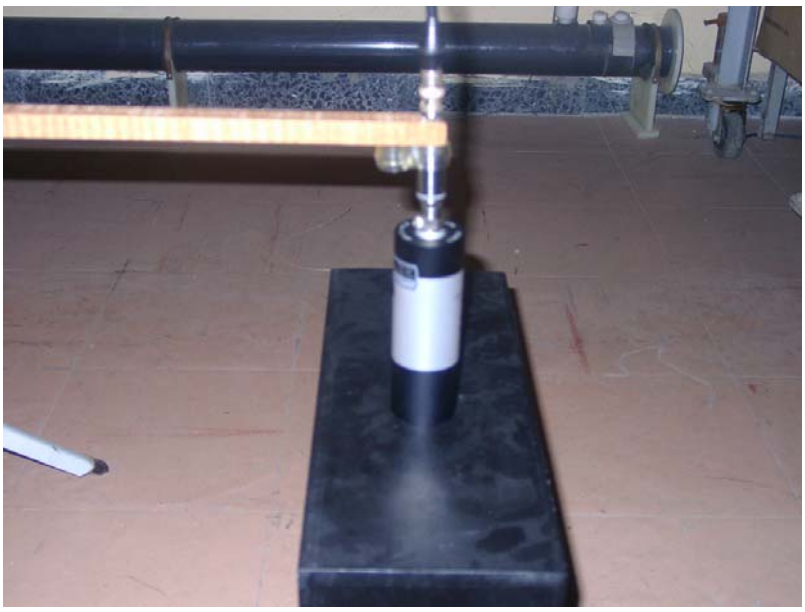

Figure 4.5 Calibration of the Displacement Transducer with the Calibration Exciter

After the distance between the accelerometer's flat surface and the displacement transducer is fixed by using the plastic spacer of a known thickness of 1 mm, plastic spacer is removed from the gap. Then, the calibration exciter which provides a known displacement value is turned on and the calibration is accomplished at a frequency of 159.15 Hz. Plastic spacer is also used to provide the same calibration distance between the probe and the plate. Surface intensity is measured by the probe configuration shown in Figure 4.6 with a spacing of 7 mm in between the acoustical center of the lower microphone of the sound intensity probe and the plate's surface. Utilization of the two probes together in a measurement enables one to measure the sound intensity, surface intensity and to determine the modal behavior of the plate, simultaneously.

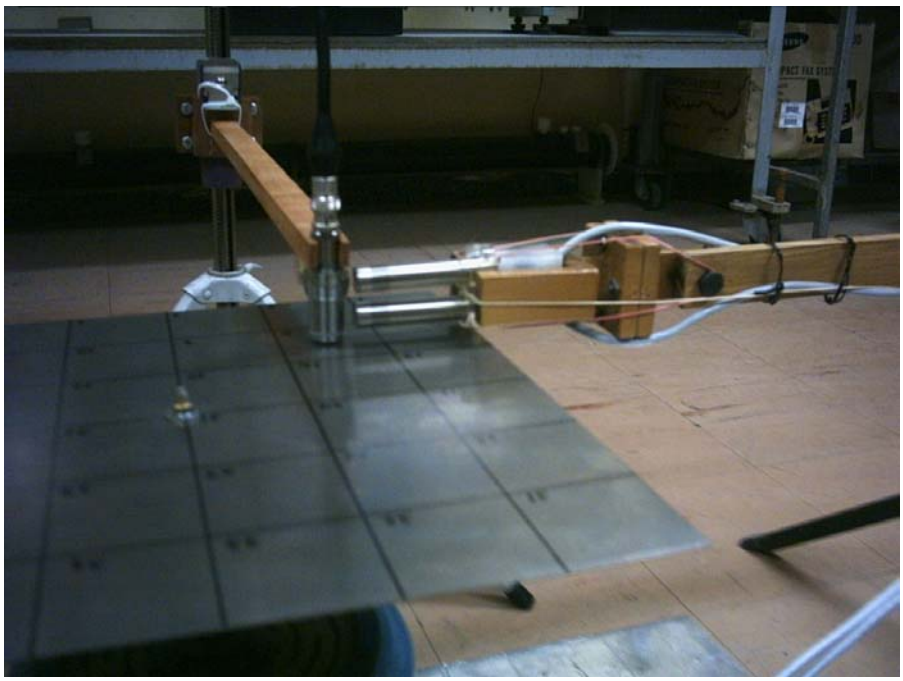

Figure 4.6 Measurement of Surface Intensity Utilizing the Two Probes Together

As it is already mentioned, structural intensity in one direction is measured by using two accelerometers with the assumption of a one-dimensional sinusoidal wave approach. Two accelerometers (B&K Type 4344 and Type 4375), each weighing approximately 2.5 grams are used throughout the measurements to decrease the mass loading effect. Signals generated by the accelerometers are amplified by the charge amplifiers B&K Type 2635 and a force transducer (B&K Type 8200) is used to measure the force and consequently the power transmitted to the plate. This power is injected into the system from one point and flows throughout the plate. Aim of measuring structural intensity is to find how this power is transmitted through the plate from the study of transmission paths means of controlling this power to be transmitted in such a way that it results in lower vibration and noise levels. Structural intensity set-up is schematically shown in Figure 4.7 below.

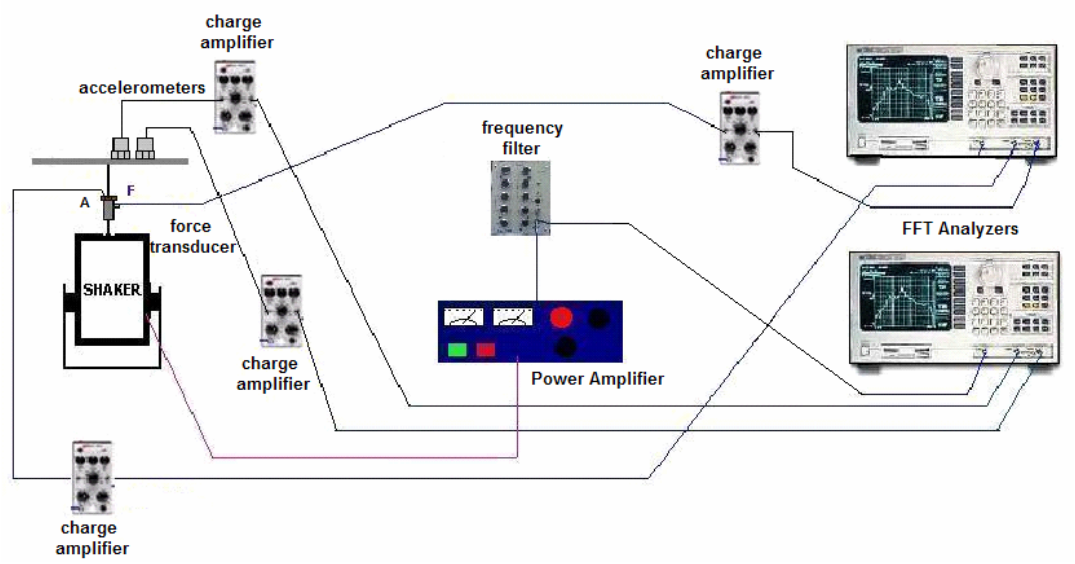

Figure 4.7 Schematical Representation of the Structural Intensity Set-Up

Calibration of the accelerometers are achieved by mounting one of the accelerometers on the plate at its midpoint where the stringer is attached and the other accelerometer onto this accelerometer directly. The plate is excited with random noise so that the accelerometers are calibrated by means of both amplitude and phase for a broadband frequency range.

Number of ensemble averages used for all subsequent measurements are 64. Data obtained from the measurements are converted from DAT format to MAT format using the original program "SDF TO ML" of the Hewlett Packard Company and post-processed via the commercial mathematical software MATLAB®.

4.2 Determination of Modal Behavior of the Plate

A common technique of acoustic source and modal behavior identification on complex structures has been to compare the frequency content of the structural

responses to that of the radiated sound. Structural behavior is observed from the spectra measured by the displacement transducer. Structural response of the plate to random excitation is shown in Figure 4.8. It should be noted that the plate is excited at its center point and the response shown below is measured at the mid-point of the partition 1 of the plate.

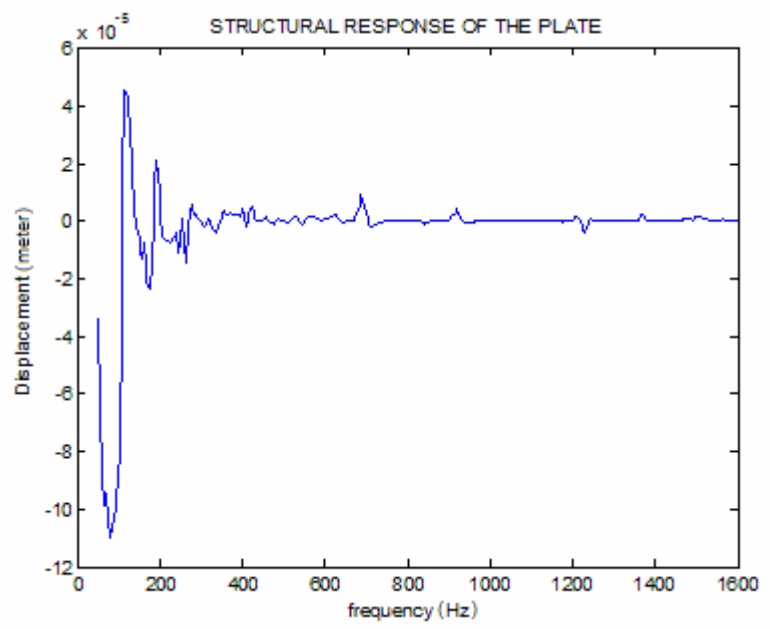

Figure 4.8 A Typical Structural Response of the Plate to Random Excitation

Some of the resonant frequencies can not be easily detected from the structural response plot because of the reason that the rigid body modes of the plate cause the amplification of the amplitude of the vibration at low frequencies in the measurement range. At this stage, pressure spectra both in logarithmic and linear settings that are measured just above the center point of the plate are utilized for extraction of the natural frequencies and displayed in Figures 4.9 and 4.10.

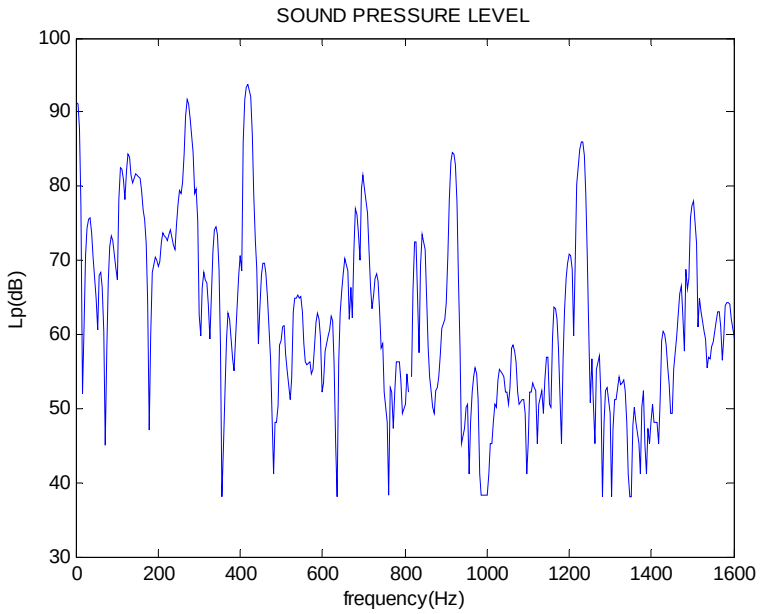

Figure 4.9 Typical Sound Pressure Level Measured over the Plate

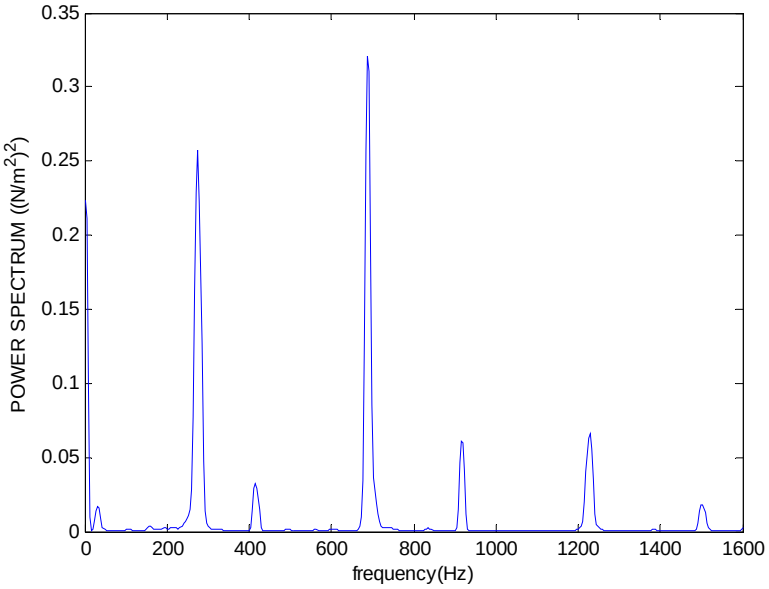

Figure 4.10 Typical Power Spectrum of Pressure Measured over the Plate

Resonant frequencies estimated from the peaks in the power spectrum and the structural response plots given above are found to be located at 32 Hz, 276 Hz, 420 Hz, 688 Hz, 920 Hz, 1232 Hz and 1504 Hz. Corresponding mode shapes are determined for the resonant frequencies of the plate using cubic interpolation and two of such modal behavior are displayed in Figures 4.11 and 4.12.

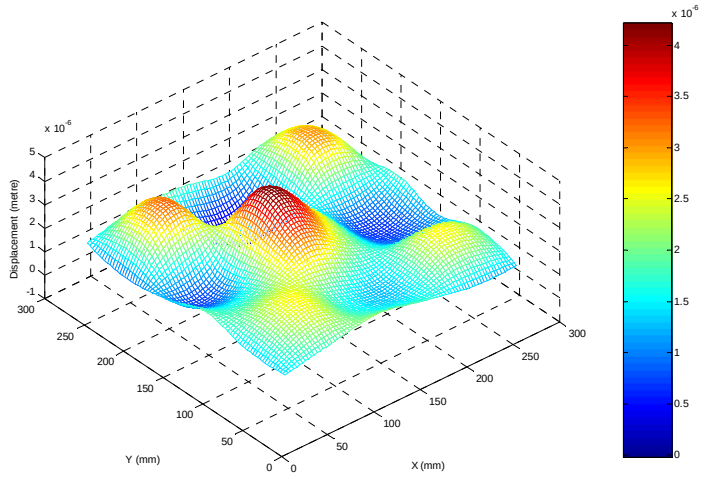

Figure 4.11 Mode Shape at 688 Hz

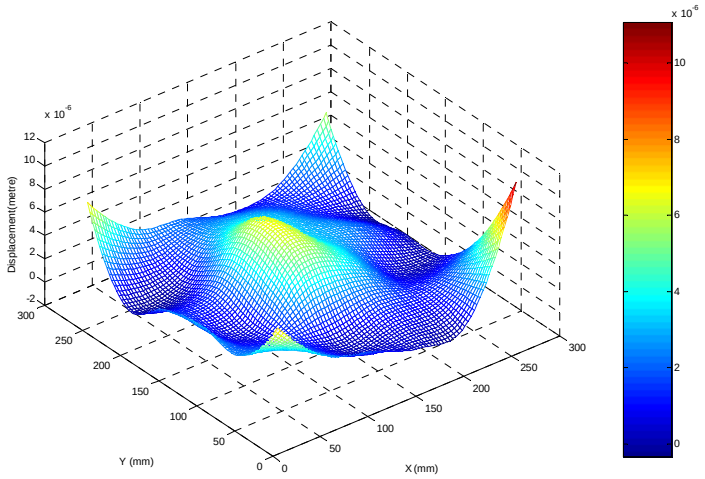

Figure 4.12 Mode Shape at 920 Hz

It is rather straightforward to calculate the velocity spectrum of each partition on the plate after acquisition of the displacement data. An example velocity spectrum for partition 1 of the plate is illustrated in Figure 4.13.

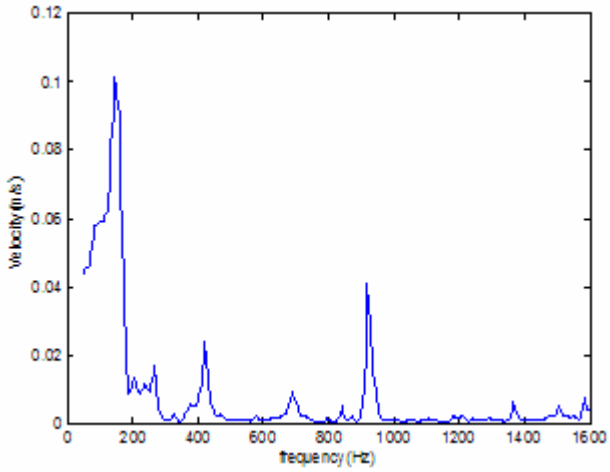

Figure 4.13 Velocity Spectrum of Partition 1 of the Plate

4.3 Measurement of Total Sound Power Radiated by the Plate

In this section, total power radiated by the plate is determined and the resulting plot is analyzed to rank the contributions of the modes to the total sound power radiated. The equipment used for this measurement is shown in Figure 4.4. The frame with 36 partitions is used to form the measurement surfaces of the hypothetical cubic box. Total sound power radiated by the plate is given in Figure 4.14. Moreover, phase-mismatch elimination is accomplished by using both the Microphone Switching Method (MSM) and the Transfer Function Method (TFM) and the resulting spectra are illustrated in Figure 4.15.

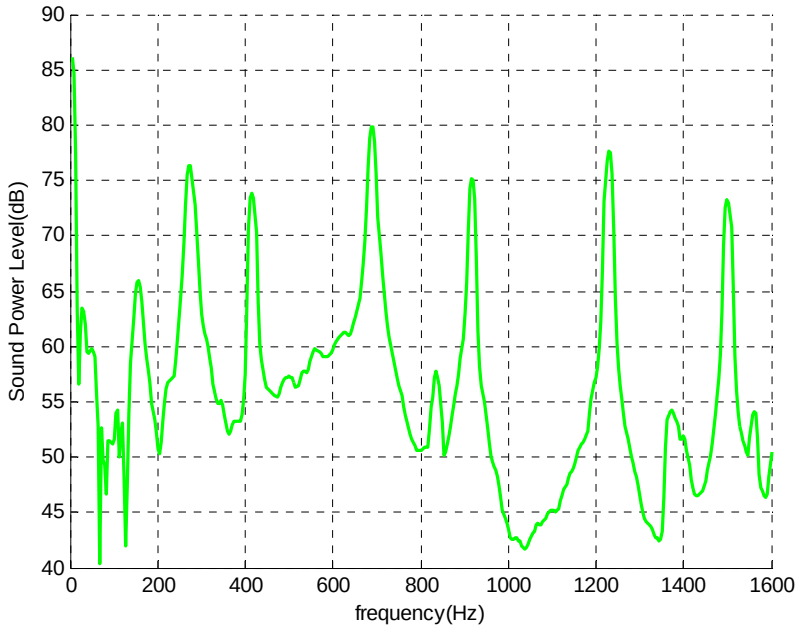

Figure 4.14 Total Sound Power Radiated by the Plate

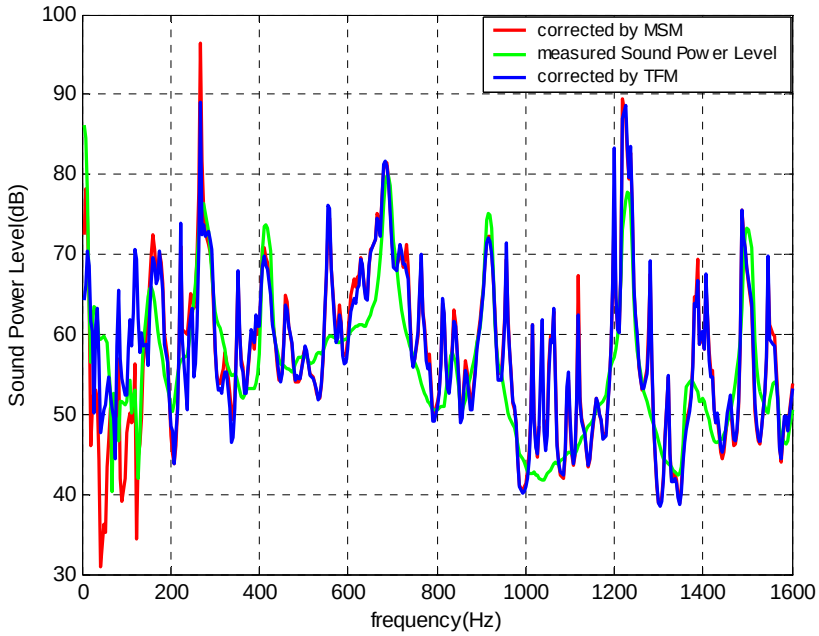

Figure 4.15 Comparison of the Phase-Mismatch Elimination Methods

From the comparison of these three spectra, it can be easily said that the elimination of the phase mismatch between the two measurement channels is much more effective within the frequency range of 0 to 200 Hz as it is expected. At the same frequency range, it is also seen that the transfer function method and the microphone switching method differs much more than that is observed for the other frequencies. This difference is due to the fact that the microphone switching method takes not only the sensitivity of the measurement system into consideration, but also considers effects of environmental conditions on each particular measurement. However, when the transfer function method is utilized, frequency responses of both channels and the transfer function between them are determined for once and then, these values are used in all subsequent calculations.

At this point, the reader is going to be informed about the background noise level of the room that the measurements take place. Sound power measured when there is no active noise source within the hypothetical surface is given in the Figure 4.16 below.

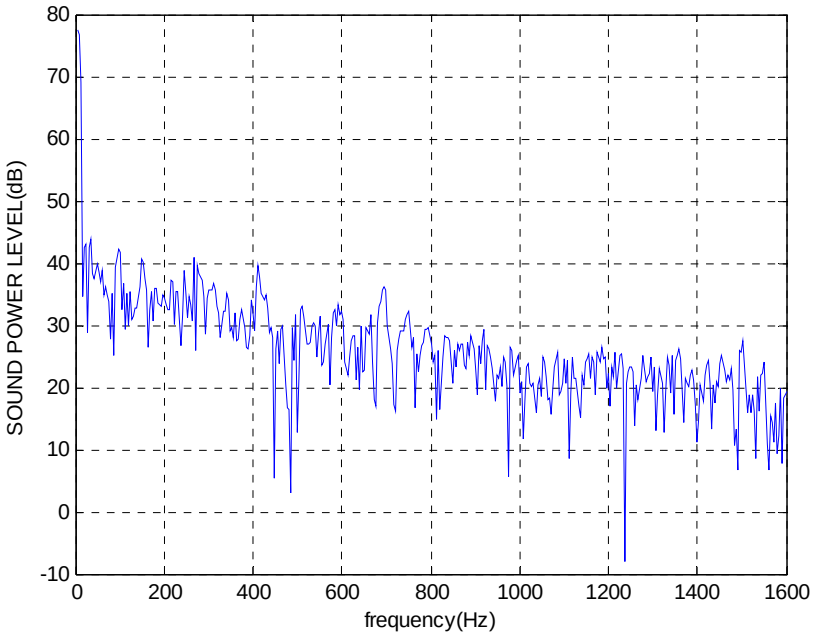

Figure 4.16 Sound Power Level due to the Background Noise

As a result, it is observed from Figure 4.14 that the five most contributing or dominant modes are the ones at 276 Hz (76.5 dB), 420 Hz (74 dB), 688 Hz (80 dB), 920 Hz (75 dB), 1232 Hz (77 dB). The mode at 688 Hz is observed to be the most contributing one and the others are the modes at 1232 Hz, 276 Hz, 920 Hz and 420 Hz, respectively when they are ranked. It is then decided to analyze the radiation patterns at these frequencies to find out the optimum locations for placement of damping patches to reduce the total sound power level. Near-field sound intensity measurements are carried out for these reasons. Surface intensity measurements are used to check the validity of the sound intensity measurements as well as to compare with the same method to present an alternative technique that can be used to identify the near-fields of structures.

4.4 Near-Field Sound Intensity Measurements

The acoustic field close to a source is predominantly reactive, i.e. the pressure and particle velocity are nearly 90° out of phase. Extension of near-field in the vicinity of the vibrating structure depends on the frequency content of the sound radiated by the structure. Near-field properties of a plate depends on its modal density, damping, critical frequency and the type of excitation. Acoustic intensity measurements made inside the near-field of a structure ignore the reactive motion and extract only the sound energy that has a capability to radiate to the far-field. This type of measurement gives the active intensity but the reactive part can also be extracted from the same data.

In this study, near-field intensity over the plate is measured to determine and understand the energy flow patterns over the surface of the plate. Two-microphone sound intensity and microphone-displacement transducer surface intensity measurements are made to determine the sound field. Intensity mapping techniques are also used to visualize the energy flow direction and magnitude. Intensity distribution, sound power level and consequently, radiation efficiency of the plate is determined using these two methods and compared to understand the

correct time to choose the most suitable method. All transducers used throughout the measurements are calibrated and the phase mismatch elimination for both procedures is achived by using the methods explained in the previous chapter.

Total sound intensity radiated by the plate's surface is measured using both the two-microphone sound intensity and the surface intensity technique and the resulting spectra are shown below.

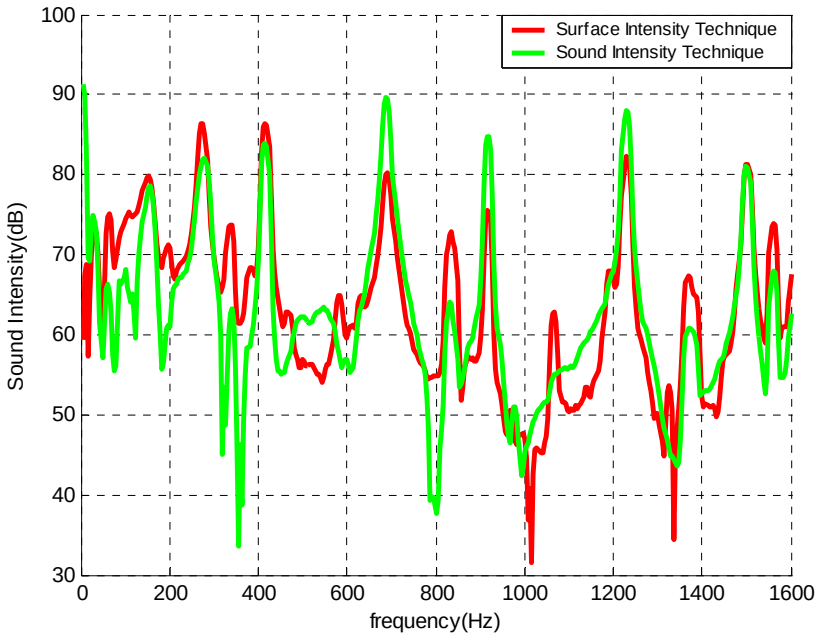

Figure 4.17 Intensity Measured by Two-Microphone Sound Intensity and Surface Intensity Techniques

Both methods give reasonably close results, especially at low frequencies and extracted vibrational and energetic behaviors seem to be quite alike. This similarity in results can be redemonstrated using the radiation efficiencies determined by using these two acoustical methods.

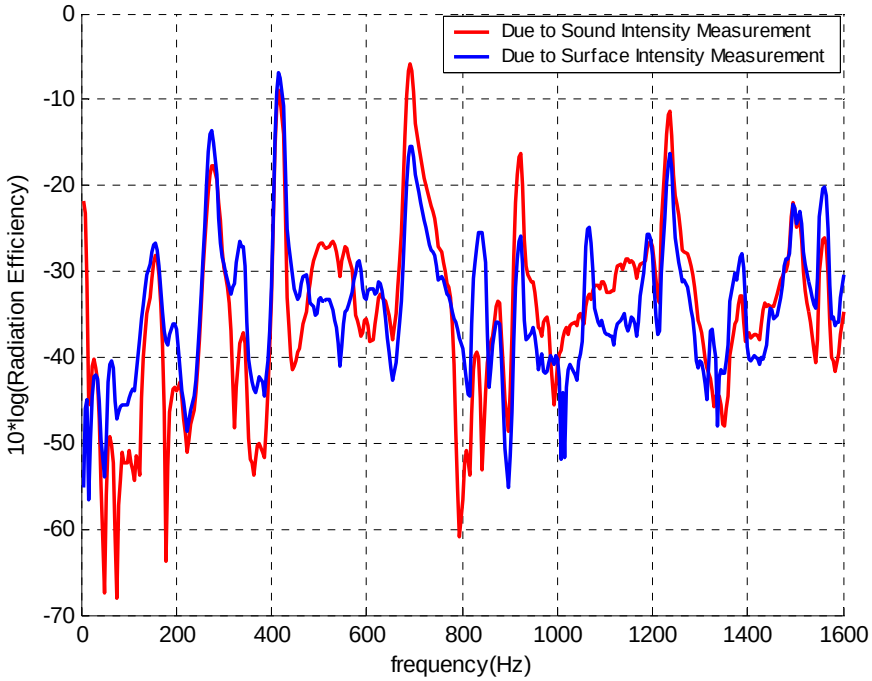

Figure 4.18 Comparison of Radiation Efficiencies by Two-Microphone and Surface Intensity Techniques

At this stage, near-field intensity maps obtained for the first five most contributing resonant frequencies are given and the sound radiation paths are determined from these maps. These measurements are taken just above the mid-point of each partition of the plate and the plots are obtained by using Matlab® routines and employing cubic interpolation technique. First, positive active intensity map and then, negative intensity map which is in fact the complimentary map of positive intensity are going to be given. They both display the amount of energy flowing in positive and negative directions. Contour plots and vector field plots are given as auxiliary plots for visualization of energy flow directions. They are plotted one on the top of the other to enrich the visualization. Reactive intensity plots are given to indicate the regions where the acoustical short-circuits are frequently seen at the corresponding frequency. In fact, it is interpreted from Equation 3.28 that when the difference between the energy passing through each individual measurement microphone differentiates more than its previous value then the reactivity can be

said to be increased. Physically, the amount of energy which passes through the microphone closer to the plate does not pass from the microphone further from the plate because it is short-circuited by another region of the plate that possesses a vibrational response nearly out-of-phase relative to the region where the energy is initially radiated.

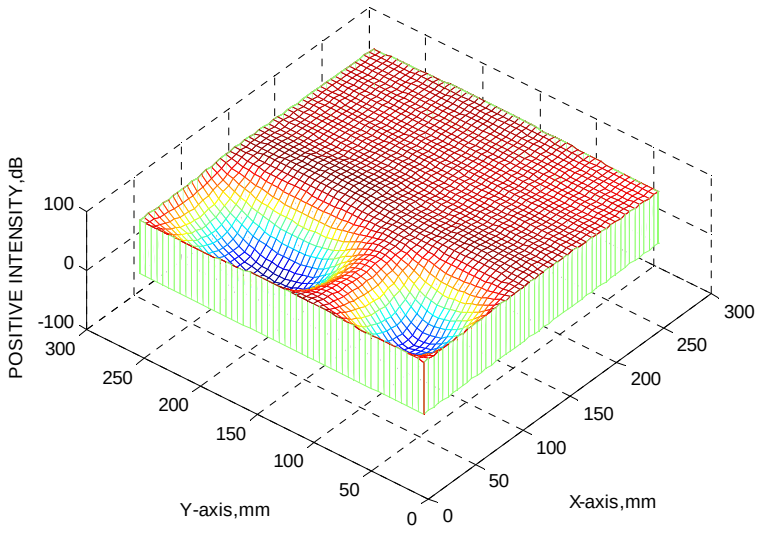

Figure 4.19 3-D Positive Intensity Plot at 276 Hz

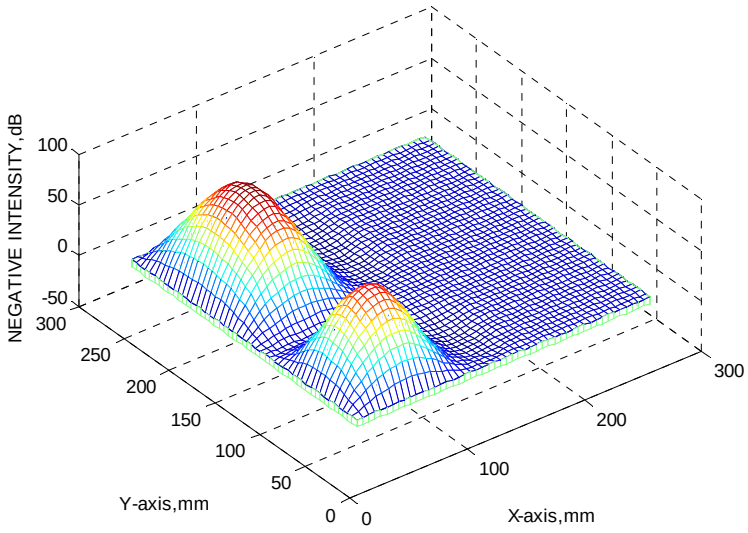

Figure 4.20 3-D Negative Intensity Plot at 276 Hz

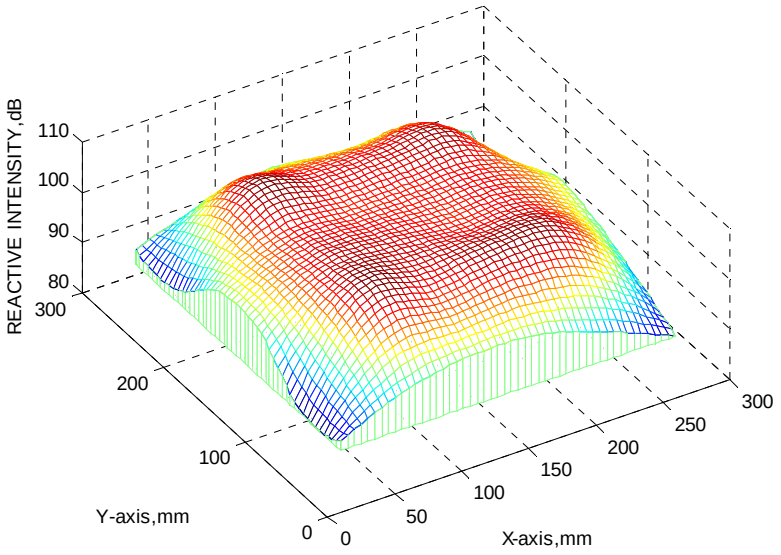

Figure 4.21 3-D Reactive Intensity Plot at 276 Hz

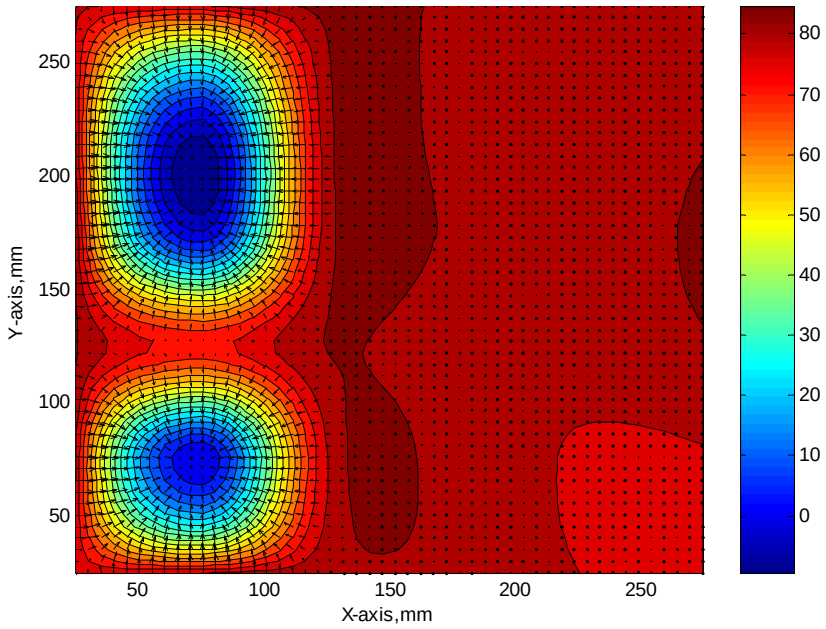

Figure 4.22 Energy Flow Direction and Intensity Contours at 276 Hz

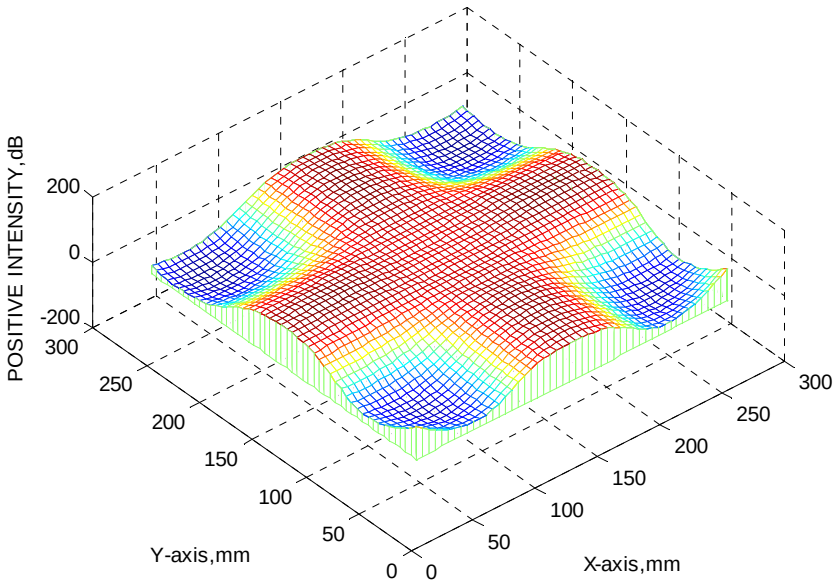

Figure 4.23 3-D Positive Intensity Plot at 420 Hz

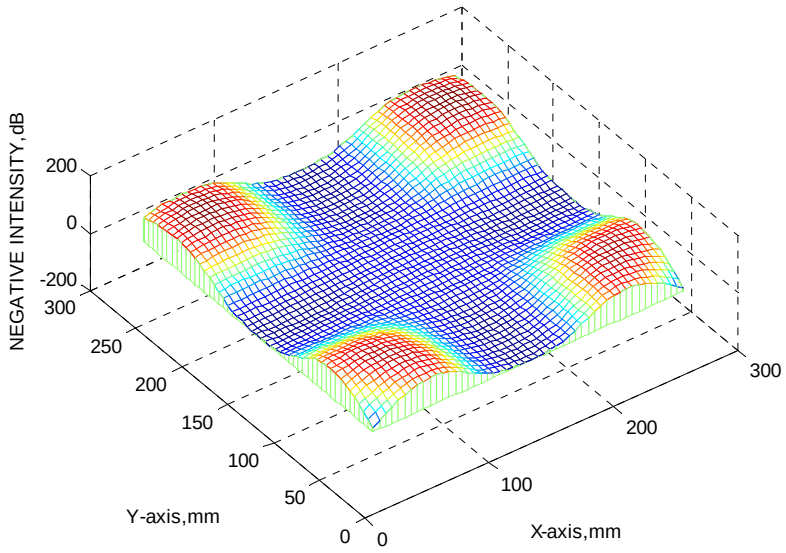

Figure 4.24 3-D Negative Intensity Plot at 420 Hz

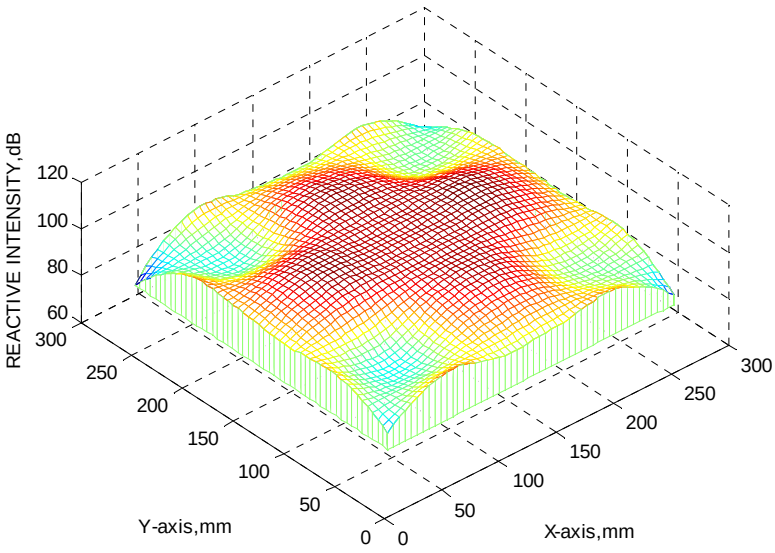

Figure 4.25 3-D Reactive Intensity Plot at 420 Hz

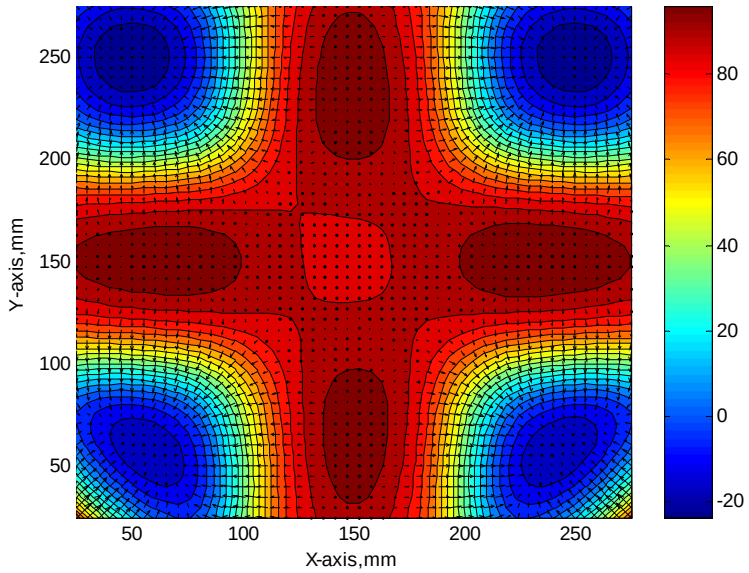

Figure 4.26 Energy Flow Direction and Intensity Contours at 420 Hz

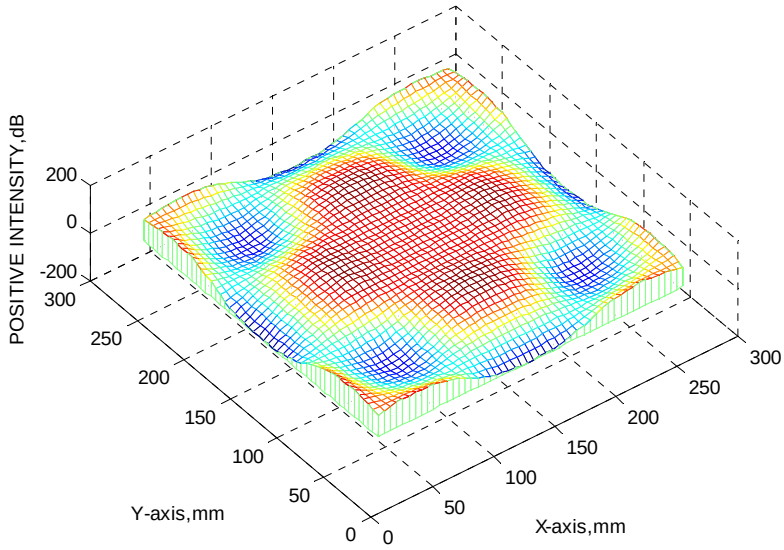

Figure 4.27 3-D Positive Intensity Plot at 688 Hz

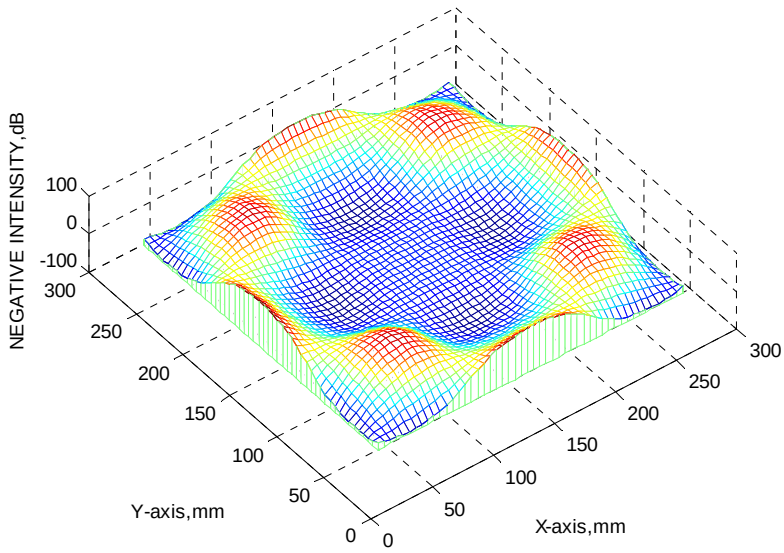

Figure 4.28 3-D Negative Intensity Plot at 688 Hz

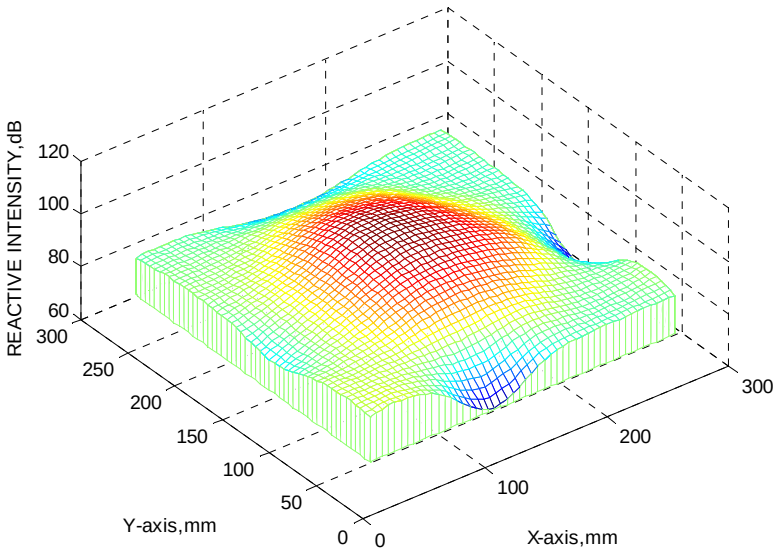

Figure 4.29 3-D Reactive Intensity Plot at 688 Hz

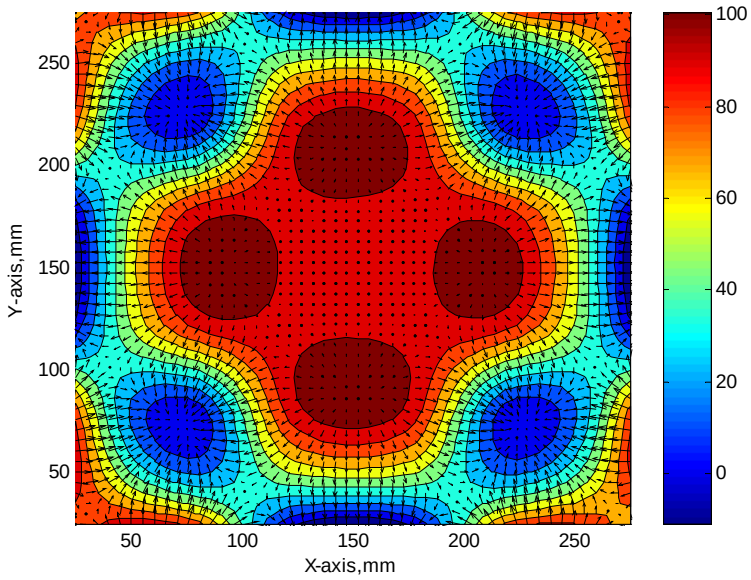

Figure 4.30 Energy Flow Direction and Intensity Contours at 688 Hz

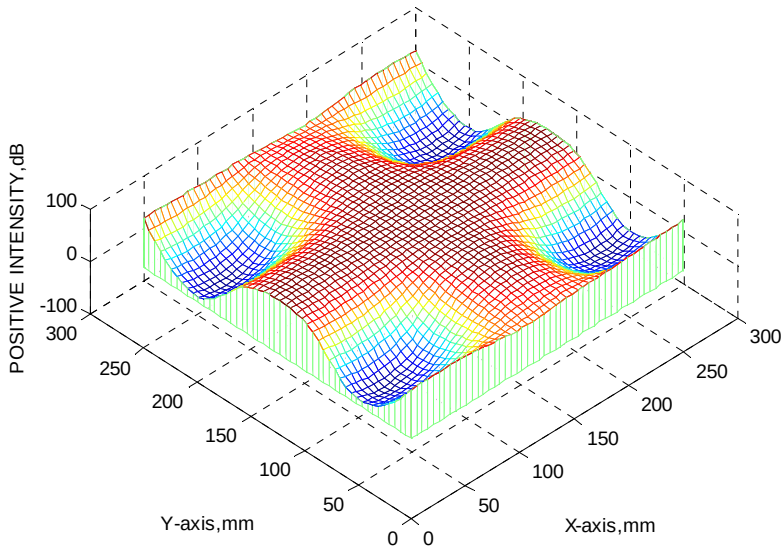

Figure 4.31 3-D Positive Intensity Plot at 920 Hz

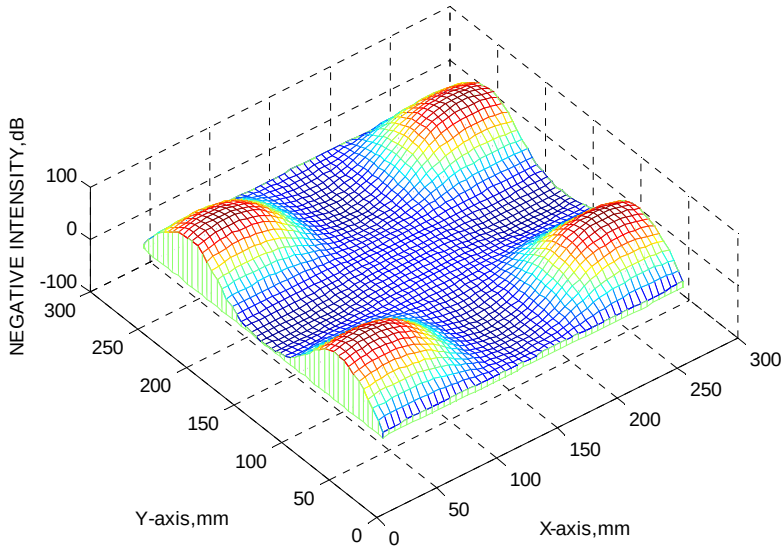

Figure 4.32 3-D Negative Intensity Plot at 920 Hz

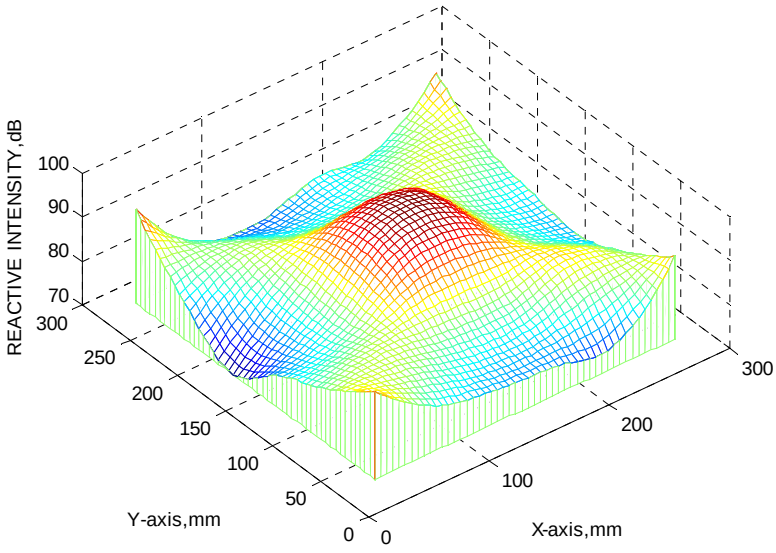

Figure 4.33 3-D Reactive Intensity Plot at 920 Hz

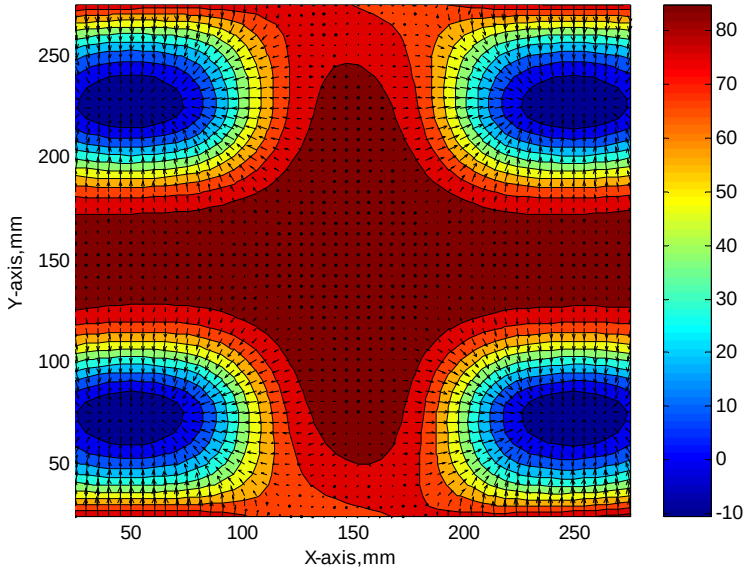

Figure 4.34 Energy Flow Direction and Intensity Contours at 920 Hz

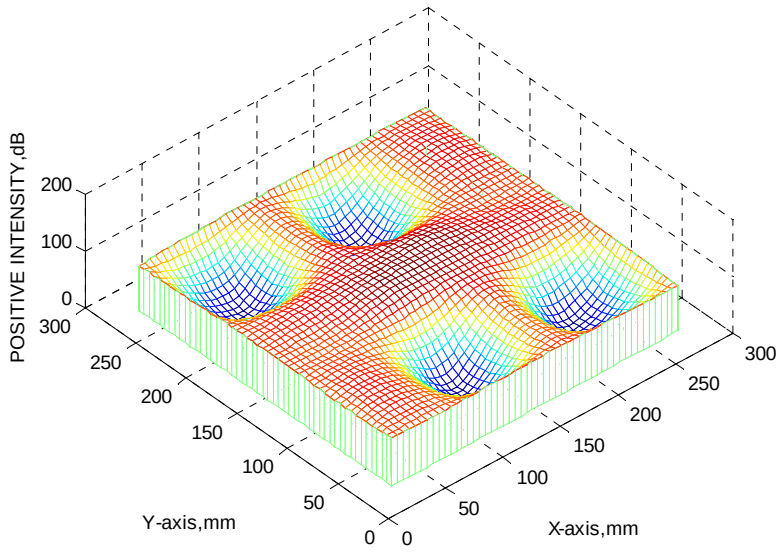

Figure 4.35 3-D Positive Intensity Plot at 1232 Hz

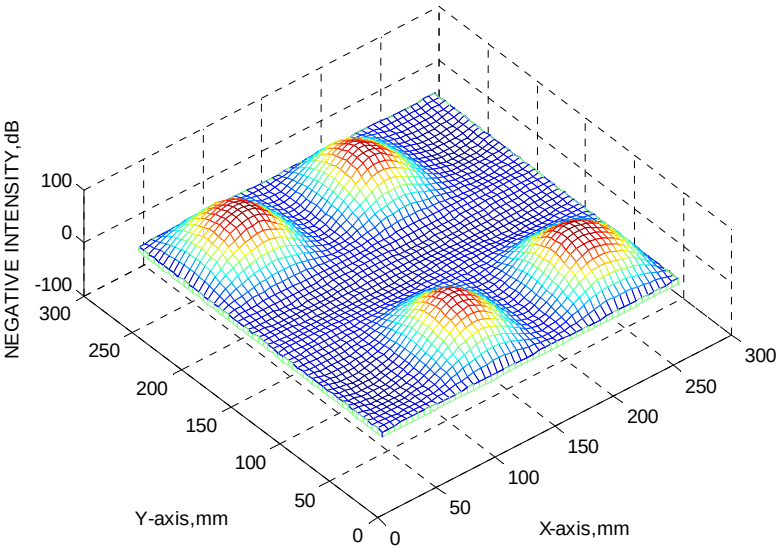

Figure 4.36 3-D Negative Intensity Plot at 1232 Hz

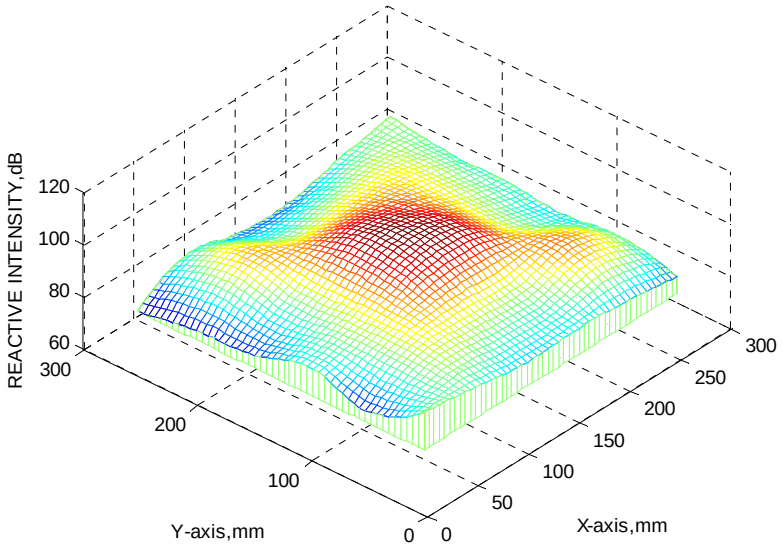

Figure 4.37 3-D Reactive Intensity Plot at 1232 Hz

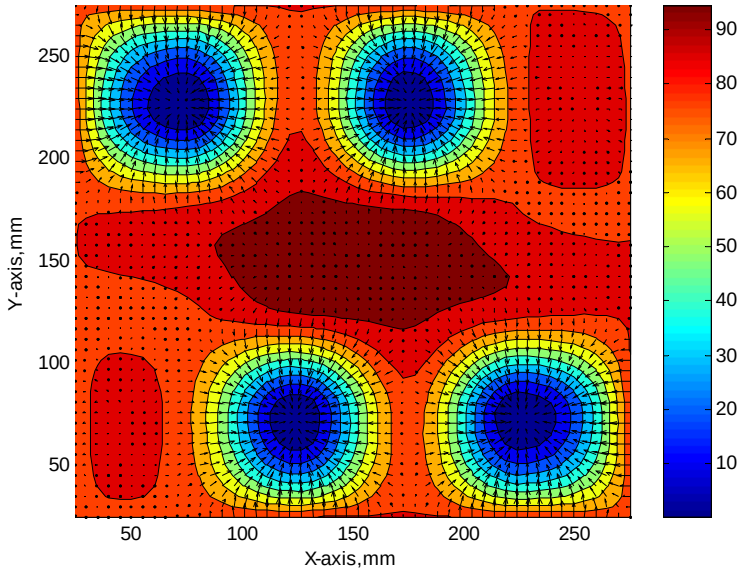

Figure 4.38 Energy Flow Direction and Intensity Contours at 1232 Hz

Likewise the above quantities, potential energy (V) and kinetic energy (T) can be calculated from the measured spectra in frequency domain as [31]:

$$V(\omega) = \frac{G_{P_1P_1}(\omega) + G_{P_2P_2}(\omega)}{8 \cdot \rho \cdot c^2} \tag{4.1}$$

$$T(\omega) = \frac{G_{P_1P_1}(\omega) + G_{P_2P_2}(\omega) - \mathrm{Re}\left[G_{P_2P_1}(\omega)\right]}{4 \cdot \omega^2 \cdot \rho \cdot \Delta r^2} \tag{4.2}$$

It is easily seen from the Equations 4.1 and 4.2 above that the potential energy is proportional to the total energy radiated at that particular frequency and the kinetic energy is proportional to the particle velocity spectrum which can be emphasized with the following equation [32]:

$$G_u(f) = \frac{G_{P_1P_1} + G_{P_2P_2} - 2 \cdot \mathrm{Re}\left[G_{P_2P_1}\right]}{(\omega \cdot \Delta r \cdot \rho)^2} \tag{4.3}$$

Since they are primarily related with the radiated energy and the particle velocity, it is expected that values of both kinds of energy are high at the mid-regions of the plate where it is driven. From the analysis of the data, this expectation has come out to be true for all frequencies of interest. Thus, only representative plots for a single frequency are given below.

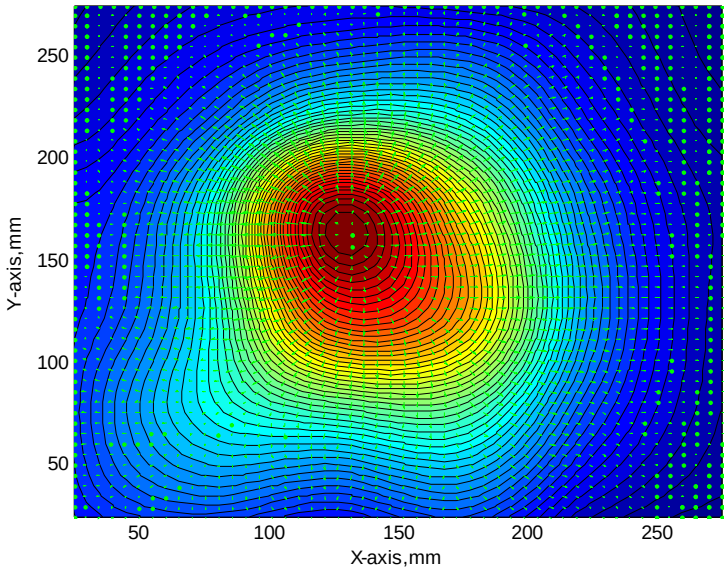

Figure 4.39 Kinetic Energy Contours and the Associated Vector Field at 688 Hz

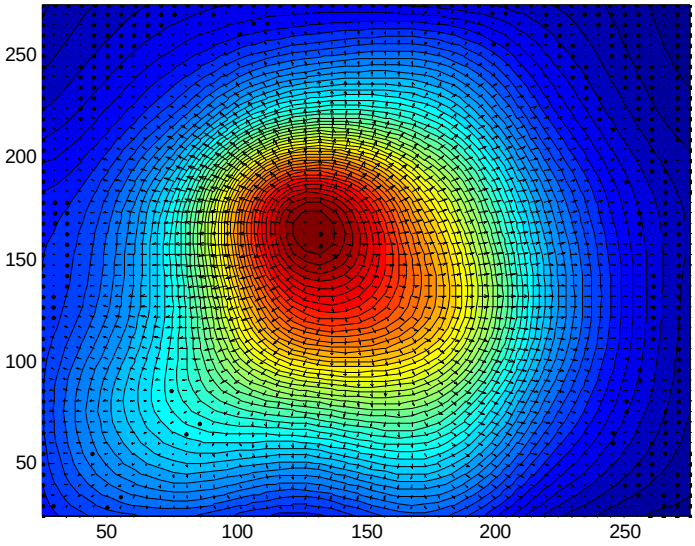

Figure 4.40 Potential Energy Contours and the Associated Vector Field at 688 Hz

Acoustical sources and sinks associated with the resonant frequencies are displayed via the near-field intensity maps. Acoustical radiation paths are obtained from these plots and structural energy propagation paths are obtained via the power flow (structural intensity) plots as a complementary part of the analysis conducted in this study. Plots of power flow in the plate are given in the next section. Before discussion of the structural intensity measurement presented, a last comparative analysis about the measurement of surface intensity will be given here. It is already mentioned that the surface intensity measurements are carried out by using non-contact displacement transducer to avoid the mass loading effect of an accelerometer. However, the phenomena of mass loading is especially observed to be effective at high frequencies, since the measurements are carried out in a relatively low frequency region, it is decided to measure surface intensity by these two different transducers independently and compare the resultant sound power levels to find the proper method for such system configurations. The resultant power spectra are given in Figure 4.41 below.

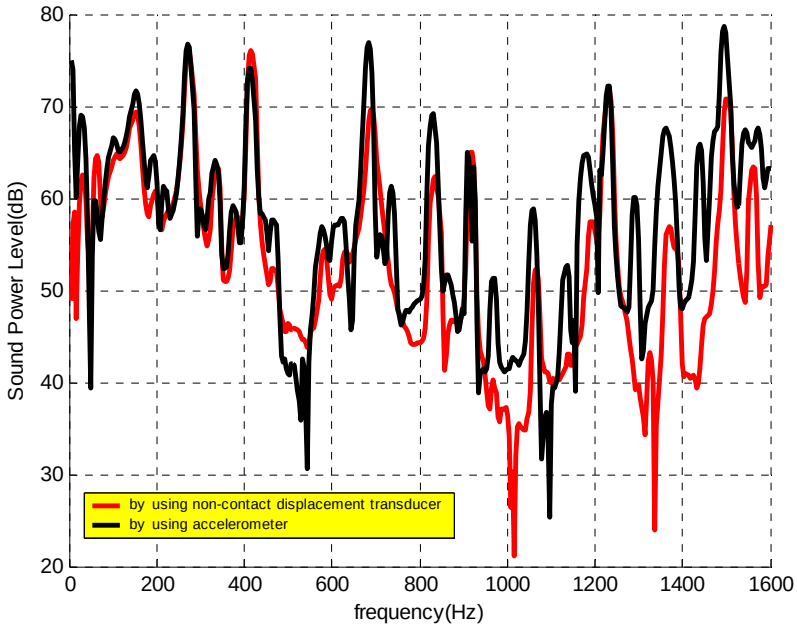

Figure 4.41 Comparison of Sound Power Level by Two Different Probe Configurations

It is observed from numerous experiments with the non-contact displacement transducer that flatness in its response at frequencies above 1 kHz can not be maintained. This fact is proven by the figure above and consequently the results start to differ much more above 1 kHz even though they are pretty close up to the same frequency. Moreover, effect of mass loading associated with the usage of the accelerometer is not observed within this frequency range. As a result, it is better to use this accelerometer (B&K Type 4344) of 2.5 grams compared with the non-contact displacement transducer within this frequency range.

4.5 Structural Intensity Measurements

Experimental set-up that has already been configured is a little bit modified to be able to measure and process the structural intensity data. Two HP 35665A Dynamic Signal Analyzers are used simultaneously. One of them is used to obtain the complex transfer functions transduced by two accelerometers, and the other one is employed to acquire and process the force data transduced by the force transducer (B&K Type 8200) located in between the stinger and the plate. Force transducer which is assembled to the system is shown in Figure 4.42 below.

Figure 4.42 Force Transducer Assembled onto the Stinger

Random noise signal delivered by the dynamic signal analyzer is fed to the shaker after amplification by a power amplifier. All of the measurements are made on a grid having 36 partitions. Acquired data is post-processed via MATLAB routines.

Firstly, mechanical power input delivered to the plate by the shaker is measured by means of a force transducer and an accelerometer mounted on the surface of the force transducer. Mechanical power is measured by implementing Equation 4.4 below [27]:

$$P_{input} = \mathrm{Re}\left\{\frac{1}{j\cdot\omega}\cdot G_{Fa}\right\} = \frac{1}{\omega}\cdot \mathrm{Im}\{G_{Fa}\} \tag{4.4}$$

Resulting spectrum is given in Figure 4.43 below. Mechanical power is plotted against a reference power value of $P_{ref} = 10^{-12}$ W.

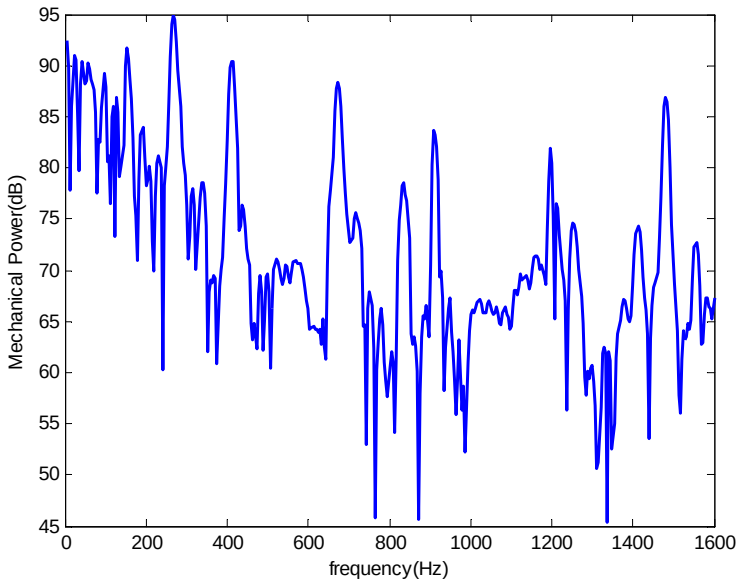

Figure 4.43 Mechanical Power Input to the Plate by the Shaker

The peaks observed in the plot coincides with the resonant frequencies of the plate. Even though the force measured displays a decreasing trend, the increase in the value of the input velocity is greater than the decrease in the value of the force due to the relaxation at the resonant frequencies causing the power delivered to increase.

Accelerometer separation distance is set as 15 mm for structural intensity measurements in both x and y directions. It has already been mentioned that the diameter of the probe mounting area must be at most equal to the one-fourth of the wavelength of bending waves propagating on the plate. Accelerometer separation distance depends on the bending wave speed and consequently, the wavelength.

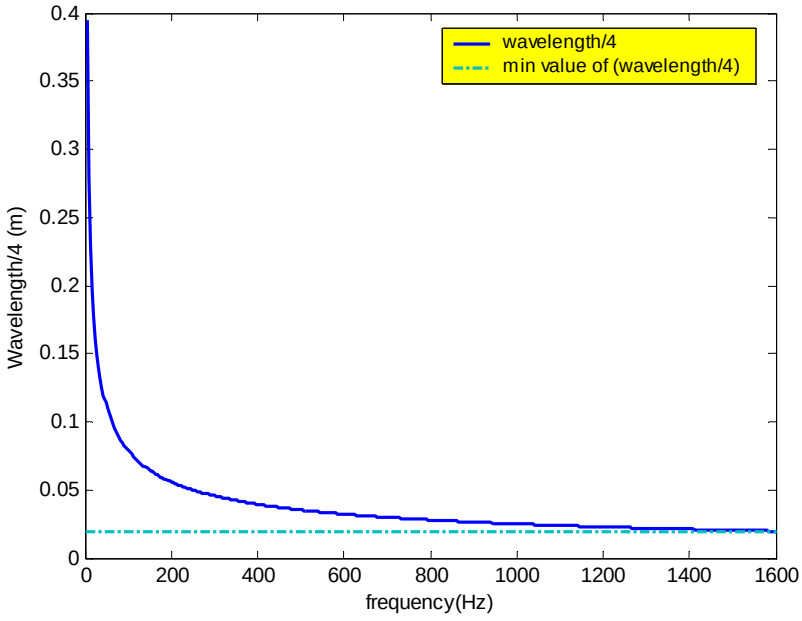

Figure 4.44 Upper Limit for the Accelerometer Separation Distance for the Plate

From Figure 4.4, it is realized that the maximum diameter of the mounting area for the accelerometers must be approximately 20 mm. Both accelerometers have radii of 5 mm, i.e. the accelerometer spacing must be 10 mm limited to measure the intensity up to 1600 Hz. Structural intensity can be measured correctly

up to 1000 Hz with this accelerometer spacing. It is also known that there will be extra finite difference errors above 1000 Hz. Spacing is set to 15 mm to be able to reduce the phase mismatch error and measure intensity in a better way at relatively low frequencies.

Different from the classical approaches, structural intensity maps are obtained for the resonant frequencies of the plate. A typical structural intensity vector plot obtained for the resonant frequency of 688 Hz is shown in Figure 4.45 below.

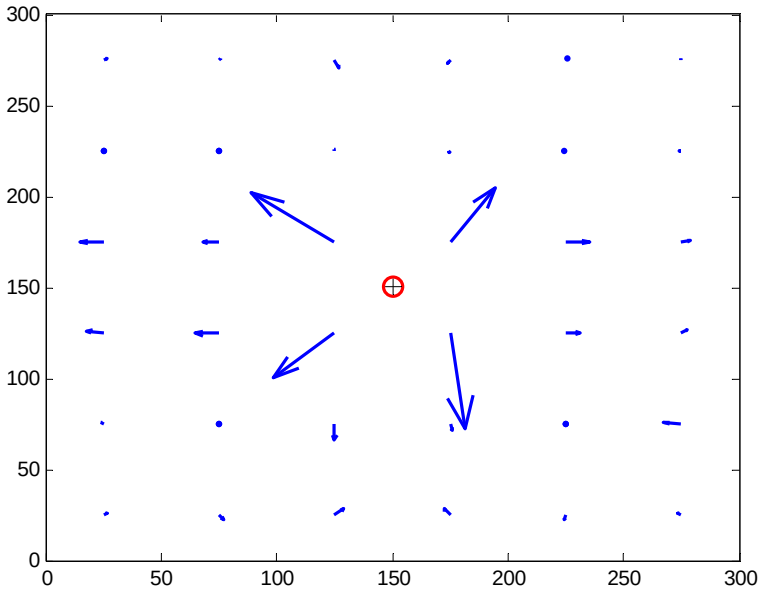

Figure 4.45 Structural Intensity Vectors at 688 Hz

All of the structural intensity maps are plotted using the raw data acquired without the application of any interpolation technique. There are 36 resultant vectors associated with the 72 separate measurements for the structural intensity in x and y directions. 64 averages are taken for each individual measurement.

Positions and the spacing of the accelerometers are shown in Figure 4.46 below illustrating the set-up for a measurement in x direction.

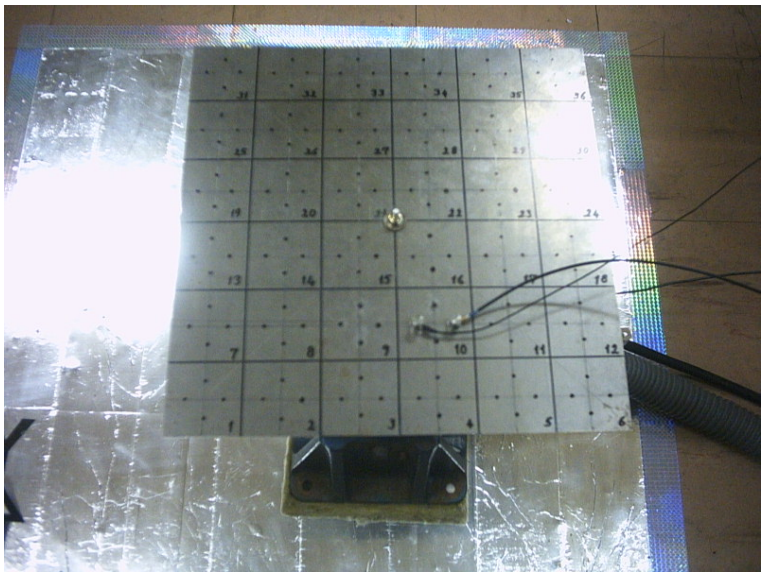

Figure 4.46 Accelerometer Configuration Used for Measurement of Power Flow

It is seen from Figure 4.45 that, at this particular frequency, there is no net power flow at the vicinity of the corners of the plate as expected. The outgoing waves and the waves reflected from the boundaries, i.e from the corners interfere at these locations forming standing waves. Consequently, these regions can be said to be the reactive regions of the plate. Source is marked with a red circle and a plus sign inside at the center of the plate. The largest value of net power flow is normally observed at the vicinity of the source point and propagate from the source to the edges of the plate. Power flow from the centre to the left and right sides are seen obviously. It is not possible to put the same interpretation on the power flow from the source to the top and the bottom edges. There seems to be a net power flow to these sides, but it is not as much as the power flow to the left and to the right edges. In addition, top and bottom sides of the plate are observed to be much more reactive. The same plot is redrawn in Figure 4.47 below by just replacing the

linear magnitudes of the structural intensity vectors with logarithmic magnitudes to enhance the visualiation of the power flow directions.

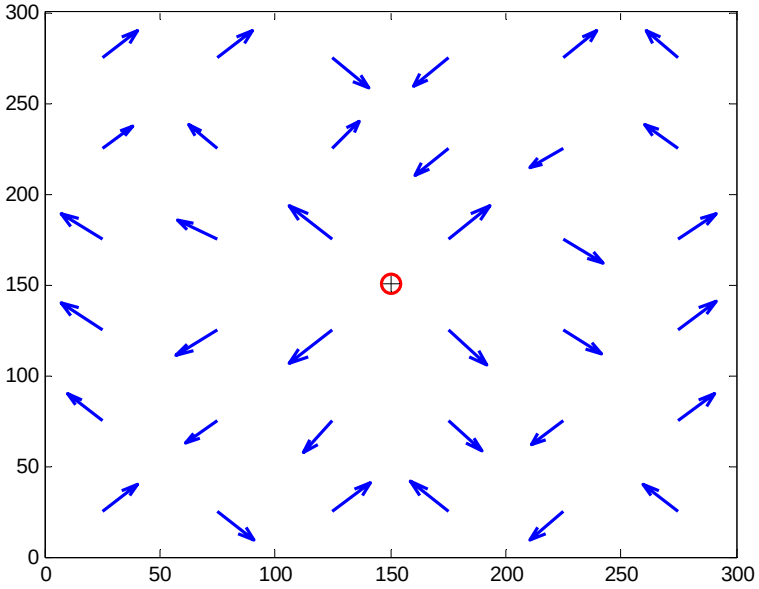

Figure 4.47 Structural Intensity Vectors Having Logarithmic Magnitude at 688 Hz

4.6 Effects of Damping Treatment on Vibroacoustical Behavior of the Plate

Structural intensity is measured by using Equation (3.76), i.e by measuring the complex frequency response functions between linear accelerations at positions 1 and 2, respectively, with respect to the reference force F. These frequency response functions are nothing but, the transfer inertances. Consequently, one can measure structural intensity and form an opinion about vibrational behavior of the plate at the same time.

In this stage of the study, constrained layer damping patches are attached to the plate's surface on some of the paths of outgoing waves generated by the source as shown schematically in Figure 4.48 below. Regions where damping patches applied are colored in grey.

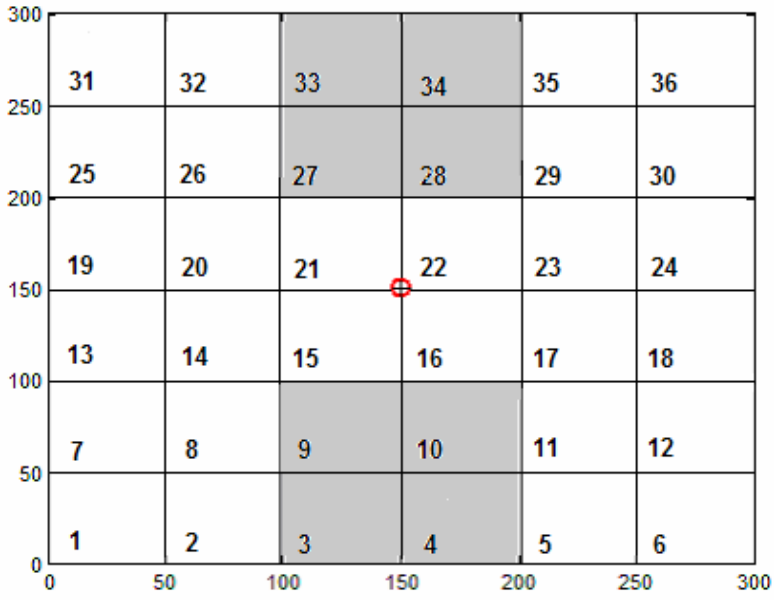

Figure 4.48 Regions where Damping Patches are applied

Resulting structural intensity vectors at 688 Hz are given in Figure 4.49. It can be easily seen that the power flow into the damped regions are increased with the influence of dissipation effect of the damping patches when compared with Figure 4.45.

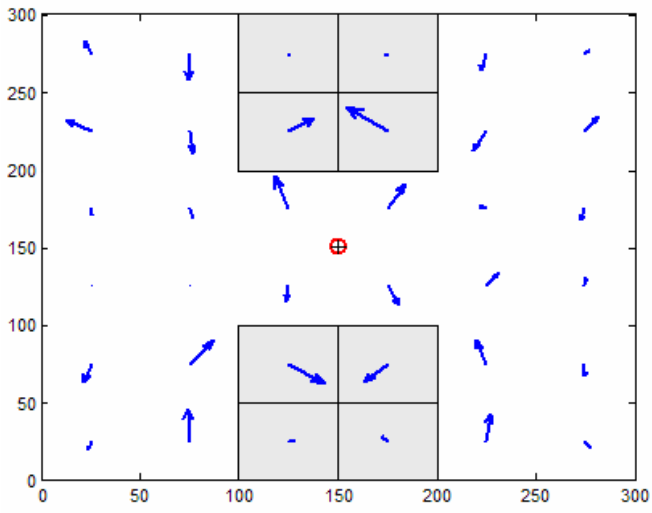

Figure 4.49 Effect of Damping on Structural Intensity Vectors at 688 Hz

It is also observed that the power flow into the middle left and middle right sides of the plate is reduced and directed to the corners. Consequently, corners are activated in a stabilized manner and get out of the resonant behavior. The same plot is given below by just replacing the linear magnitudes of the structural intensity vectors with logarithmic magnitudes to enhance the visualiation of the power flow directions.

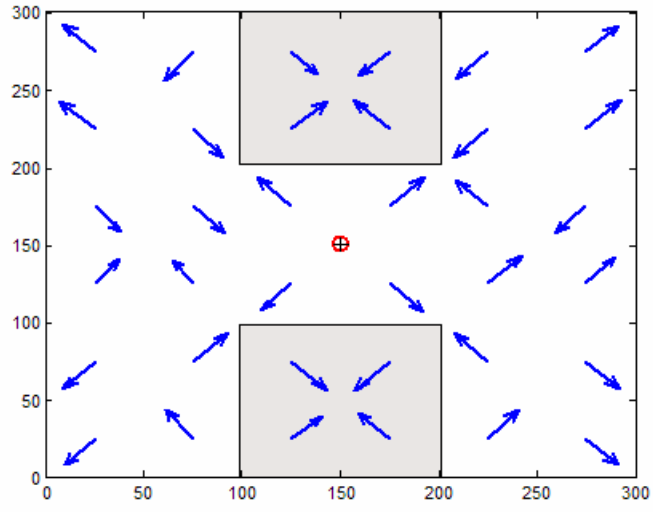

Figure 4.50 Structural Intensity Vectors with Logarithmic Magnitude at 688 Hz

Near-field sound intensity maps obtained for the resonant frequencies of the damped plate are given below.

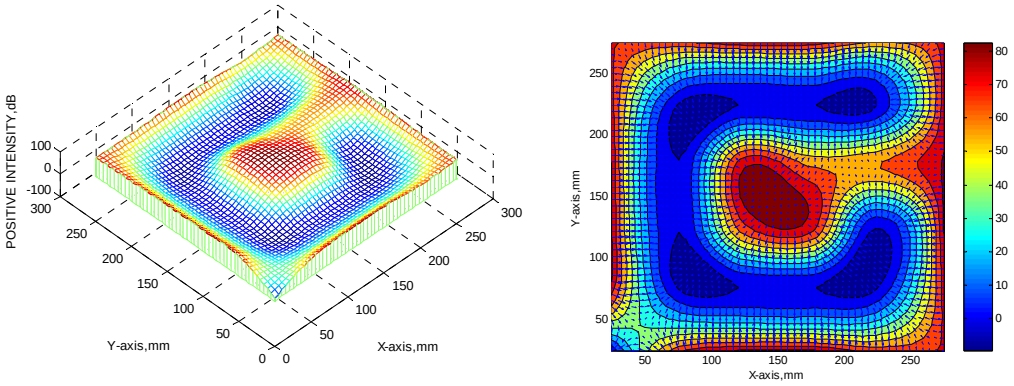

Figure 4.51 Positive Intensity Distribution over the Damped Plate at 276 Hz

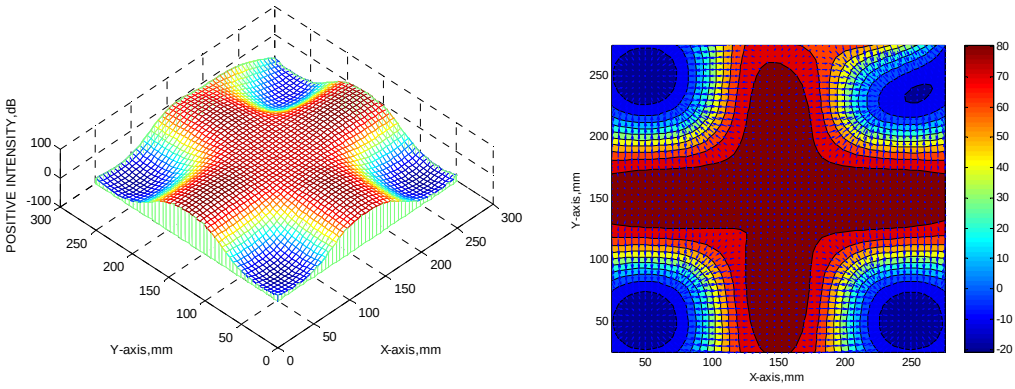

Figure 4.52 Positive Intensity Distribution over the Damped Plate at 420 Hz

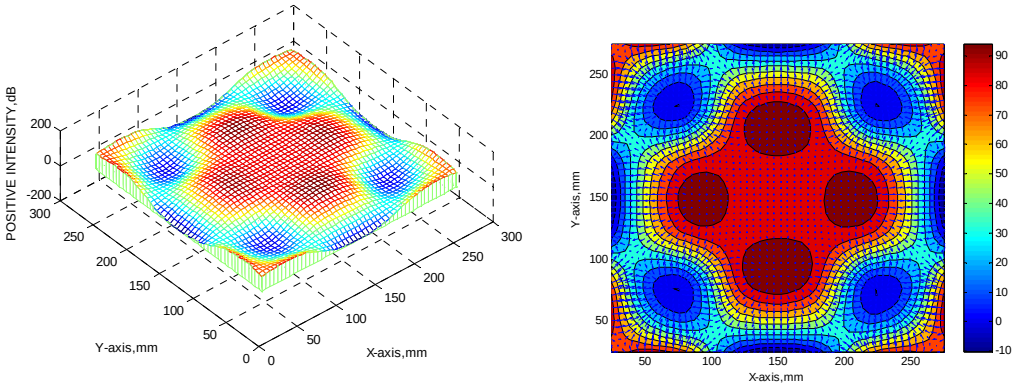

Figure 4.53 Positive Intensity Distribution over the Damped Plate at 688 Hz

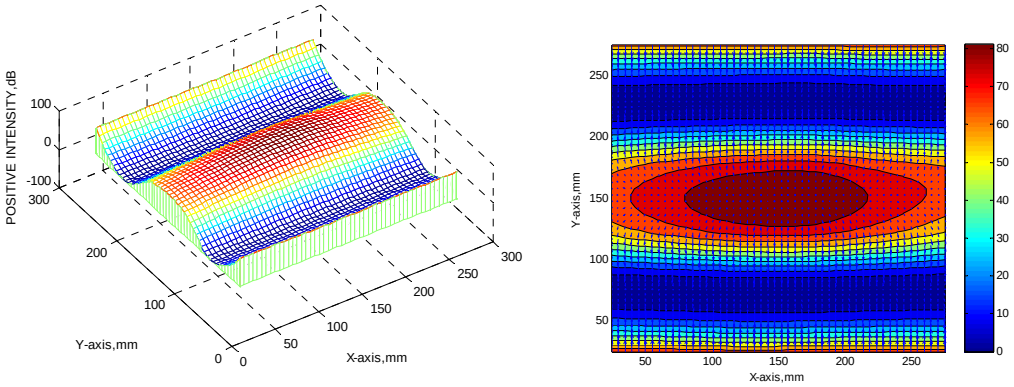

Figure 4.54 Positive Intensity Distribution over the Damped Plate at 920 Hz

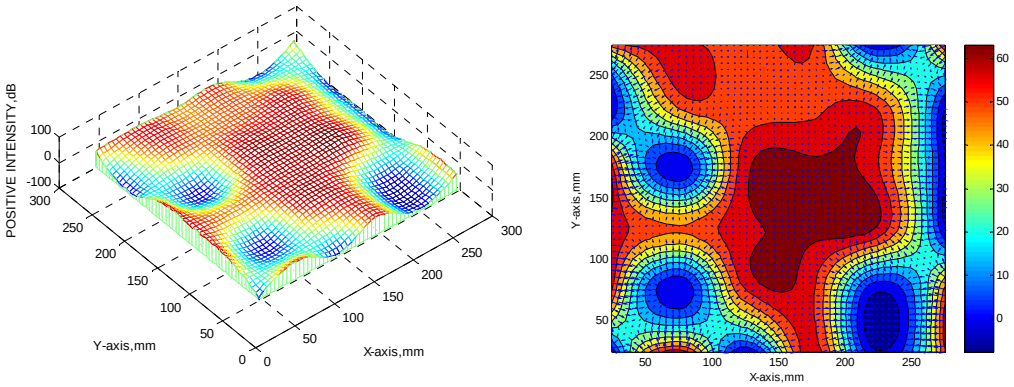

Figure 4.55 Positive Intensity Distribution over the Damped Plate at 1232 Hz

Comparing with mapping of the case of no externally applied damping, it is seen that radiation paths are changed in an unpredictable manner except the change at 920 Hz, where the radiation paths are completely vanished at the locations of the damping patches. Yet, it is definite that the radiated sound power is reduced at all frequencies between the frequency range of 0-1600 Hz. Comparison of the sound power levels radiated by the damped and undamped states of the plate is presented in Figure 4.56 below.

It is seen that there is a level drop of nearly 6 dB for all of the resonant frequencies and the effect of damping can be observed by means of the expansion in the necks of peaks corresponding resonant frequencies. It should be also noted that the shifts of the resonant frequencies, especially seen after 1 kHz, is due to the mass loading effect of the damping patches.

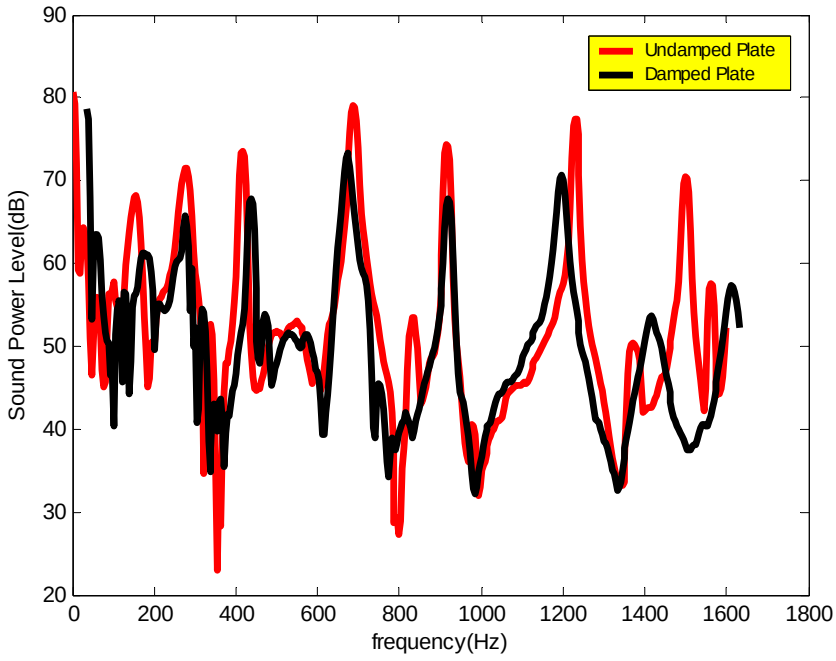

Figure 4.56 Effect of Damping Treatment on Total Sound Power Level

4.7 Errors Associated with the Measurement Techniques Employed

Error analysis is carried out especially for sound intensity measurement procedure by using the approach mentioned in the previous chapter. Bias errors will be analysed at first and then, random errors will be analysed. The most important bias errors are phase mismatch errors and finite difference errors for the measurement of sound intensity.

A measurement set-up is established to investigate the error due to the phase mismatch between channels of the analyzing system used. It consists of an impedance tube (Hilton), random noise generator (B&K Type 1405) and the sound intensity probe itself. The measurement set-up is shown in the below figure.

Figure 4.57 Phase Mismatch Error Measurement Set-Up

Sound intensity probe is assembled into the impedance tube that has a cut-off frequency of 3000 Hz with a connector having an anechoical termination on its

surface facing the impedance tube. The configuration with the connector is shown in Figure 4.58.

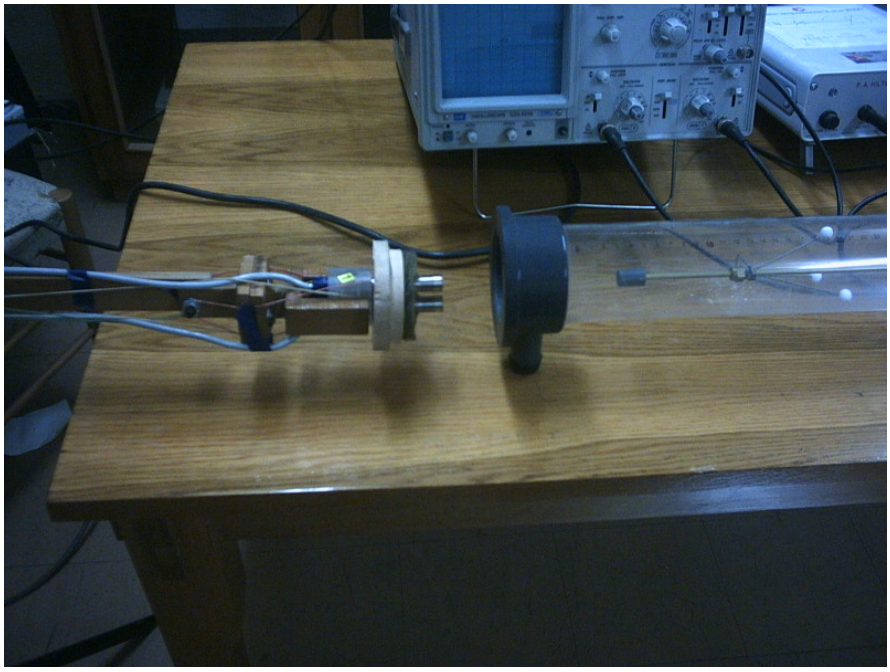

Figure 4.58 Special Connector and Its Anechoically Terminated Surface

One-dimensional plane waves are produced by the loudspeaker of the impedance tube to be sensed by the intensity probe. Since there is no spacing between the microphones, there is no field phase to measure. The measured phase (Φ_{err}) is only due to the phase mismatch between the channels of the measurement system for this configuration. The resulting phase mismatch error is shown in Figure 4.59.

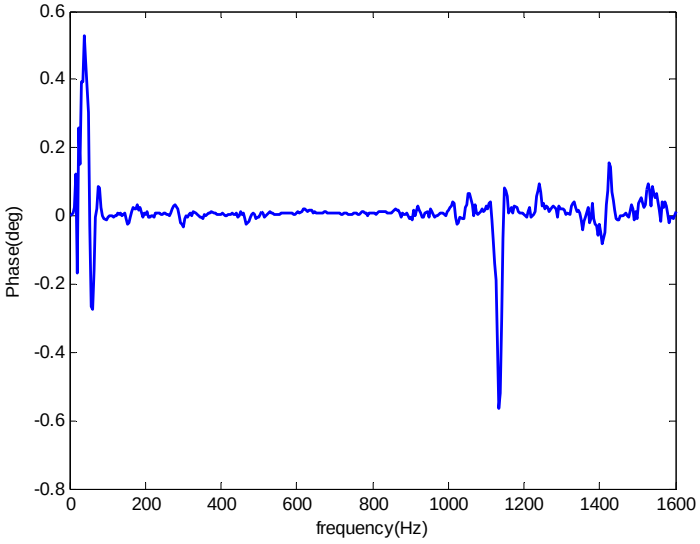

Figure 4.59 Phase Mismatch (Φ_{err}) between Channels of the Measurement System

It is seen from Figure 4.59 that the sound intensity measurement with this probe configuration is safe between the frequencies 100-1100 Hz from phase mismatch error standpoint. An ideal probe configuration is declared to have a maximum phase mismatch value of 0.3 degrees [1]. This probe configuration can be said to be an ideal probe between the frequency range of 100-1100 Hz.

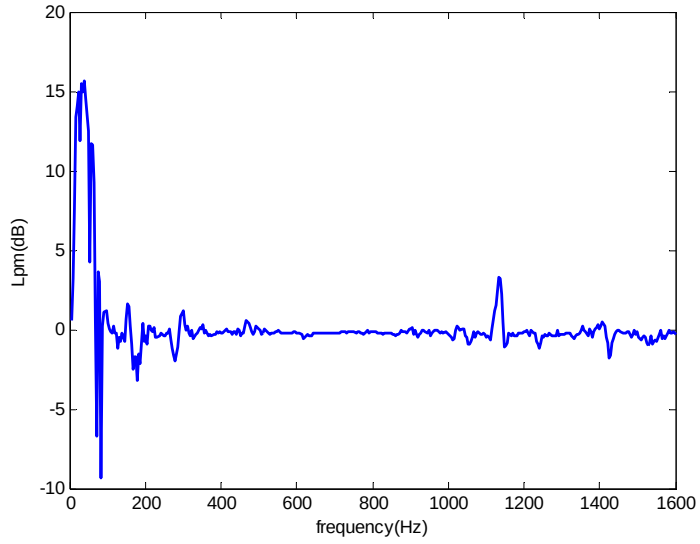

Figure 4.60 Residual Intensity due to the Phase Mismatch

Residual intensity due to the phase mismatch is also determined and given in Figure 4.60 .

Second type of bias errors is the finite difference aproximation error and can be calculated for ideal sound fields and ideal sound sources [1]. For a plane sinusoidal wave, for simplicity, assumed to propagate along the axis joining the microphones, the estimate of error in intensity measurement due to the finite difference approximation error (L_{en}) is calculated using Equation 3.30 and the resulting spectrum is given below for this particular study. It can be easily observed from the graph that the intensity is underestimated because of this type of error.

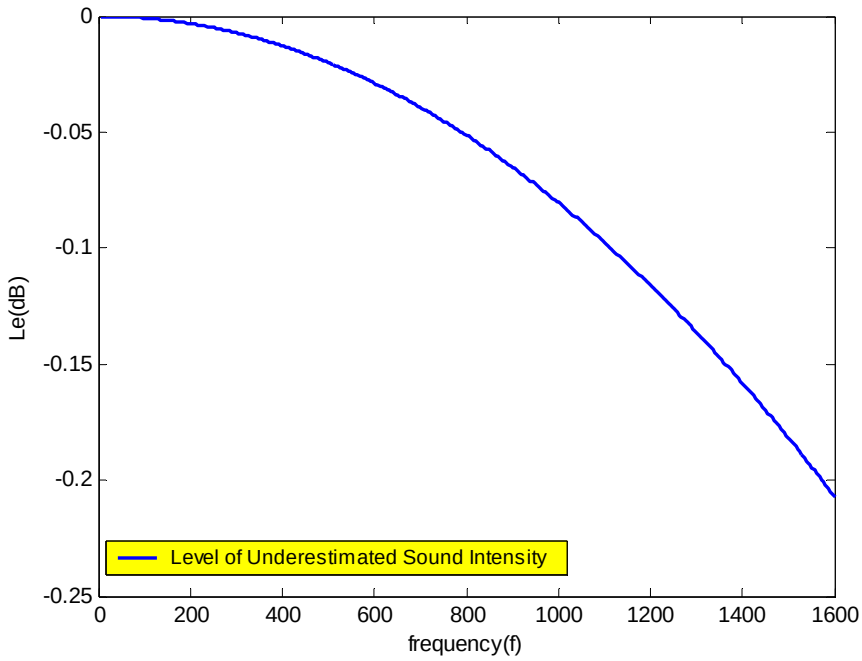

Figure 4.61 Level of Underestimated Intensity due to Finite Difference Error

Another bias error occurs, if the intensity changes along the probe, i.e. if the intensity is different at the two measurement positions and it is called as near-field approximation error. For a spherical wave originating from a monopole source, sound intensity level is overestimated due to the near-field approximation error and is shown below for this particular case.

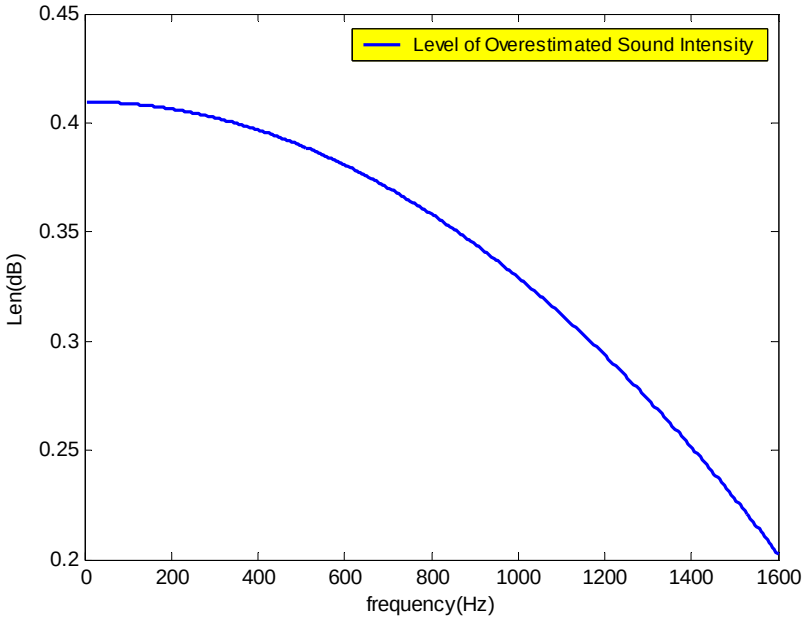

Figure 4.62 Overestimated Intensity Level due to Near-Field Approximation Error

Random errors are classified as spatial sampling error and spectral estimation error. There are some formulations that are used to evaluate the spatial sampling error. But in this study, it is minimized by increasing the measurement points and checked whether there is a change in the resultant total intensity value. It is experienced that, it is not effective to increase the total number of measurement points more than 36. Spectral estimation errors are again classified as bias and random errors. All of the methods employed in this study are in terms of the cross-

spectra of the measured physical quantities so that spectral estimation errors are analysed for cross-spectra estimates. Normalized bias error is given as [9],

$$\varepsilon_b = \frac{B_e^2}{24} \cdot \left[\frac{G''_{P_2P_1}(f)}{G_{P_2P_1}(f)} \right] \tag{4.5}$$

where $G''_{P_2P_1}(f)$ is the second derivative of cross-spectrum in frequency domain and B_e is the resolution bandwidth. Resolution bandwidth is equal to 4 Hz for the measurements carried out for this study. Normalized bias error spectrum is shown below.

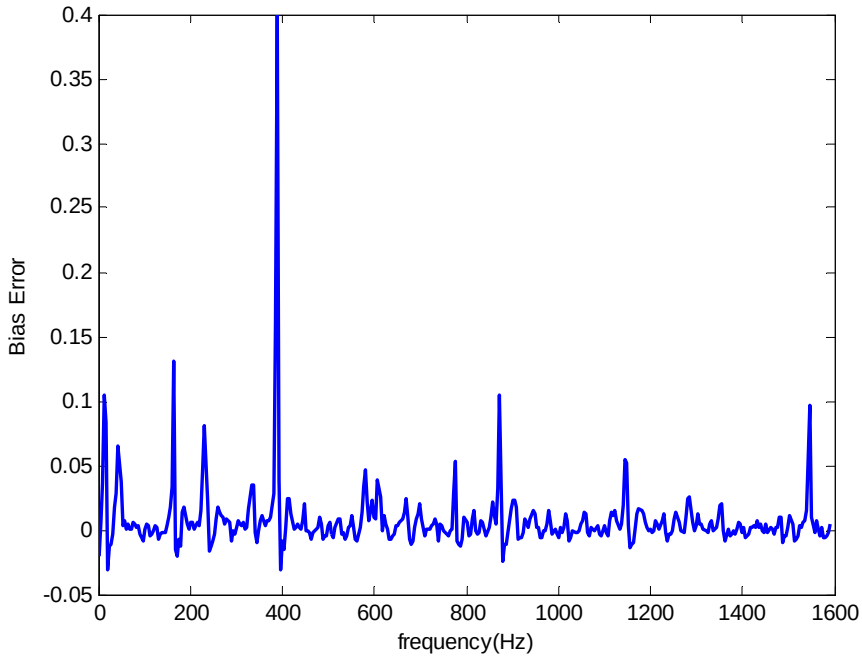

Figure 4.63 Normalized Bias Error due to the Cross-Spectrum Estimation

Normalized random error is given as [9],

$$\varepsilon_r = \frac{1}{\left|\gamma_{P_2P_1}(f)\right| \cdot n_d} \tag{4.6}$$

where $\left|\gamma_{P_2P_1}(f)\right|$ is the positive root of $\gamma^2_{P_2P_1}(f)$ which is the coherence between the two pressure signals and n_d is the number of averages taken and it is equal to 64 for this particular study. Normalized random error for sound intensity measurements carried within this study is given in Figure 4.63 below.

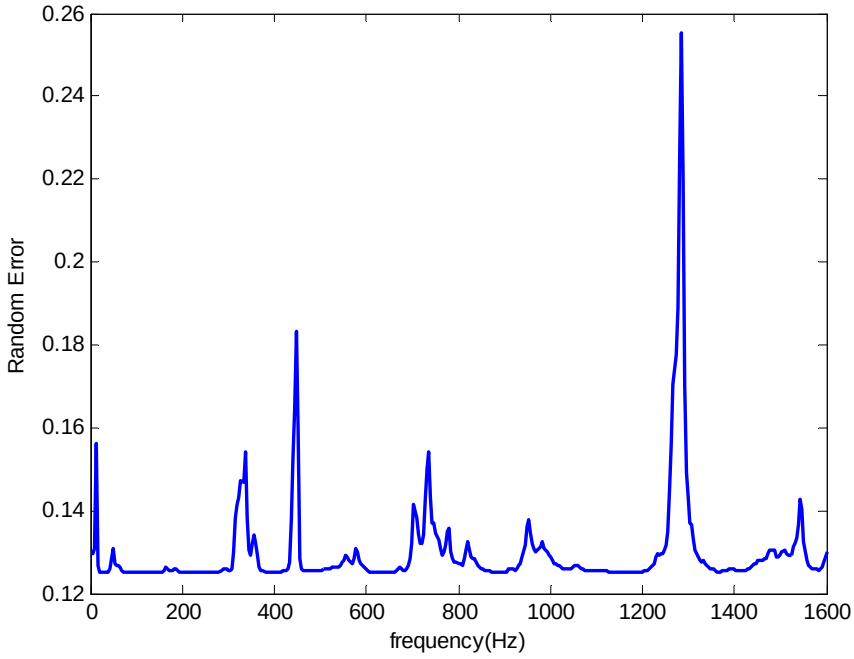

Figure 4.64 Normalized Random Error due to the Cross-Spectrum Estimation

Error analysis procedure for structural intensity is very similar to the procedure used for sound intensity. It is not going to be discussed here in detail. However, only the phase mismatch between the two measurement channels is measured and displayed in Figure 4.64 below. Please note that the two transducers are still working within the same type of media, i.e. plate, as it has been the case in the sound intensity measurement. The phase mismatch error is measured by mounting one of the accelerometers on the top of the other and mounting the lower one on the plate and exciting the plate with a random noise signal fed by the shaker.

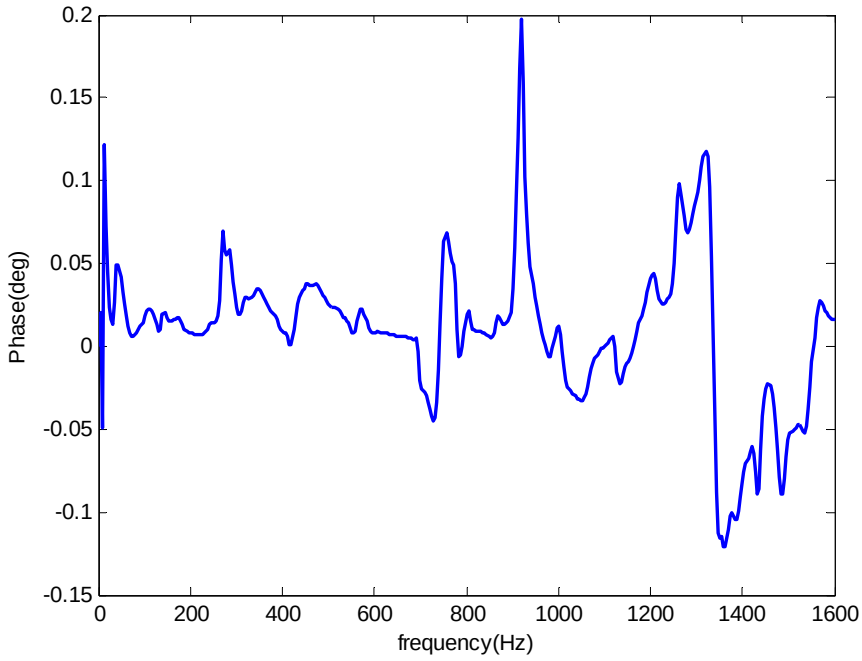

Figure 4.65 Phase Mismatch (Φ_{err}) Between Channels of the Measurement System

Even though the methods given in the literature are applied for error analysis of surface intensity measurement technique, none of them are found to be sufficient enough and will not be given here. This is primarily due to the fact that this measurement technique utilizes the cross-spectrum between the signals

measured at two different media, i.e plate and air. Although the wave speed is constant within air, it changes on the plate due to the dispersive behavior of this type of media.

CHAPTER 5

LUMPED PARAMETER MODELLING OF PLATES

5.1 Introduction

The goal of the analysis in this chapter is to develop an easily adoptable lumped parameter model of plate-like structures to compute the sound power radiated by the structure. The analysis is specifically concerned with computing acoustic power output because it is the single global quantity which can be used to assess the noise radiated by a source [33]. Even though total sound power of a structure can be determined by using numerical techniques like finite elements and boundary elements at the design stage, it may sometimes be cumbersome, expensive or unnecessary to use these methods. Instead, a relatively simple, fast and inexpensive method is needed. This is achieved by a lumped parameter model for the analysis of plates at especially low frequencies.

5.2 Lumped Parameter Modelling

At low frequencies where the acoustic wavelength is much larger than the characteristic dimension of the vibrating structure, acoustic radiation can be modelled as equivalent to that of a pulsating sphere or a vibrating piston. Moreover whole structure can be thought as if it is composed of many pulsating spheres or vibrating pistons. These simple source models may be combined in such a way that they all radiate in phase as a very rough model. Another method is to combine all of the simple sources that are of the same strength and where neighbouring sources

are 180° out of phase with each other [25]. As a last model, it is recommended in this particular study to combine all of the simple sources such that they radiate in their own true phases. Their relative true phases are determined from the measurement of the surface velocity of the structure. The plate that has been used in experimental part of the study is modeled by using the pulsating sphere and vibrating piston as the elementary source types, respectively, to compare the results obtained from these models to the results of the experimental work. Firstly, the plate is going to be modelled using pulsating sphere type sound sources in the next section.

5.3 Modelling the Plate by Using Pulsating Sphere Type Sound Sources

In this model, each partition on the plate is thought to be replaced by a pulsating sphere with a surface area equal to the corresponding partition of the plate radiating in its own true phase and the corresponding model is shown in Figure 5.1 below.

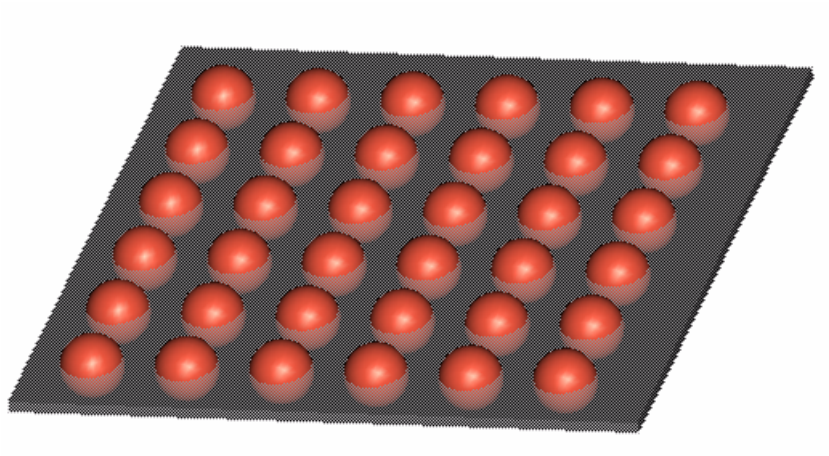

Figure 5.1 Lattice of Pulsating Spheres on the Plate

It is assumed that the pulsating sphere radiates harmonic spherical waves due to harmonically alternating surface velocity amplitude of U at the surface of

the sphere as shown in Figure 5.2. This means that the surface velocity of the pulsating sphere is assumed to be equal to the outgoing sound wave speed at the boundary and this can be used as a boundary condition in the derivation of the surface pressure.

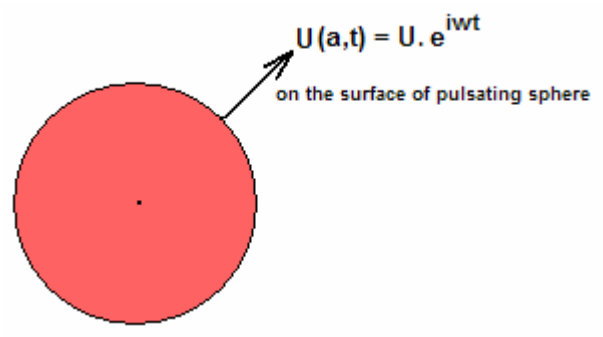

Figure 5.2 Velocity Amplitude at the Surface of the Pulsating Sphere

At this stage, derivation of the sound power radiated by each particular pulsating sphere will be carried out starting from the linearized equation for conservation of momentum as given below.

$$\rho_o \cdot \frac{\partial u}{\partial t} = -\frac{\partial p}{\partial r} \tag{5.1}$$

where the pressure is given for outgoing spherical waves as,

$$p = \frac{A}{r} \cdot e^{i(\omega t - kr)} \tag{5.2}$$

The particle velocity near the surface of the sphere u(r,t) can be obtained by using Equations 5.1 and 5.2 as,

$$u(r,t) = p(r,t) \cdot \left[\frac{k}{\omega \cdot \rho_o} + \frac{1}{i \cdot \omega \cdot \rho_o \cdot r} \right] \tag{5.3}$$

when the velocity equivalence condition given at the surface of the sphere is used as the boundary condition, one gets

$$u(a,t) = U \cdot e^{i\omega t} = p(a,t) \cdot \left[\frac{k}{\omega \cdot \rho_o} + \frac{1}{i \cdot \omega \cdot \rho_o \cdot a} \right] \tag{5.4}$$

where a is the radius of the pulsating sphere. Velocity amplitude can be determined as,

$$U = \frac{A}{a} \cdot e^{-ika} \cdot \left[\frac{i \cdot \rho_o \cdot \omega}{i \cdot k \cdot a + 1} \right] \tag{5.5}$$

Inserting the value of A found from Equation 5.5 into Equation 5.2 and rearranging the terms, the pressure expression is found as,

$$p(r,t) = \frac{a}{r} \cdot \frac{i \cdot k \cdot a}{1 + i \cdot k \cdot a} \cdot \rho_o \cdot c \cdot U \cdot e^{i(\omega t - k(r-a))} \tag{5.6}$$

where all of the terms in front of the exponential function is the pressure amplitude P. Then the root mean square (rms) value of the pressure can be given as,

$$P_{rms} = |P| \cdot \frac{1}{\sqrt{2}} \tag{5.7}$$

Substitution of the expression for P into the above equation and rearranging the terms, yields the rms value of the pressure as,

$$P_{rms} = \left[\left(\frac{a}{r} \right)^2 \cdot (\rho_o \cdot c \cdot U)^2 \cdot (k \cdot a)^2 \cdot \left(1 + (k \cdot a)^2 \right)^{-1} \right]^{\frac{1}{2}} \cdot \frac{1}{\sqrt{2}} \tag{5.8}$$

Sound waves become “plane wave” at the infinity, so the rms velocity becomes,

$$U_{rms} = \frac{P_{rms}}{\rho_o \cdot c} \tag{5.9}$$

and the intensity at far field can be written as,

$$I_{rms} = P_{rms} \cdot U_{rms} \tag{5.10}$$

$$I_{rms} = \frac{(P_{rms})^2}{\rho_o \cdot c} \tag{5.11}$$

and rearranging, one gets

$$I_{rms} = \left(\frac{a}{r}\right)^2 \cdot \left(\rho_o \cdot c \cdot U\right)^2 \cdot \left(k \cdot a\right)^2 \cdot \left(1 + \left(k \cdot a\right)^2\right)^{-1} \cdot \frac{1}{2 \cdot \rho_o \cdot c} \tag{5.12}$$

Sound power radiated can be written in terms of the sound intensity as,

$$W = \int_S I \cdot dS \tag{5.13}$$

where S is the total surface area of a sphere and it can be written in terms of solid angle Ω of the sphere as,

$$W = \int_0^{4\pi} I \cdot r^2 \cdot d\Omega \tag{5.14}$$

Solid angle is the three dimensional analog of the ordinary angle. It is the angle that is seen from the center of a sphere where it includes a given area or patch on the surface of that sphere. The value of the solid angle is numerially equal to the size of that area divided by the square of the radius of the sphere and can be written as,

$$\Omega = \frac{S}{r^2} \tag{5.15}$$

The term 4π as a boundary value for the integration in Equation 5.14 is the value for the full area of a unit sphere. Solid angle can be written in terms of azimuth angle (θ) and polar angle (Ø) in spherical coordinates. These angles are shown in Figure 5.3 below [34].

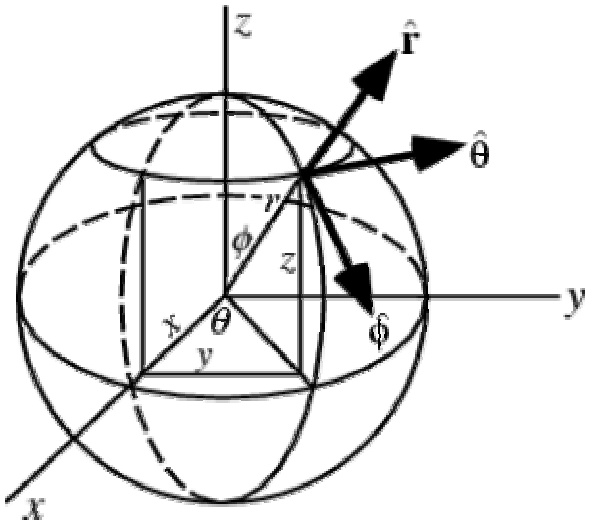

Figure 5.3 Angles Defining a Sphere in Spherical Coordinate System

The polar angle expression is given as,

$$\Omega = \iint_S \sin\varnothing \cdot d\theta \cdot d\varnothing \tag{5.16}$$

Inserting Equation 5.16 into Equation 5.14, the power is found to be,

$$W = \int_0^{2\pi}\int_0^{\pi} I \cdot r^2 \cdot \sin\varnothing \cdot d\varnothing \cdot d\theta \tag{5.17}$$

It should be noted that the azimuth angle is defined between the angles 0 to 2π and the polar angle is defined between the angles 0 to π. Evaluating the integration,

$$\int_0^{\pi} \sin\varnothing \cdot d\varnothing = 2 \tag{5.18}$$

and inserting the resulting value into Equation 5.17, one can get:

$$W = I_{rms} \cdot r^2 \cdot \int_0^{2\pi} 2 \cdot d\theta \tag{5.19}$$

and integrating,

$$W = I_{rms} \cdot 4 \cdot \pi \cdot r^2 \tag{5.20}$$

Substituting Equation 5.12 into Equation 5.20 and rearranging all of the terms, the power expression due to the radiation of a pulsating sphere is found to be,

$$W = \frac{2 \cdot \pi \cdot \rho_o \cdot \left(U_{rms}\right)^2 \cdot a^4 \cdot \omega^2}{c \cdot \left[1 + \left(k \cdot a\right)^2\right]} \tag{5.21}$$

This is the resultant power equation which is implemented into the Matlab® routine to find the total power radiated by the plate. U_{rms} is the surface velocity measured on each particular partition of the plate. The resultant power spectrum of the plate obtained from the model is plotted together with the total power spectra obtained from the measurement of sound intensity and surface intensity to test the analytical model with the experimental results.

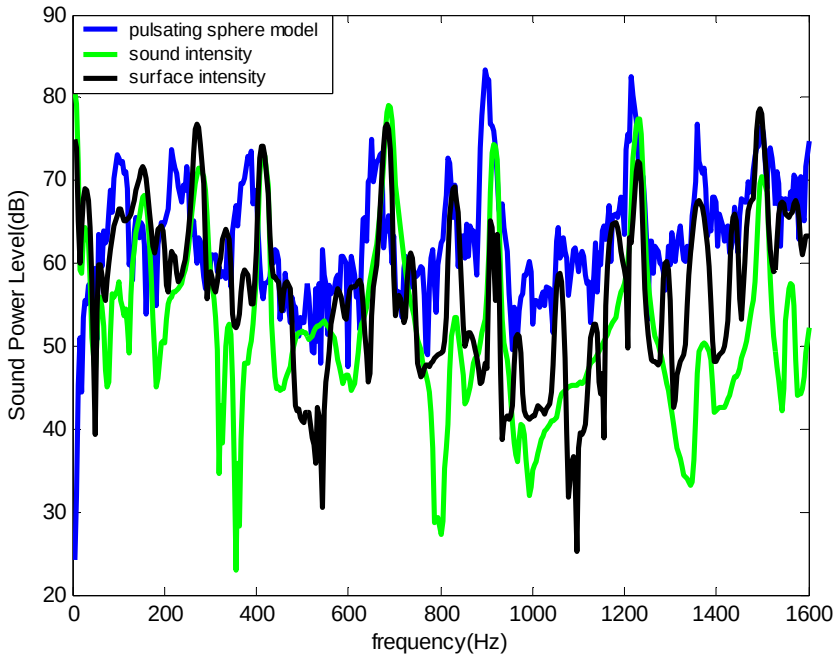

Figure 5.4 Sound Power Spectra Obtained from the Model and the Experiments

It is seen from the sound power spectra in Figure 5.4 obtained from both experimental methods together with the pulsating sphere model yield reasonably close results, at especially low frequencies where the acoustic wavelength is longer than the characteristic dimension of the vibrating structure, i.e. length of one side of a partition of the plate. It is also seen that the pulsating sphere is more efficient than the plate itself and this can also be seen from the radiation efficiency spectra shown in Figure 5.5 below.

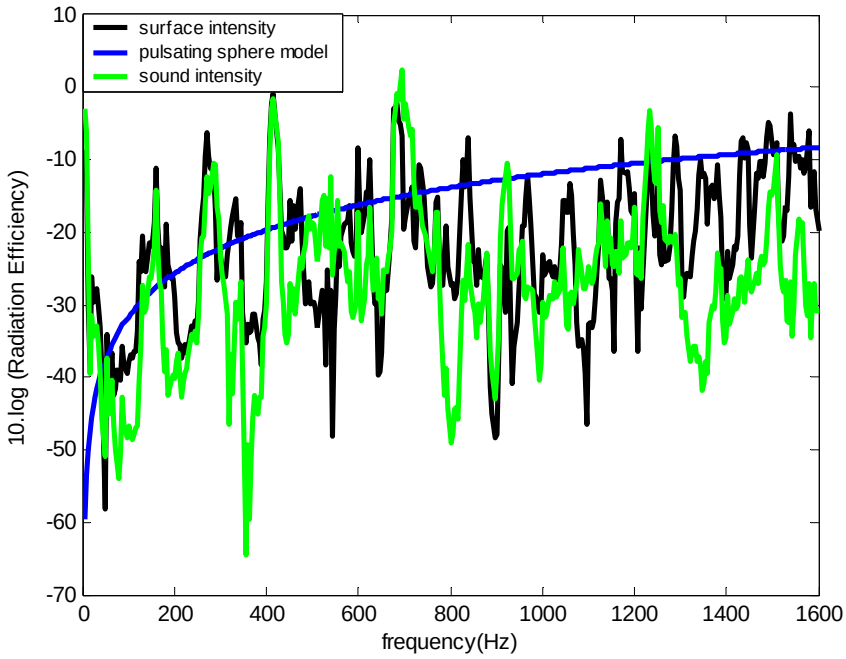

Figure 5.5 Radiation Efficiency of the Plate due to the Model and the Experiments

5.4 Modelling the Plate by Using Circular Piston Type Sound Sources

It is aimed to model the plate by a collection of another type of simple sources for more realistic representation of the acoustic radiation such that analytical results are expected to display a trend closer to the results of the experimental techniques employed. Circular, baffled vibrating piston model is used to accomplish this objective. In this model, each partition on the plate is thought to be replaced by a circular vibrating piston with a surface area equal to the corresponding partition of the plate radiating in its own true phase. The purpose of the baffle is to restrict the sound field to the forward hemisphere. More generally, it is used to decouple the sound fields in the forward and backward directions.

Otherwise, the piston would tend to act as a dipole, which radiates poorly [35]. The model is shown in Figure 5.6 below.

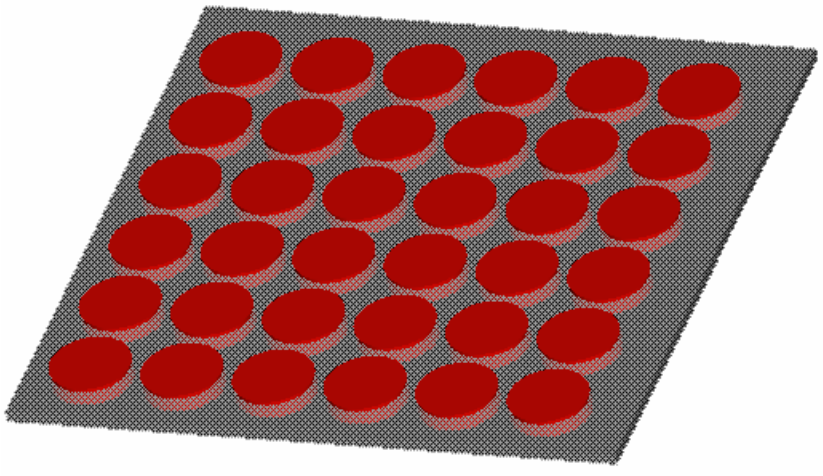

Figure 5.6 Lattice of Circular Vibrating Pistons on the Plate

Even though it is possible to calculate the total power radiated by the piston by integrating the farfield value of $P_{rms}^2/\rho_o \cdot c$ over a hemisphere surrounding the source, here, the power at the face of the piston is calculated instead. Sound power radiated by each piston in the baffle is given by [35],

$$W_i = \pi \cdot a^2 \cdot \left(U_{rms}\right)_i^2 \cdot \rho_o \cdot c \cdot R_1\left(2 \cdot k \cdot a\right) \tag{5.22}$$

where R_1 is the real part of the self radiation impedance which is given as,

$$Z_{mm} = \rho_o \cdot c \cdot S_m \left[1 - \frac{J_1(2 \cdot k \cdot a_m)}{k \cdot a_m} + i \cdot \frac{2 \cdot S_1(2 \cdot k \cdot a_m)}{k \cdot a_m}\right] \tag{5.23}$$

with J_1 is the Bessel function of the first order, S_1 is the Struve function of the first order, k is the wavenumber and a is the equivalent radius of the pistons. The plate is already thought to be divided into 36 partitions. Each partition is replaced by a vibrating piston with an area S_m, that is equal to the area of the corresponding

partition and with a uniform surface velocity U_{rms} obtained from the direct measurements on the plate's surface. Sound power radiated by the plate can be found by superposition of results from Equation 5.22 where there is no mutual interaction assumed between the pistons [36]. It should be noted that the radiation impedance of a piston can be obtained by integrating the elemental pressure distribution over the surface area of the piston to obtain the total sound pressure at a point in the field and subsequently integrating this again over the surface to obtain the force on the piston due to the acoustic pressure fluctuations [37].

Although it is not included in the model mentioned above, there is an acoustical interaction between each vibrating piston. Surface velocity of a piston influences the pressure field above another piston and vice versa. This is mathematically explained by the mutual radiation impedance term. In this section, results are both obtained for the original model above where there is no acoustical interaction between the partitions and for modified model where the interaction takes place via the mutual radiation impedance terms given by [38],

$$Z_{mn} = \frac{\rho_o \cdot c \cdot k^2 \cdot S_m \cdot S_n}{2 \cdot \pi} \cdot \left[2 \cdot \frac{J_1(k \cdot a_m)}{k \cdot a_m} \right] \cdot \left[2 \cdot \frac{J_1(k \cdot a_n)}{k \cdot a_n} \right] \cdot \left(\frac{\sin kd_{mn}}{kd_{mn}} + i \cdot \frac{\cos kd_{mn}}{kd_{mn}} \right) \quad (5.24)$$

where S is the area of a piston and d is the distance between the centers of the m^{th} and the n^{th} pistons as they are shown in Figure 5.7.

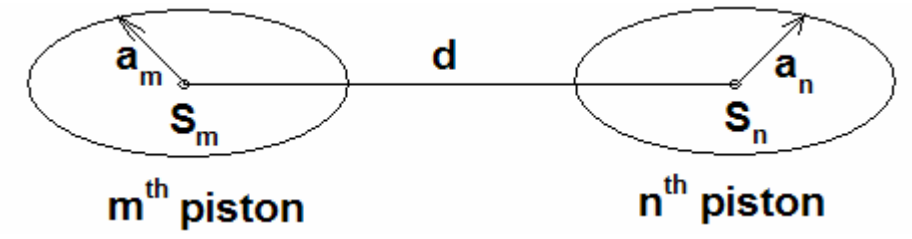

Figure 5.7 Calculation of the Mutual Radiation Impedance

Then the total sound power radiated can be given as,

$$W_i = \mathrm{Re}\left(Z_{mm}\right)\cdot\left|U_m\right|^2\cdot S_m + \sum_n \mathrm{Re}\left(Z_{mn}\cdot U_m\cdot U_n^*\right)\cdot S_n \qquad (5.25)$$

Consequently, total sound power radiated by the plate can be found by summing the Equation 5.25 for the latter model where U represents the complex velocity of each particular partition, asterisk denotes the complex conjugate and Re indicates the real part of the complex-valued quantities.

Results of the circular vibrating piston model with and without mutual interaction are compared with the result obtained by the two-microphone sound intensity measurement and the result of the pulsating sphere model of the plate as shown in Figure 5.8.

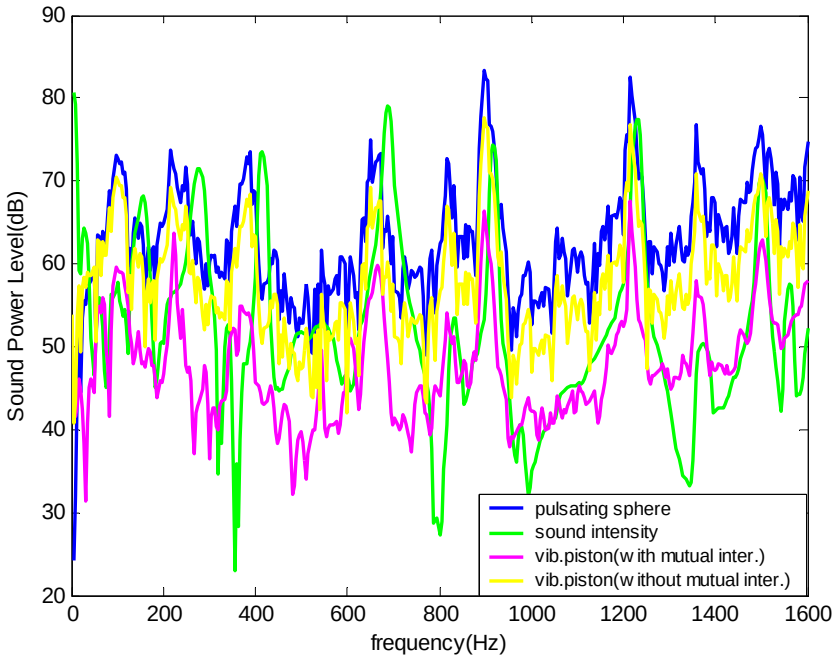

Figure 5.8 Sound Power Spectra Obtained from the Models and the Experiments

Pulsating sphere type sound source is observed to be the most efficient radiator as expected. The same result can be seen from the comparison of the radiation efficiencies given in Figure 5.9.

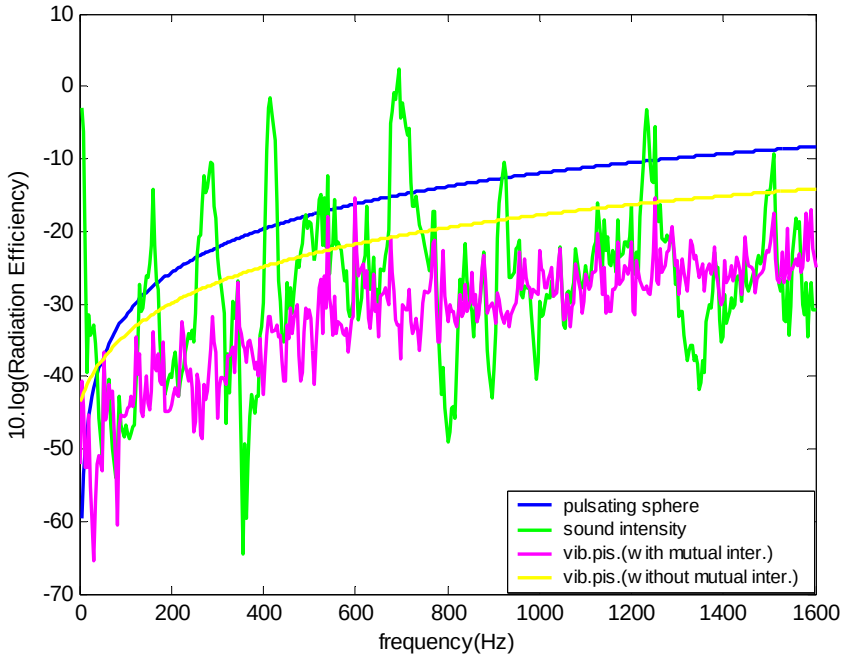

Figure 5.9 Radiation Efficiency of the Plate due to the Models and the Experiment

Although it is not necessary to calculate the value of the Struve function in the self radiation impedance formulation given by Equation 5.23 for power calculations, it is required in the calculation of the impedance itself. Struve function of the first order is approximated by a function given by Equation 5.26 in this study [39].

$$S_1(2ka) \approx \frac{2}{\pi} - J_0(2ka) + \left(\frac{16}{\pi} - 5\right) \cdot \frac{\sin(2ka)}{2ka} + \left(12 - \frac{36}{\pi}\right) \cdot \frac{1 - \cos(2ka)}{(2ka)^2} \qquad (5.26)$$

The term J_0 given in Equation 5.26 is the Bessel Funtion of order zero. The approximate function given by Equation 5.26 yields a very close spectrum to the spectrum of the real Struve function. Approximate function is mainly used to shorten the calculation time. Though there is no direct command in Matlab®, one must write a rather long subroutine to calculate the exact Struve Function. Instead, it is found more practicle to use the approximate function given by Equation 5.26.

5.5 Results and Discussions

At last, sound power level and radiation efficiency spectra belonging to the results of all of the measurement techniques employed and the analytical models applied are given on the same graph for ease of comparison in Figure 5.10, respectively.

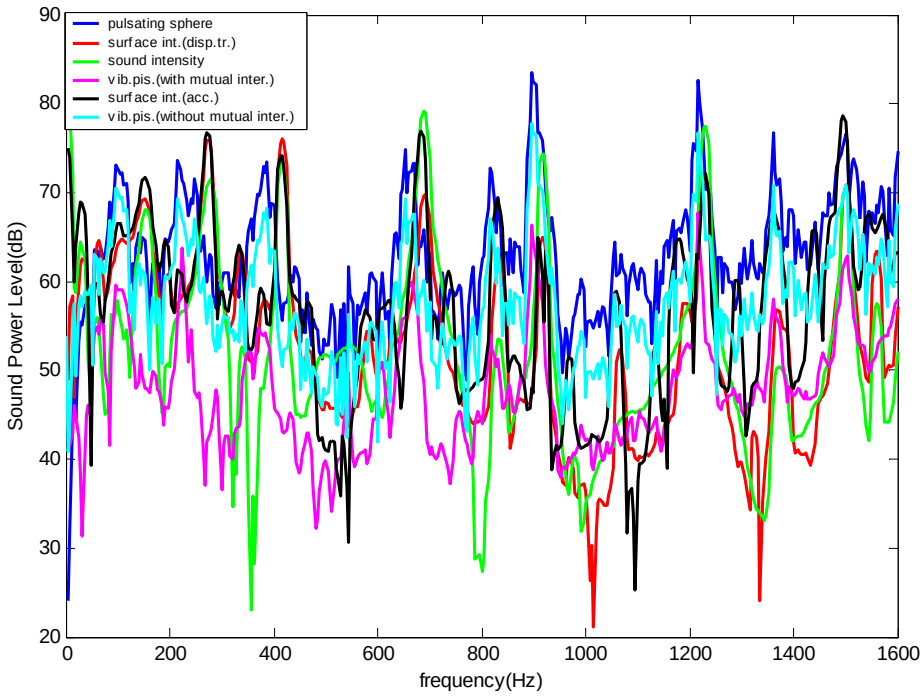

Figure 5.10 Sound Power Level Spectra due to the Models and the Experiments

It is observed from Figure 5.10 that the model that displays the closest results to the results obtained from the experimental methods employed is the baffled circular vibrating piston model without mutual interaction. Pulsating sphere is the most efficient radiator and the vibrating piston model with included mutual interaction terms is the most inefficient radiator. Moreover, it is observed to be the worst model to represent the plate analysed throughout this study from standpoint of deviation from experimental results. Comparative evaluation of the radiation efficiencies can be easily made via the graph given in Figure 5.11 below.

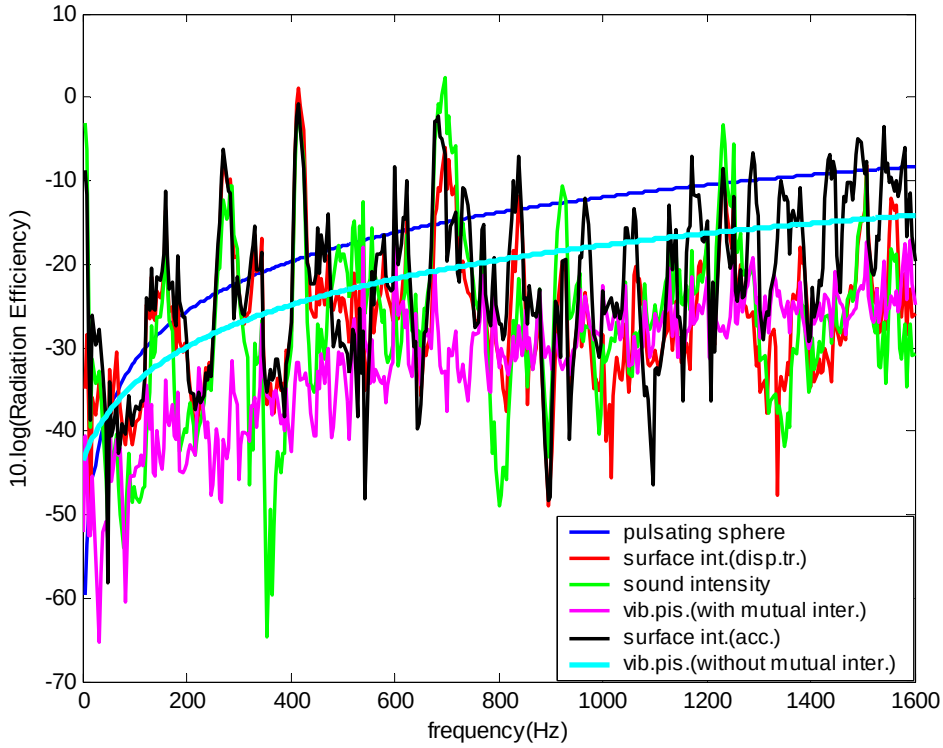

Figure 5.11 Radiation Efficiency Spectra due to the Models and the Experiments

CHAPTER 6

SUMMARY OF RESULTS AND DISCUSSIONS

The experimental and analytical results of this investigation have described an integrated approach to determine the vibroacoustical characteristics of plate-like structures at low frequency range, corresponding to the working frequency range of machinery in everyday use. Three different techniques have been employed to understand both the sound radiation and the power flow paths to establish the relationship between the dynamics of the waves propagating in two different media. The results and conclusions of most significance are briefly summarized below.

1. The most fundamental acoustical measurement tehniques are utilized in this study. Three measurement probes are designed to measure sound intensity, surface intensity and structural intensity respectively. It has been shown that, integrated use of these three techniques is possible even with the basic probes designed. The experimental results are so encouraging that these techniques can be used in an integrated manner and the vibroacoustical properties of machinery in situ can be determined in a practical and inexpensive fashion.

2. Calibration of the probes are achieved by using the techniques available in the literature. However, some of the calibration techniques are a little bit modified to conform to the laboratory conditions. For instance, amplitude calibration of the non-contact displacement transducer is achieved by using a calibration exciter which is usually employed to achieve the amplitude calibration of accelerometers. Since the probe can only transduce the displacement of metallic surfaces, an accelerometer is screwed onto the calibration exciter to form a metal and flat vibrating surface.

3. Sound intensity probe and the displacement probe is used together to measure sound intensity and surface intensity simultaneously. Results obtained from these two acoustical methods seemed to be in harmony up to 1000 Hz which is in fact the frequency value where the displacement transducer starts to loose its flatness in response.

4. Even though the plate used in the experimental part of this study is considered to be small in dimensions which implies that the plate is a very reverberant media for structural intensity measurement, classical two-accelerometer probe is successfully employed in the experiments. Frequency domain formulation of structural intensity is derived both with a cross-spectral approach and with a transfer function approach. Transfer function formulation of structural intensity is achieved by treating the measurement system as a single-input/multiple-output system where the forcing applied by the shaker is assumed to be the input and the two acceleration signals sensed by the accelerometers are assumed to be the two outputs of the system. Power flow maps are given for the resonant frequencies of the plate.

5. Modal behavior of the plate is determined by using both the non-contact eddy-current displacement probe and an accelerometer. Results are observed to be the same as expected. Power spectrum acquired by the accelerometer is used to detect the structural resonances of the plate.

6. Total sound power radiated by the plate is measured by using the two-microphone sound intensity technique. Results are analyzed to rank the contributions of the modes to the total sound power radiated within the frequency range of interest.

Phase mismatch elimination is achieved by using both the ***microphone switching method*** and the ***transfer function method***. Results are compared with the one obtained from measurement of sound power involving phase mismatch. It is observed that the elimination of the phase mismatch between the two measurement channels is much more effective within the frequency range of 0 to 200 Hz as expected. At the same frequency range, it is also seen that the transfer function method and the microphone switching method differs much more than that

is observed for other frequencies. This difference is due to the fact that the microphone switching method takes not only the sensitivity of the measurement system into consideration, but also the effects of the environmental conditions on each particular measurement. When the transfer function method is utilized, frequency responses of both channels and the transfer function between them are determined for once and then, these values are used for all subsequent calculations.

7. Side-by-side microphone configuration is used for the two-microphone sound intensity measurements and near-field energy radiation paths are successfully identified. This allows one to hinder the excess sound radiated by the dominant sources on the plate by using different noise control methods.

8. Surface intensity is measured to compare its results with the results obtained from the two-microphone sound intensity measurements. The measurements are carried out by using two different types of probe configurations. First, a non-contact, eddy-current displacement transducer is used with a condenser microphone and as a second configuration, an accelerometer is used with a condenser microphone to measure surface intensity. Results obtained are compared and evaluated. Since the effect of mass loading associated with the use of the accelerometer is not observed within this frequency range and it is observed that the non-contact displacement transducer looses its flatness in response at frequencies above 1 kHz, it is concluded that, it is better to use the accelerometer (B&K Type 4344) of 2.5 grams for this application within this frequency range.

9. Damping patches are attached onto the plate's surface to see the difference in the paths of outgoing structural waves as well as in the sound radiation paths on the plate . The regions where the damping patches are attached are chosen as a result of the analysis of the near-field intensity results of the undamped plate. Results of sound intensity and structural intensity measurements carried out both on the undamped and damped configuration of the same plate are compared. Results have shown that the application of the damping patches have been successful in reducing the total sound power radiated by the plate. They are also effective in changing density and direction of the power flow on the plate. Yet, both sound and structural intensity maps have revealed that, the change in the

direction of sound energy radiation paths and power flow paths are not found as striking as they have been expected. This is especially due to the reverberant characteristic of the plate used and possible inhomogeneity in the structure of the damping patches attached.

10. Error analysis is carried out for both two-microphone sound intensity and structural intensity methods and confidence intervals for frequency range of measurement and transducer spacing value are determined by the help of the results obtained from the error analysis.

11. Easily adoptable two lumped parameter models of the plate are developed to compute the sound power radiated by the structure. In these models, the plate is modeled by employing the pulsating sphere and vibrating piston as the elementary source types alternatively. Results obtained from these models are compared with the experimental results. The plate is thought to be divided into 36 partitions. In the first model, each partition is replaced by a pulsating sphere whereas the second model utilizes a vibrating piston. Surface areas of the sphere and piston are taken equal to the area of the corresponding partition. A uniform surface velocity U_{rms} obtained from the measurements on the plate's surface is assigned in corresponding models. In the model employing piston in the baffle, results are obtained with and without mutual interaction among partitions. Analytical results of the models are compared to the results of the experimental work. They are found to be encouraging at especially low frequency range for both cases where effect of mutual impedances is taken into account or not for the vibrating piston model and the pulsating sphere model. Yet, vibrating piston model which does not take the effect of mutual impedances into account is found to display a closer trend with the experimental results for this particular study.

Future work in this area should concentrate on the phase mismatch elimination inherent in the surface intensity technique. In fact, a new generation surface intensity probe should be designed to eliminate the phase mismatch.

Further work should also focus on the analytical and experimental comparison of mass, stiffness and damping addition on the predetermined regions on plates. This topic may be supported by another study involving the application

of both finite element and boundary element methods in an integrated manner to compare the results obtained with the results obtained from the experimental studies that have been completed.

REFERENCES

[1] Sound Intensity (Theory), Technical Review, Bruel & Kjaer, No: 3, 1982

[2] F.J. Fahy, Sound Intensity,Elsevier, London, 1990

[3] R. Raangs, W.F. Druyvesteyn and H.E. de Bree, "A low cost Intensity Probe", Audio Engineering Society Convention Paper, 2001, Netherlands

[4] F. Jacobsen, V. Cutanda and P.M. Juhl, Journal of Acoustical Society of America, 103, 953 (1998)

[5] M.J. Crocker and J.P. Arenas, "Fundamentals of the Direct Measurement of Sound Intensity and Practical Applications", Acoustical Physics, Vol.49, No.2, pp. 163-175, 2003

[6] F.J. Fahy, "Measurement of Acoustic Intensity using the Cross-Spectral Density of two microphone signals", Journal of Acoustical Society of America, Vol.62, No.4, October, 1977

[7] J.Y. Chung, "Cross-Spectral Method of Measuring Acoustic Intensity", Research Publication, General Motors Research Laboratory, GMR-2617, Warren, Michigan, 1977

[8] R.B. Coleman, "Sound Radiation from Repetitive Transient Vibrations using Multi-Channel Digital Signal Processing with Application to Impact Machinery", PhD Thesis Submitted to NCSU, 1984, Raleigh

[9] J.S. Bendat, A.G. Piersol, Engineering Applications of Correlation and Spectral Analysis, Wiley-Science, New York, 1980

[10] Sound Intensity, Technical Review, Bruel & Kjaer, 1986

[11] J.K Thompson and D.R. Tree, "Finite Difference Approximation Errors in Acoustic Intensity Measurements", Journal of Sound and Vibration, 1981, 75(2), pp. 229-238

[12] J.Y. Chung, "Cross-spectral method of measuring acoustic intensity without error caused by instrument phase mismatch", Journal of Acoustical Society of America, Vol.62, No.6, December, 1978

[13] Sound Intensity (Instrumentation & Applications), Technical Review, Bruel & Kjaer, No: 4, 1982

[14] G. Krishnappa, "Cross-spectral method of measuring acoustic intensity by correcting gain and phase mismatch errors by microphone calibration", Journal of Acoustical Society of America, Vol.69, No.1, January, 1981

[15] D.M. Yeager, “A Comparison of Intensity and Mean-Square Pressure Methods for Determining Sound Power Using a Nine-Point Microphone Array”, Noise Control Engineering Journal, Vol.22, No.3, May-June, 1984

[16] T.H. Hodgson, “Investigation of the surface acoustical intensity method for determining the noise sound power of a large machine in situ”, Journal of Acoustical Society of America, Vol.61, No.2, February, 1977

[17] D.E. Boone, “A Surface Acoustic Intensity Probe using a Pressure Microphone and A Fiber Optic Lever Displacement Transducer”, MSc Thesis Submitted to NCSU, 1981, Raleigh

[18] Driesch, Iwata, Koopmann and Dosch, “Development and evaluation of a surface acoustic intensity probe”, Review of Scientific Instruments (American Institute of Physics), Vol.71, No.10, October 2000

[19] W. Reinicke, “When to apply surface intensity measurements”, Proceedings of Inter-Noise 88, pp. 101-104

[20] M.C. McGary and M.J. Crocker, “Phase Shift Errors in the Theory and Practice of Surface Intensity Measurements”, Journal of Sound and Vibration, 82(2), 1982, pp. 275-288

[21] D.U. Noiseux, “Measurement of Power Flow in Uniform Beams and Plates”, Journal of Acoustical Society of America, Vol.47, No.1, Part 2, 1970

[22] G. Pavic, “Measurement of Structure Borne Wave Intensity, Part1: Formulation of the Methods”, Journal of Sound and Vibration, 49(2), 1976, pp. 221-230

[23] E.G. Williams, H.D. Dardy and R.G. Fink, “A technique for measurement of structure-borne intensity in plates”, Journal of Acoustical Society of America, Vol.78, No.6, December, 1985

[24] Gunnar Rasmussen, “Intensity Measurements”, Bruel & Kjaer publications, September, 1987

[25] L.Cremer, M. Heckl and E.E. Ungar, “Structure Borne Sound”, Springer-Verlag, 1973, Berlin

[26] J.W. Verheij, “Cross Spectral Density Mehods for Structure Borne Power Flow on Beams and Pipes”, Journal of Sound and Vibration, 70(1), 1980, pp. 133-139

[27] H.S. Kim and J. Tichy, “Measurement error minimization of bending wave power flow on a structural beam by using the structural intensity techniques”, Applied Acoustics, Vol.60, 2000, pp. 95-105

[28] D. A. Bies and C. H. Hansen, Engineering Noise Control: Theory and Practice, E & FN SPON, London, 1996

[29] A.D. Pierce, Acoustics : An Introduction to Its Physical Principles and Applications, McGraw Hill, New York, 1981, Chapter 1

[30] R.H. Lyon, Machinery Noise and Diagnostics, Butterworth Publishers, 1987

[31] J.A. Mann III and J. Tichy, "Near-field identification of vibration sources, resonant cavities and diffraction using acoustic intensity measurements", Journal of Acoustical Society of America, Vol.90, No.2, Part 1, 1991

[32] B. Forssen and M.J. Crocker, "Estimation of acoustic velocity, surface velocity and radiation efficiency by use of the two-microphone technique", Journal of Acoustical Society of America, Vol.73, No.3, 1983

[33] G.H. Koopmann and J.B. Fahnline, Designing Quiet Structures : A Sound Power Minimization Approach", Academic Press, 1997

[34] http://mathworld.wolfram.com , 07.05.2004

[35] D.T. Blackstock, Fundamentals of Physical Acoustics, Wiley-Interscience, New York, 2000

[36] M. İnalpolat and M. Çalışkan, "An Integrated Approach for Determination of Radiation Characteristics of Plates by Sound and Structural Intensity Techniques", Proceedings of ICSV11(to be published), July 2004, St.Petersburg, Russia

[37] M.P. Norton, Fundamentals of Noise and Vibration Analysis for Engineers, Cambridge University Press, 1989

[38] N. Hashimoto, "Measurement of sound radiation efficiency by the discrete calculation method", Applied Acoustics, Vol.62, pp. 429-446, 2001

[39] R.M. Aarts and A.J.E.M. Janssen, "Approximation of the Struve Function H_1 Occuring inImpedance Calculations", Journal of Acoustical Society of America, Vol.113, No.5, May, 2003

[40] H.F. Olson, "System responsive to the energy flow of sound waves", U.S. Patent No.1, 892, 644, December 1932

[41] H.F. Olson, "Field-type acoustic wattmeter", Journal of Audio Engineering Society, Vol.22, No.5, June 1974

[42] C.W. Clapp and F.A. Firestone, “The acoustic wattmeter, an instrument for measuring sound energy flow”, Journal of Acoustical Society of America, Vol.13, October, 1941

[43] R.H. Bolt and A.A. Petrauskas, “An acoustic impedance meter for rapid field measurements”, Journal of Acoustical Society of America, Vol.15,79(A), 1943

[44] S. Baker, “An acoustic intensity meter”, Journal of Acoustical Society of America, Vol.27, No.2, March, 1955

[45] T.J. Schultz, “Acoustic Wattmeter”, Journal of Acoustical Society of America, Vol.28, No.4, July, 1956

[46] B.G. Van Zyl and F. Anderson, “Evaluation of the intensity method of sound power determination”, Journal of Acoustical Society of America, Vol.57, No.3, March, 1975

[47] G. Pavic, “Measurement of sound intensity”, Journal of Sound and Vibration, Vol.51, 1977

[48] J.F. Burger, G.J.J. Van der Merwe, B.G. Van Zyland, L. Joffe, “Measurement of sound intensity applied to the determination of radiated sound power”, Journal of Acoustical Society of America, Vol.53, No.4, 1973

[49] J.Y. Chung, J. Pope and D.A. Feldmaier, “Application of acoustic intensity measurement to engine noise evaluation”, Proceedings of the Diesel Engine Noise Conference, Michigan, February, 1979

[50] M.P. Waser and M.J. Crocker, “Introduction to the two-microphone cross-spectral method of determining sound intensity”, Noise Control Engineering Journal, May-June, 1984

[51] J. Buffa II and M.J. Crocker, “Background noise effects on the measurement of sound power of small machines using sound intensity techniques, Noise Control Engineering Journal, July-August, 1985

[52] U.S. Shirahatti and M.J. Crocker, “Studies on sound power measurements using the sound intensity technique”, Noise Control Engineering Journal, September-October, 1993

[53] T. Astrup, “Measurement of sound power using the acoustic intensity technique – A consultant’s viewpoint”, Applied Acoustics, Vol.50, No.2, pp.111-123, 1997

[54] P.S. Watkinson, “The practical assessment of errors in sound intensity measurement”, Journal of Sound and Vibration, Vol.105, No.2, pp. 255-263, 1986

[55] F. Jacobsen, “Random errors in sound intensity estimation”, Journal of Sound and Vibration, Vol.128, No.2, pp. 247-257, 1989

[56] F. Jacobsen, “Spatial sampling errors in sound power estimation based upon intensity”, Journal of Sound and Vibration, Vol.145, No.1, pp. 129-149, 1991

[57] B.S. Cazzolato and C.H. Hansen, “Errors in the measurement of acoustic energy density in one-dimensional sound fields”, Journal of Sound and Vibration, Vol.236, No.5, pp. 801-831, 2000

[58] N. Atalla and J. Nicolas, “A new tool for predicting rapidly and rigorously the radiation efficiency of plate-like structures”, Journal of Acoustical Society of America, Vol.95, No.6, June, 1994

[59] J. Tichy and T. Kihlman, “Sound intensity field in front of plates with and without damping”, Proceedings of Inter-Noise 88, pp. 111-114

[60] F. Cervera, H. Estelles, F. Galvez and F. Belmar, “Sound intensity in the near-field above a vibrating flat plate, Noise Control Engineering Journal, Vol.45, No.5, September-October, 1997

[61] M.F. Jacobsen, R. Singh and F.B. Oswald, “Acoustic radiation efficiency models of a simple gearbox”, Army Research Laboratory Technical Report, ARL-TR-1111, 1996

[62] F.J. Fahy and R. Pierri, “Applications of cross-spectral density to a measurement of vibration power flow between connected plates”, Journal of Acoustical Society of America, Vol.62, No.5, November, 1977

[63] Y. Zhang and J.A. Mann III, “Examples of using structural intensity and the force distribution to study vibrating plates”, Journal of Acoustical Society of America, Vol.99, No.1, January, 1996

[64] M.E. Johnson and S.J. Elliott, “Active control of sound radiation using volume velocity cancellation”, Journal of Acoustical Society of America, Vol.98, No.4, October, 1995

[65] G. Rasmussen and P. Rasmussen, “Structural Intensity Measurements using Vibrational and Acoustical Techniques”, Proceedings of Inter-Noise 92, pp. 549-552, Canada